High-resolution wave forecasting
The Catalan coast case

Modelling, coupling and validation

Elena Pallares

Thesis directors:
Agustin Sánchez-Arcilla Conejo
Manuel Espino Infantes

A thesis presented for the degree of Doctor

Laboratori d'Enginyeria Marítima
UPC - BARCELONATECH

Spain
July 2016

Per la meva mare Esperança i la meva germana Marta.

High resolution wave forecasting. The Catalan coast case.

Modelling, coupling and validation

Elena Pallares

Abstract

It is widely known that wind and wave predictions in the nearshore are less precise for semi enclosed domains than in the open ocean. The Catalan coast is a clear example of this situation, with a wave climate controlled by short fetches, complex bathymetry, high wind field variability in time and space, and sea and swell waves combined that generate bimodal spectra. These characteristics, typical for a semi-enclosed basin, limit the reliability of wave predictions in the area, with errors on the significant wave height around 10% and a clear under-prediction of the wave period with errors around 30%.

The motivation of this work is to improve the actual wave forecasting abilities for the Catalan Coast using the SWAN v.4091 wave model. In order to achieve this goal, three working lines are considered: (1)adapting the model to the Catalan coast conditions, tuning the wave growth rates included in the model to better reproduce the observed values, (2) evaluate the effect of the currents and wind into the wave field by using a coupled system and (3) consider the use of unstructured grids as an alternative to the traditionally nested systems in order to obtain high resolution wave forecasts in coastal areas reducing the computational time and avoiding the use of internal boundary conditions with their associated errors.

The results obtained support previous studies where the limited ability of the models to reproduce wave growth rates in young seas have been detected. The white-capping term correction proposed in this document helps reducing under-prediction of the wave period observed with almost no effect on the significant wave height. This correction can be applied to similar environments. However, the proposed formulation is only suitable for the early stages of generation and should be discontinued after waves reach a certain maturity.

Two coupling strategies are considered, a one-way coupling where current fields are directly introduced into the wave model, and a two-way coupling where the waves, currents and winds models run in parallel. The effects of the coupling are evaluated during calm periods but also during energetic events. The results show that during calm conditions the coupling does hardly improve the results while during energetic events, such as superficial currents intensifications or wind jet events, the coupling has greater importance. However, the two-way coupling has extremely high computational requirements, not always available.

In this sense, the use of unstructured grids as an alternative to the traditional nested systems is presented. The main benefit of unstructured grids is that allows working with a single grid with different resolutions in each sub-domain, improving

the resolution in coastal areas. Other advantage is the capacity to better reproduce the sharp coastline and the areas around the islands. The design of unstructured grids has been shown as one of the most delicate parts of this methodology, requiring special attention for the grid generation criteria. The validation of the results, performed with buoy measurements in the nearshore but also for the entire domain with altimetry measurements, allows stating that unstructured grids perform correctly in the study area.

Finally, the proposed work suitability for an operational forecasting system has been considered. The whitecapping term modification is proven to be decisive in the quality of the wave forecast, while the coupling is not always recommended depending on computational capabilities. The use of unstructured grids with a regional triangular mesh covering the entire Western Mediterranean sea is considered as the first option, providing accurate high resolution wave conditions near the coast with a clear reduction of the computational time in comparison with a traditional nested system.

Publications

Peer Reviewed Internationa Journals

Pallares, E, A Sanchez-Arcilla, M Espino (2014), "Wave energy balance in wave models (SWAN) for semi-enclosed domains: application to the Catalan Coast." *Continental Shelf Research*, 87, 41-53.

Grifoll, M, J Navarro, E Pallares, L Rafols, M Espino, A Palomares (2016), "Ocean-atmosphere – wave characterization of a wind jet (Ebro shelf, NW Mediterranean Sea)." *Nonlinear Processes in Geophysics*, Revised Submission.

Publications under preparation or under review

Pallares, E, J Lopez, M Espino, A Sanchez-Arcilla (expected 2016), "Comparison between nested grids and unstructured grids for a high-resolution wave forecasting system in the Western Mediterranean Sea." *Journal of Operational Oceanography.* Under Review.

Pallares, E, G van Vledder, M Espino, A Sanchez-Arcilla (under preparation), "Design and validation of unstructured grids in SWAN for the Western Mediterranean Sea." *Journal of Operational Oceanography.* Under preparation.

Conference contributions

Pallares, E, M Grifolll, M Alomar, R Tolosana-Delgado, C Mosso, M Espino, A Sanchez-Arcilla (2011), " Campos de oleaje y corrientes frente a la costa de Barcelona." *XI Jornadas Españolas de Costas y Puertos.* Las Palmas de Gran Canaria, Spain. Oral presentation.

Pallares, E, M Grifoll, M Alomar, R Tolosana-Delgado, M Espino, A Sanchez-Arcilla (2011), "Wave and current fields at the Barceona coast." *6th EuroGOOS Conference: Sustainable operational oceanography.* Sopot, Poland. Oral presentation.

Pallares, E, M Espino, A Sanchez-Arcilla (2012), "Efectos de los wind jets en la generación y propagación del oleaje cerca de la costa." *II Encuentro Oceanografía Física Española.* Madrid, Spain. Poster.

Pallares, E, M Espino, A Sanchez-Arcilla (2013), "The relevance of the whitecapping term in wave forecasting: an analysis for the wave period of the Catalan coast." *EGU2013 - European Geoscience Union General Assembly 2013.* Viena, Austria. Oral presentation.

Pallares, E, A Sanchez-Arcilla, M Espino (2014), "Improving the wave forecast in the Catalan Coast." *EGU2014 - European Geoscience Union General Assembly 2014.* Vienna, Austria. Poster.

Pallares, E, G van Vledder, A Sanchez-Arcilla, M Espino (2014), "Design and validation of unstructured grids in SWAN for the Western Mediterranean Sea." *The WISE 2014 meeting – Waves in Shallow Water Environment.* Reading, United Kingdom. Poster.

Pallares, E, L Rafols, M Espino, M Grifoll, J Lopez, M Bravo, A Sairouni, V Gracia, M Garcia (2014), "High resolution ocean modelling forecast for a coastal early warning system in the Catalan Coast." *7th EuroGOOS Conference: Operational Oceanography for Sustainable Blue Growth.* Lisbon, Portugal. Poster.

Pallares, E, A Sanchez-Arcilla, M Grifoll, M Espino (2015) "Coastal zone requirements for satellite products supported by coupled meteo-oceanographic numerical models." *Sentinel -3 for Science workshop. European Space Agency (ESA).* Venice, Italy. Poster.

Pallares, E, H Hernandez, J Moré, M Espino, A Sairouni (2015), "Wave ensemble forecast in the Western Mediterranean Sea, application to an early warning system." *EGU2015 - European Geoscience Union General Assembly 2015.* Vienna, Austria. Poster.

Pallares, E, J Lopez, M Espino, A Sanchez-Arcilla (2016), "The benefits of unstructured grids for wave modelling in semi-enclosed domains." *EGU2016 – European Geoscience Union General Assembly 2016.* Vienna, Austria. Oral presentation.

Pallares, E., Sanchez-Arcilla, A. Lopez, J., Espino, M. (2016), "The benefits of unstructured grids for wave modelling in semi-enclosed domains. Application to the Western Mediterranean Sea." *III Encuentro de la Oceanografía Física Española.* Alicante, Spain. Oral presentation.

Contents

List of Figures

List of Tables

There are some things you can only learn in a storm.

Joel Osteen (1963 -)

Blue, green, grey, white or black;
smooth, ruffled, or montainous;
that ocean is not silent.

H. P. Lovecraft (1890 - 1937)

Chapter 1

Introduction

1.1 Motivation

The need for information and the easy access to it is one of the characteristics that defines the actual society. Due to modern technology, people can now have immediate access to almost any kind of data just using their smartphone or laptop. The ocean state, including the wave forecast, does not escape from the technical development.

Users require information in different areas and with different purposes. In this sense, wave forecasting data can be divided into two general groups, on one hand the information provided by global models, covering almost the entire globe with a coarse resolution, and on the other hand the local models, which provides information in delimited areas usually near the coast with better resolution.

The first kind of models provides useful information for route mapping, navigation, and also for large-scale fishing, while the second type are allied to other activities that involve a lot of people and money, since the majority of human activities on the ocean occur in the first kilometres near the shore. Some examples of users requiring information in the coastal areas are related to leisure (e.g. tourism, uses of the coast, surfing or recreation sailing), to engineering and economic activities (e.g. design of coastal structures, beach restoring, offshore platforms design, renewal energy assessment or aquaculture), and also to hazard assessment by authorities, especially when a storm event reaches the coast. The accuracy of the wave forecasts, together with the wind and current information, is the key point to propitiate better support to management decisions for harbour, coastal and navigation authorities, and particularly interesting for hazard assessment and coastal vulnerability during energetic events.

It should be remarked that for the two wave forecast options different model configurations are used.

The first global wave operational models appeared in the 80s and the 90s, implemented by national weather services in Australia, Japan, Europe and North America. Forecast information for a horizon of up to 6 days was provided once a day. During the first years the errors were considerable. A comparison between five of the most noted wave forecasting systems between 1996 and 1999 is presented in Bidlot et al. (2002), obtaining root mean square errors for the significant wave height between the 17% and the 22% for the first day of simulation that increased up to 24% to 31% after 48 hours. The errors for the peak period moved between 23% and 37% depending on the model. In 2013 the errors of global models in open waters had decreased to 10% for the significant wave heights and to the 30% for the wave period (Ardhuin and Roland, 2013), and are continuously evolving up to the present. Some of the betterments implemented consist of progressing on the quality and resolution of the wind forcing (Janssen, 2008), improving the grid design in areas near the equator or the poles (e.g. Tolman, 2008; Chawla et al., 2013), assimilating wave height data from satellite or including the ice coverage and icebergs (Ardhuin et al., 2011) among others.

When moving to coastal areas the wave forecast becomes more complicated. The transition from global wave models to coastal scales applications in an operational real-time has been the focus of interest for many decades, and has promoted new research projects like the NOPP project (Tolman et al., 2013) or the European MyWave project (FP7-SPACE project nº.284455), involving a great number of wave modellers. Then it can be assured that the operational systems in coastal scales have progressed considerably the last years. However, an equilibrium between the scientific advances in new physics parametrizations or the evolution of the numerical schemes and the forecasting efficiency is not yet reached. These deficiencies are more evident when applying the models to complex environments, where the accuracy of the models is diminished (Tolman et al., 2013).

The Catalan coast and the Western Mediterranean Sea are clear examples that there is still work to be done in wave modelling and forecasting in complex environments.

Previous studies describe the wave climate in the area controlled by short fetches, complex bathymetry with deep canyons close to the coast, high wind field variability in time and space, wave calms combined with energetic storms, the presence of wind jets canalized by the river valleys and the consequent sea and swell waves combination that generate bimodal spectra (Bolaños, 2004; Sanchez-Arcilla et al., 2008; Alomar, 2012). These characteristics, some of them typical for a semi-enclosed

basin, limit the reliability of wave predictions in the area (Sanchez-Arcilla et al., 2014).

More specifically, an underestimation of the significant wave height and wave period has been observed in this area by different authors. Bolaños (2004) considered that part of the error was due to the limited spatial and time scales of the processes to reproduce, around 10 km and 12 hours, and recommended using an atmospheric model nested with enough resolution to reproduce the different phenomena. Alomar (2012), continuing with this work, presented two ways to improve the wave predictions. One option consisted in increasing the temporal and spatial resolution of the wave modelling system to capture the wind and wave gradients in the geographic dimension. She proved that using a wind input with better temporal resolution improve the maximum values for a storm event, while a higher wind spatial resolution only improved the timing of the peaks but not the magnitude. The second modification proposed was adjusting the wave growth rate. The author confirmed that the observed rate of wave growth in the region of study was faster than the simulations and faster than the rates derived for more homogeneous wind conditions. However, she was not able to tune enough the wave model in order to amend the sub-prediction problem associated to the wave period (only improved by 4%).

The first results obtained by the author in the framework of this thesis (not shown), by comparing the wave model simulations during a storm event (using the configuration detailed in chapter 2) with buoy measurements in a location 50 km offshore, presented root mean square errors for the wave height around 10%, with a clear under-prediction of the storm peaks up to 1 m, despite the timing of the storm peak was well reproduced. The errors for the peak period moved around 30%, with a clear under-prediction bias of 2 s with respect to the buoy measurements that made up 40% of the total error. When analysing the validation results in locations nearer the coast the errors became slightly worse. These errors were of the same order of magnitude as those obtained by previous authors in the study area.

The requirements of information for the Catalan coast, motivated by social and economic interests, together with the lack of ability of the models to provide wave forecast with the accuracy expected, have been the main motivation of the present work. Previous and important works have been already carried out in the area, considered as a starting point, enabling to produce the actual wave predictions. However, a step forward should be done in order to adapt the new products to the user's necessities.

1.2 Objectives

As previously mentioned, the wave simulations in the Catalan coast present important inaccuracies, mainly for the significant wave height during storm events, but also during all the year for the wave period. The forecasting systems available in the area only provide general information about wave conditions in coastal areas, with poor spatial and temporal resolution and with a lack of accuracy during energetic events. The main objective of this thesis is then to **improve the actual wave forecasting abilities for the Catalan coast.**

In general, the main issues affecting the wave accuracy are reported to be, in decreasing order of importance: (1) the accuracy of the forcing fields, (2) the accuracy of the source term parametrizations, and (3) the effect of numerical schemes. Additionally, some other effects are specifically involved in coastal areas like (4) the interaction between the currents and the wave field or (5) the boundary conditions quality from the coarser domain in nested grids (Ardhuin and Roland, 2013). Consequently, for coastal areas the wave models gain in complexity in order to better reproduce the reality. This is driven by more physical processes affecting the wave evolution in shallow and intermediate waters together with the important variability of the wind fields and the orography on those areas.

Previous works on the Catalan coast have addressed the topic of wind accuracy with interesting conclusions and good improvements of the wave forecasts in coastal areas (Bolaños, 2004; Alomar, 2012). The accuracy of the source terms parametrizations has been treated in Alomar (2012), focusing on the wave growth in variable wind conditions and the capability of models to reproduce it, with also very stimulating conclusions. However, still some progress may be achieved in this line of work.

With regard to specific topics referring to local domains in coastal areas, like the effect of the boundary conditions or the wave modifications due to the ambient currents, it had not been deeply treated for the study area at the beginning of this study, in 2011. However, similar studies carried out in other areas present promising results.

The coupling between oceanic, atmospheric and wave models takes more relevance during energetic events (Jorda et al., 2007; Warner et al., 2010) due to the intense wind, currents and wave fields involved. The Western Mediterranean sea is an area mainly defined by calm periods most of the year. However, coastal areas are often characterized by highly variable and heterogeneous conditions, which make the numerical prediction of the meteo-oceanographic processes difficult. Some examples of this local energetic events in coastal areas, when the effect of the coupling may be

decisive, are the wind jets or the surface current intensifications, frequently observed along the Catalan coast.

Moreover, the usage of unstructured grids as an alternative to the nested regular grids has been considered by several authors in the last years (Siadatmousavi et al., 2015; van Vledder and Akpinar, 2015) in order to improve the wave modelling. The main advantages of the unstructured grids is that a refinement of the grid resolution near the coast is possible removing the internal boundaries and so the complications associated. Additionally, the unstructured grids better fit the shoreline and easily reproduce the bathymetric gradients.

Finally, a reflection should be performed about the viability of applying the proposed measures in an operational forecasting system. The computational cost and the expected improvements need to be analysed in order to find an equilibrium adapted to the user's demands.

In this sense, five specific objectives are defined:

- **Improve the wave forecasting in the Catalan coast by tuning the wave model parametrizations related to the wave growth.**
- **Evaluate the effect of the coupling between the wave model and the current and atmospheric models for different situations.**
- **Consider the use of unstructured grids as an alternative of the regular nested grids.**
- **Define the criteria necessary to generate an efficient unstructured grids, considering the grid resolution and the distribution of cells in the domains.**
- **Asses the viability of these improvements into an operational forecasting system.**

1.3 Outline

In order to achieve the specific objectives defined in previous lines, the work has been structured in four main blocks, so it is with this document.

After presenting the motivation and the main objectives of the study in Chapter 1, a general review of the background is presented in Chapter 2, where the study area, the wave models history and evolution, together with the SWAN third-generation wave model and the measurements and validation techniques used in the thesis are detailed. A more specific background would be presented in each of the following main chapters.

The four chapters comprising the core work performed in the framework of this thesis topic come next.

In Chapter 3 a review of the wave model implementation to the Catalan coast is presented, focusing on the wave growth problems detected in previous studies. Two modifications are proposed, one concerning the whitecapping dissipation and the other related to the comparison between wave model results and buoy measurements.

The different coupling alternatives are analysed in Chapter 4, including a one-way coupling with a current model and a two-way coupling with both an atmospheric model and a current model. Both alternatives are applied to calm periods and to energetic events.

In Chapter 5 the design of two unstructured grids covering the study domain is performed, in order to achieve an efficient equilibrium between grid resolution and computational time requirement. The quality of the results obtained from wave model simulations is assessed validating it with buoy measurements and satellite wave data.

In the last Chapter 6, an evaluation of the mentioned improvements in operational systems is performed through a comparison between the unstructured grids and the traditional nested systems for a one year hindcast.

The final discussion and conclusions are presented in Chapter 7, together with the future lines of work.

The common structure of chapters 3 to 6 is as follows:

- Introduction of the topic.
- Specific background review.
- Methodology used, including the forcing required, the measurements available for the selected period and the wave model configuration and grids used.

- Analysis of the results obtained.
- Discussion.
- Final conclusions.

The structure of these chapters is motivated by part of the work that has already been published (chapter 3 and part of chapter 4) or is intended to be published soon (chapters 5 (paper under preparation) and 6 (paper under review)), so the structure of the chapter follows somehow a paper structure. In the publication section a list of the papers and conferences related to this thesis is detailed.

Chapter 2

Background

2.1 Study area : The Catalan coast

The Catalan coast is located in the north-western Mediterranean Sea. It corresponds to the northern section of the Spanish coast, located between latitudes 40º45' N and 42º25' N and longitudes 0º45' E and 3º15' E, with an extent of around 600 km (figure 2.1). The Balear Sea is located between this coast and the Balearic Islands.

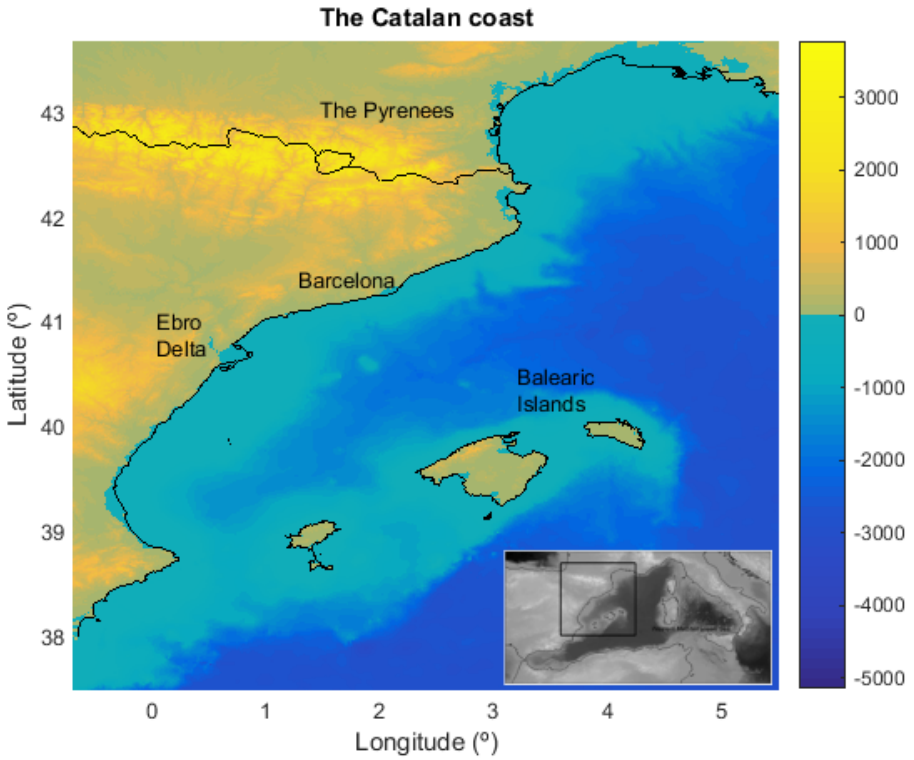

Figure 2.1: The Catalan coast orography and bathymetry.

In the subsequent lines a description of the meto-oceanic conditions is presented, followed by a description of the socio-economic activity in the area.

2.1.1 Meteorology and oceanic conditions

Winds:

The meteorological situation in the area is mainly controlled by orographic patterns, air-sea temperature differences and the passage of low-pressure centres from the Atlantic. The Pyrenees mountain range, situated at the north of the Catalan coast, acts as a physical barrier that strongly modifies the wind patterns and produces the Mistral (north-west) and Tramontana (north) winds, whose influence can be noticed hundreds of kilometeres offshore (Bolaños et al., 2009).

When the wind blows from the north, the mountain ranges induce wind channelling through river valleys, with the most important being the Ebro Delta wind jet. These characteristic land-to-sea winds are highly variable both in space and time (Sanchez-Arcilla et al., 2008) and are particularly intense and persistent during autumn and winter (Alomar et al., 2014).

The prevalent winds come from the north and north-west, primarily during December and January; southerly and easterly winds are also important, particularly during the months of February, March, April and November (Arnau, 2000). On average, the winds are not very intense. The maximum velocities correspond to easterly winds, in agreement with storm conditions; in addition, the most energetic storms registered in the area are associated with this directional sector and affect the full length of the Catalan coast (Mendoza et al., 2011).

Waves:

Wave climate is one of the characteristic properties on coastal areas due to the important energy associated with it, its impact on coastal structures and the associated sediment transport. Measurements along the Catalan coast for more than 25 years have allowed several authors to study the characteristics of the area (Garcia et al., 1993; Bolaños and Sanchez-Arcilla, 2006).

From these studies it can be stated that the predominant wave directions, as with the wind, vary along the coast, showing clearly the topographic control due to complex bathymetry, with submarine canyons and a heterogeneous continental shelf width (Sanchez-Arcilla et al., 2008; Bolaños et al., 2009).

Sanchez-Arcilla et al. (2008) describe how the southern and northern sections of the coast show a predominance of north-west and north wave conditions, while the central part of the Catalan coast is dominated by east and south wave conditions. The largest waves come from the east, where the largest fetches and stronger winds coincide. In the areas where the wind blows from the north-west (offshore winds), like the Ebro Delta (see fig 2.1) there is a tendency to develop a large amount of bimodal spectra due to the co-existence of sea and swell waves (Bolaños et al., 2007).

The Western Mediterranean Sea is an area mainly defined by calm periods most of the year. However, when analysing the buoy records in the area, important storms are detected despite the fetch-limited conditions (Bolaños et al., 2009). Recent studies define the significant wave height threshold as 2.2 m and set a minimum duration of 6 h for the study area (Lin-Ye et al., 2016). Forecasting these fast and energetic storms near the coast, characteristic of the area, is a challenge for operational oceanography.

Currents:

The region is characterized by a micro-tidal condition. The bathymetry varies in the domain from a quite narrow shelf in the northern areas to a wider shelf in the southern part (fig 2.1), controlling the hydrodynamics of the Catalan coast.

The ocean dynamics are mainly dominated by the associated quasi-permanent slope current at the regional Northern Current (Jorda, 2005; Millot, 1999), which may be affected by mesoscale phenomena. These mesoscale events are usually current meanders and eddies (Font et al., 1995) and are the main dynamic agent of the coastal ecosystem (Font, 1990).

In general terms, the mean intensity of the superficial currents is not very strong, around 10 to 20 cm /s, but current intensifications have been observed by several authors (Palanques et al., 2002; Jorda et al., 2007; Grifoll et al., 2015) within the study area, associated with strong local events.

According to Mestres et al. (2016), a flow intensification can be defined as an intense water flow lasting more than 12 h and exceeding a threshold defined as the surface current monthly 95^{th} percentile. With these criteria Mestres et al. (2016) detected up to 14 events on the Catalan coast during a three-year period (from June 2008 to July 2011) mainly during spring (6) and summer (5), and less frequently in autumn (1) and winter (2). The mean superficial current for the entire study period in front of the Barcelona harbour was 0.20 m/s, while the events selected reached values around 0.75 m/s, with an extreme of 1.39 m/s during an event tat occurred in October 2010.

As concluded Mestres et al. (2016), the current intensifications in front of the Barcelona harbour area are mainly induced by locally strong and persistent winds blowing from north-east to south-east, typically associated with the presence of lows in the south-western Mediterranean and highs over central Europe.

2.1.2 Potential social and economic impacts

A significant part of the European Mediterranean coast is limited in its ability to deal with environmental, physical and hydro-meteorological hazards due to the inhabitation of the first few hundred metres inland. This inhabitation has progressed in most of the locations, on the assumption of a stable coastal fringe. This idea is probably reinforced by a gentle sea state during most of the year, resulting in a false perception of security by society. However, energetic storm events are not rare at all and, when combined together with high water levels, can cause significant damages (figure 2.2). In the last 20 years, extreme storm events have been responsible for at least 50 casualties on the north-western Mediterranean coast and for significant damages in coastal defences, harbours and infrastructure, amounting to over EUR 30 million (Gracia et al., 2014).

Figure 2.2: Train hit by waves in a railway located along the coast line (left) and damages in a promenade after a storm event (right) on the Catalan coast.

The Catalan coast is no exception. Located in the north-east corner of Spain, on the north-western Mediterranean Sea, Catalonia is a Spanish region that in 2014 received 16.8 million tourists, who spent around EUR 15,000 million. The harbour facilities together with the touristic attractions of Barcelona city, the nice weather and its strategic location on the Western Mediterranean Sea and in Europe have been the main reasons for several cruise companies picking Barcelona as their main port of call. But tourism is not the only activity affecting the coastal areas in Catalonia. On the one hand, there are several economical activities affected by

the ocean conditions, such as maritime transport or fisheries. On the other hand, along the Catalan coast it is easy to find promenades, buildings, roads and even railways very close to the coast that are highly exposed to the meteo-oceanographic conditions.

2.2 Wave modelling

2.2.1 Evolution of wave models

The prediction of the wave height distribution, wave direction and wave periods has always been a point of interest for coastal engineers for different purposes. The first attempts to estimate the sea state date back to the Second World War, when information was required for landing. After that some experiments were carried out in order to better understand the physics behind the wind wave generation and propagation (e.g. the Joint North Sea Project, JONSWAP; Hasselmann et al., 1973).

With the emergence of the first high-computing-capacity computers and the consequent appearance of supercomputing centres, in parallel with improvements upon theknowledge of physical parametrizations, wind wave forecasting was driven on.

Estimations of the sea state can be performed using different types of models that - using information about meteorological conditions, especially the wind intensity and direction on the sea surface - provide information about the sea state. The obtained results are then propagated to coastal areas.

The propagation and dissipation of wind waves can be reproduced with two classes of numerical models:

- *Phase-resolving models*

  These models, also named deterministic models, describe the form of the sea surface itself. Among their advantages is that the models account for processes like diffraction, reflection and nonlinear interactions in shallow waters. However, they cannot describe the momentum transfer from the atmosphere to the sea, so generation is not reproduced. This class of models is valid for small domains, usually located near-shore, for example inside a harbour.

- *Phase-averaged models*

  In contrast with phase-resolving models, phase-averaged models (also named spectral models) do not describe the surface evolution but rather the evolution of the wave energy in each cell forming the domain. The parameters provided consist of statistical values representative of the sea surface in space and time. This class of models accounts for the most important processes governing the evolution of wind waves and can be used in larger areas.

In the first-generation of spectral wave models the growth and dissipation of the waves was predicted from empirical expressions, and the absence of the nonlinear interactions was compensated for by the better reproduction of the wave growth (e.g. Ewing, 1971). Following upon this, the second-generation wave models introduced some parametrizations of the nonlinear interactions (Young, 1988) or limited the spectral density as a function of the wind conditions (Holthuijsen and DeBoer, 1988) in order to improve the estimations.

In the middle of the 1980s a group of wave modellers who called themselves the Wave Modelling Group (WAM) considered that a wave model that solves the energy balance equation for surface wind waves including nonlinear wave interactions was feasible (SWAMPgroup, 1985). Although the previous models performed reasonably well in some situations, they realized that under rapidly varying wind conditions the results of the different models considerably diverged (Janssen et al., 1997). That was how the third-generation models appeared. The models were based on the Hasselmann spectral balance equation (equation 2.1, Hasselmann, 1960), where the source terms were explicitly parameterized and integrated in time without assuming the spectral shape. This was possible by improving the nonlinear interactions with the development of a computationally inexpensive parametrization of this term, known as the discrete interaction approximation (DIA; Hasselmann et al., 1985), and the related developments of the Wave Modelling Group (WAMDIgroup, 1988; Komen et al., 1994).

The resulting model was known as the WAM spectral wave model (WAMDI-group, 1988) and sparked the development of some other third-generation spectral wave models, the most renowned of which being SWAN (Booij et al., 1999; Ris et al., 1999) and WAVEWATCHIII (Tolman et al., 2002; Tolman, 2008).

In those first years, the third-generation spectra wave models were not adapted to coastal areas for two main reasons: some coastal processes were not implemented in the models, and the computational cost was too high to solve the balance equation at those scales. The SWAN model was the first model to introduce most of the missing processes and adapted the numerical scheme in order to be able to provide accurate sea state estimations in coastal areas. Nowadays almost all models include this option.

The latest developments in this sense include, among others, the coupling of wave models with current and atmospheric models (Warner et al., 2010; Bolaños et al., 2011), the assimilation of buoy and satellite information (Abdalla et al., 2006), the continuous development of the physical parametrizations (Ardhuin and Roland, 2013) and the improving of the numerical schemes to include two-way nesting and unstructured grids (Zijlema, 2010).

2.2.2 The SWAN wave model

The SWAN Cycle III v.4091A code has been used to simulate wave evolution in the area. SWAN (Simulating Waves Nearshore) is a third-generation wave model that computes random, short-crested wind generated waves in coastal regions and inland waters (Booij et al., 1999; Ris et al., 1999).

SWAN simulates wind wave generation and propagation in coastal waters and includes the processes of refraction; diffraction; shoaling; wave–wave interactions; and dissipation due to whitecapping, wave breaking and bottom friction. Based on the wave action balance equation with sources and sinks, the shallow-water wave model SWAN is an extension of the deep-water third-generation wave models. It incorporates the state-of-the-art formulas for the deep-water processes of wave generation, dissipation and the quadruplet wave-wave interactions from the WAM model (Komen et al., 1994), while in shallow water these processes have been supplemented with the state-of-the-art formulas for dissipation due to bottom friction, triad wave-wave interactions and depth-induced breaking; it also admits ambient currents as an input.

The SWAN model works with the action density, defined as $N(\sigma, \theta) = E(\omega, \theta)/\sigma$ (where E is the energy density and ω and σ are the absolute and the relative radian frequency, respectively), rather than the energy density, because during the propagation in the presence of ambient currents this magnitude is conserved whereas the energy density is not (Whitham, 1974). The action balance equation thus reads:

$$\frac{\partial N}{\partial t} + \frac{\partial c_x N}{\partial x} + \frac{\partial c_y N}{\partial y} + \frac{\partial c_\theta N}{\partial \theta} + \frac{\partial c_\sigma N}{\partial \sigma} = \frac{S_{tot}}{\sigma} \tag{2.1}$$

The first term of the equation represents the local rate of change of action density in time; the second and the third terms represent the propagation of action density in geographic space (with propagation velocities c_x and c_y thus accounting for shoaling process). The fourth term represents the depth-induced and current-induced refraction (with propagation velocity c_θ), and the fifth term represents the shifting of relative frequency due to variations in depth and currents.

The right term of equation 2.1 is the source term in terms of energy density. In shallow waters, six processes contribute to the sinks and sources term:

$$S_{tot} = S_{in} + S_{nl3} + S_{nl4} + S_{ds,w} + S_{ds,b} + S_{ds,bd} \tag{2.2}$$

Where the first term denotes the wave growth due to wind (S_{in}); the second and third terms correspond to the nonlinear transfer of wave energy through three-wave

(S_{nl3}) and four-wave (S_{nl4}) interactions, respectively, and the next three terms represent the action density dissipation due to whitecapping ($S_{ds,w}$), bottom friction ($S_{ds,b}$) and depth-induced breaking ($S_{ds,db}$). The parametrizations used for wave simulations in the study area are presented in section 2.2.3. For an extended description of these terms, calibrated for fully-developed wave conditions, it is recommended to consult the SWAN manual (SWANteam, 2015b) and the SWAN scientific and technical documentation (SWANteam, 2015a).

One of the main differences between SWAN and the other third-generation wave models is the numerical scheme. Traditionally, explicit finite-differences schemes are used to propagate the waves through geographic space. These schemes are simple, robust and economical for applications in oceanic waters. However, in coastal areas such schemes are not quite as adequate because the time step necessary would be very small (Holthuijsen, 2007). This is caused by the Courant criterion limitation of the explicit schemes, which states that the wave energy may not travel more than one geographic cell in one time step.

The SWAN model is therefore based on an implicit finite-differences numerical scheme, and such schemes are always numerically stable. Thus, the criterion for choosing the time step is mainly based on the phenomena scales that are being computed. The implicit schemes may lead to non-physical solutions of equation 2.1 under some circumstances, when the c_θ or the c_σ are too big in comparison to the x and y dimensions so the action density travels more than one geographic cell, accumulating at one point. More details on this issue will be presented in section 5.3.3; however, it can be said in advance that the proposed solution consists in introducing a limiter of the spectral velocities (Dietrich et al., 2013; SWANteam, 2015a).

2.2.3 The model setup for the Catalan coast

In this thesis the SWAN model Cycle III version 40.91A has been implemented in the Catalan coast as a third-generation model for non-stationary conditions.

Spherical coordinates and nautical convention have been selected.

The wind growth is obtained as the sum of a linear term, following Cavaleri and Malanotte-Rizzoli (1981), and an exponential term that is the same one used by WAM Cycle 3, following Snyder et al. (1981) and rescaled by Komen et al. (1984). The alternative exponential formulation (Janssen, 1991a) implemented in the WAM Cycle 4 model (Komen et al., 1984) was initially tested but dismissed because it presented worse results for the study area, with over-predictions of the significant wave height up to 1 m during storm events.

The quadruplet nonlinear wave-wave interactions are computed using the DIA proposed by Hasselmann et al. (1985), while the triad-wave interactions are not activated.

The whitecapping term used is the Komen et al. (1984) formulation. However, a correction is proposed, as detailed in chapter 3 and used thereafter, to adapt the action energy balance to the wave growth rates observed in the study area.

The depth-induced wave breaking in shallow water is treated by Battjes and Janssen (1978) spectral formulation with $\alpha = 1$ and $\gamma = 0.73$. Bottom friction is not activated.

The geographic space and time discretization used is known as the first-order backward space, backward time (BSBT) scheme. The advantage of this method is that it is fully monotone, so it cannot generate spurious oscillations. On the other hand the main disadvantage is that the scheme is numerically diffusive. The numerical diffusion is caused by gradients of wave action across geographic space, due to refraction processes for example, which may be considered small in coastal areas.

The numerical scheme for geographic propagation has a maximum number of iterations per time step up to 15. A time step of 15 min has been chosen, which is small enough to reproduce the wind and wave variability but keeps the computational cost affordable (Alomar, 2012).

The frequency range considered is 0.01-1 Hz, with 49 values logarithmically spaced with a frequency resolution of $df/f = 0.1$ as recommended by the SWAN manual (SWANteam, 2015a), and the directional resolution is 10^{o}.

Finally, the SWAN model has been run in a shared memory parallel environment. Using the OpenMP protocol, the tasks are divided in different processors using a unique memory.

2.3 Validation techniques

The SWAN wave model implementations for the Catalan coast presented in this document are validated against buoy measurements and satellite data using different techniques. In this section the measurement instruments used and the validation tools applied are presented.

2.3.1 Measurements

The measurement techniques of surface waves over the ocean can be divided into two main group; the in situ measurements (instruments deployed in the water, near the sea surface) and remote-sensing techniques (instruments measuring from a certain distance above the sea surface). The first group includes not only the buoys located on the sea surface but also some other instruments like the AWACs deployed at the sea bottom, while the second group is mainly formed by radar measurements, which can be mounted not only on a structure near the shore or on a ship but also on a satellite.

Each kind of measurement presents different characteristics, including different spatial and temporal coverage, resolutions and accuracy, as well as different maintenance and costs.

In situ measurements

The in situ measurements are located near the sea surface water, floating at the surface (e.g. a buoy) or some meteres below (e.g. an AWAC mounted on a structure on the seabed), and are used to obtain time series of the sea surface evolution at a fixed location.

The buoys are able to measure the vertical acceleration of the sea surface while floating on the ocean by using an accelerometer included in the instrument. The buoys also move horizontally, but this movement is generally considered negligible. By integrating the vertical acceleration twice, it is possible to obtain the sea surface vertical movements.

The size and weight of the buoy, together with these small horizontal movements, affect the measurements, creating time series with more smooth crests and troughs and underestimating short waves (Holthuijsen, 2007). Some of these effects are widely known and can be corrected with the instrument software, so the buoys can be considered to perform well in general.

The buoys are usually provided with radio communication to send their signals to a land or a platform receiving station. Most recently, satellite communication and positioning protocols are also included.

In order to obtain directional information from a buoy measurement, some additional parameters need to be recorded, so in this sense two different types of directional buoys have been developed. The first one is based in a flat buoy that measures the slope of the sea surface by incorporating some extra inclinometer sensors. Then the tilt of the buoy in two orthogonal directions is measured (including a positioning sensor to determine the angle with respect to the geographic north). With these parameters the mean wave direction can be obtained in addition to the evolution of the sea surface at the mooring location. Directional buoys of the second type measure the horizontal movements in two orthogonal directions with some extra accelerometers and, using a similar procedure to the one previously explained, obtain the mean wave direction of the waves.

Other instruments deployed in the study area are the AWACs. The AWAC is an instrument composed of three current meters and an acoustic surface tracker located under the surface at the sea bottom.

The current meters measure the wave-induced orbital motion (with magnitude and direction) and the pressure. Then, the directional wave characteristics can be easily obtained from these measurements. Some of the limitations of this method are that it can only be deployed in shallow waters (maximum 10-15 m) and that measurements of waves with periods shorter than 4 s are not possible due to the attenuation of the signal. In order to overcome these limitations, new techniques appeared at the end of the twentieth century that consist in obtaining these measurements closer to the sea surface. In doing so, the pressure is no longer obtained from the current meters but from the acoustic surface tracker. The AWAC instruments can be deployed at the sea bottom or in a subsurface buoy positioned closer to the surface (e.g. 30 m below the surface).

In conclusion, the in situ instruments provide detailed information about the evolution of the sea surface in time at a fixed location. The accuracy of these instruments is around 0.5% of the measured value (Datawell, 2006). However, no spatial distribution is offered, so a large number of instruments should be deployed throughout the study area in order to monitor the sea state.

Remote-sensing measurements

The remote-sensing instruments are located over the sea surface, from a few meteres above when located on an observation tower to hundreds of kilometeres above when

the instrument is located on a satellite. The principle of these instruments is to receive signal reflections off the sea surface and transform them into sea surface elevation. The most important difference from previous instruments mentioned is that large areas can be covered almost instantaneously; however, it is also a more expensive technique.

The altimetry satellites determine the distance from the satellite to the sea surface by measuring the time required by a radar pulse to travel from the satellite to the surface and back to the satellite. The surface height is the difference between the satellite's position in orbit with respect to a reference ellipsoid, so extremely precise knowledge of the satellite's position is needed in order to obtain accurate results.

The altimeter emits a spherical microwave radiation with one or two known frequencies (the Ku-band with 13.575 GHz and the S-band with 3.2 GHz). These pulse are emitted at regular intervals defined by the pulse repetition frequency; in order to reduce the statistical fluctuations and to perform a time tracking, these pulses are averaged over time. The return echo power, affected by the sea surface shape, is recorded in a tracking window (with 64 or 128 waveform samples) which, when represented as a function of time, provides the echo waveform (ESA and CNES, 2016).

The waveform has a characteristic shape that can be described analytically with the Brown model (Brown, 1997). When comparing a measured waveform with the theoretical curve, six parameters can be obtained. By looking at the return signal characteristics (amplitude and waveform parameters), the sea surface roughness (and so the significant wave height) and the wind speed over the oceans can be obtained. No information about the wave period or wave direction is provided by the remote-sensing altimetry measurements.

When a satellite is launched and the instruments are properly working, the common procedure consists in comparing the measurements with analysed modelled fields and buoy measurements on a global scale to check the main errors and, if necessary, to retune the geophysical algorithms (Janssen et al., 2007; Queffeulou et al., 2011). The comparison with buoy data (Queffeulou, 2004) shows that the altimeter significant wave height is in general agreement with the in situ data, with differences of the order of 0.30 m, and tends to slightly overestimate the low significant wave heights and underestimate the higher significant wave heights. In order to solve this, global corrections to the wave measurements were established. These corrections, in general linear, correspond to a few percent of the measurements (Queffeulou and Croize-Fillon, 2016). For more details on the wave height corrections, the reader is recommended to consult Queffeulou (2004) and Queffeulou and Croize-Fillon (2016).

After the corrections, the reported error for altimetry radar measurements is of the order of a few centimetres (e.g. Dinardo et al., 2014), which is usually higher than buoy measurement accuracy. However, the spatial coverage of these measurements provides an interesting opportunity to evaluate the model performance in areas where in situ measurements are not available.

2.3.2 Validation tools

Traditional wave measurements, obtained from a buoy, consisted of time-record series of the sea surface elevation at a fixed location. In contrast, satellite measurements present the sea surface variations over time along a track. The combination of both measurements allows an even better image of the reality to be created.

The validation tools used to evaluate the wave model results with time series at a fixed location or in satellite trackdata are presented below. It should be remarked that no spectrum validation has been possible due to the absence of spectra measurements in the study area.

Time series analyses and statistics

The validation of results from the different simulations has mainly been based on time series plots, scatter diagrams and Taylor diagrams (Taylor, 2001).

A Taylor diagram is a graphical representation of the correlation coefficient (R), the root mean square difference ($RMSD$) between two fields, and the standard deviation of each field summarized at one point located in a 2D graphic (see figure 2.3). These diagrams are very useful to present a statistical evaluation of different models performance in comparison to a measurement time series. The nearer a point is located to the reference field, the better the correspondence.

The only drawback of Taylor diagrams is that the biases are eliminated when computing the $RMSD$, and thus the results may not be representative in some situations.

For these reasons, some statistical parameters have also been computed and employed for quantitative comparisons; the main ones are the root mean square error ($RMSE$), the bias, the scatter index (SI) and the correlation coefficient (R). These parameters are obtained as follows:

$$RMSE = \sqrt{\frac{\sum_{i=1}^{N}(S_i - O_i)^2}{N}} \tag{2.3}$$

$$bias = \frac{\sum_{i=1}^{N}(S_i - O_i)}{N} \tag{2.4}$$

$$SI = \frac{RMSE}{\bar{O}} \tag{2.5}$$

$$R = \frac{\sum_{i=1}^{N}\left((S_i - \bar{S}) \cdot (O_i - \bar{O})\right)}{\sqrt{\sum_{i=1}^{N}(S_i + \bar{S})^2} \cdot \sqrt{\sum_{i=1}^{N}(O_i + \bar{O}} \tag{2.6}$$

Where S corresponds to the simulated data and O to the measured data (observations); N is the number of data points; and$\bar{O}$ and $\bar{S}$ correspond to the mean value of the time series for observed and measured values, respectively. All these formulas except the bias have been adapted to analyse the wave direction, considering the minimum angle between the two data (simulated and measured).

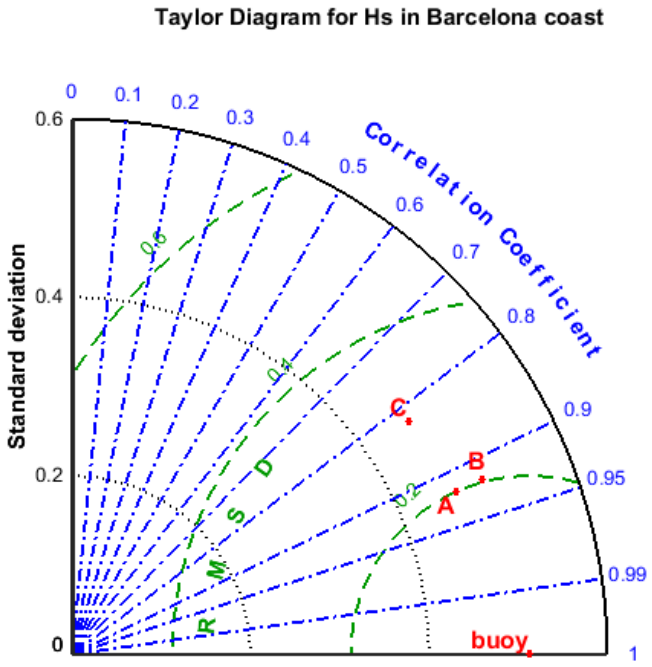

Figure 2.3: Example of a Taylor diagram in which the significant wave height obtained from three models (A, B and C) is compared with a buoy record.

The data measured by the instruments and those obtained from the SWAN simulations both correspond to 1 h time resolution for the different study periods selected in each exercise. The number of validation points varies between 1,000 and 8,000 values in most of the situations.

The parameters considered for validation are summarized in table 2.1. Results from the wave model correspond to the same location as the measurement instruments after an interpolation performed by the SWAN model: a spatial interpolation in the discrete components of the spectra; hereafter the integral parameters are computed.

Table 2.1: Definition of the bulk parameters used to compare the SWAN simulations with the instrument measurements.

Moment	m_n	$m_n = \int_{fmin}^{fmax} \int_0^{2\pi} f^n \cdot E(f,\theta) d\theta df$
Significant wave height	H_{m0}	$H_{m0} = 4\sqrt{m_0}$
Mean wave direction	Dir	$Dir = arctg\left[\frac{\int sin\theta \cdot E(f,\theta) df d\theta}{\int cos\theta \cdot E(f,\theta) df d\theta}\right]$
Mean wave period	Tm_{01}	$Tm_{01} = 2\pi\frac{m_0}{m_1}$
Mean zero up-crossing period	Tm_{02}	$Tm_{02} = 2\pi\sqrt{\frac{m_0}{m_2}}$
Peak wave period	Tp	Period corresponding to the maximum energy

Satellite collocation and model validation

The collocation process is a method to compare the satellite measurements (along tracks) with data at a fixed point (from buoy measurements or model simulation results). Once the significant wave height from the satellite is corrected, the methodology consists in selecting the satellite measurements that are included in a time interval and in a spatial region around the comparison point.

First a collocation in time is necessary, selecting a time interval of 30 min before and after the model or measurement time. Thereafter, a space collocation is performed in order to determine whether there is any measurement near the comparison point (e.g. figure 2.4). The traditional collocation radius is 50 km. If several measurements satisfy the collocation conditions, the nearest point or the mean value is usually selected. The situation can be described as a superobservation when there are more than six points available (Sepulveda et al., 2014); under these conditions the satellite data considerably improve the accuracy.

From this collocation procedure a time series of a pair of points is obtained, including the collocated satellite significant wave height measurement and corresponding fixed-point data. The series obtained are not equally distributed throughout time. From these pairs of collocated points, scatter plots can be generated together with the statistics described before (equations 2.3 to 2.6).

A previous analysis performed with several altimetry data compared with buoy measurements by Sepulveda et al. (2015) confirms that the better agreements correspond to open-ocean buoys, while in coastal areas the scatter is much larger. Additionally, for significant wave heights under 0.7 m the errors become more important. For these reasons it is common to eliminate the satellite measurements near the shore. In the present study a 30 km distance to the coast has been selected as the invalid region.

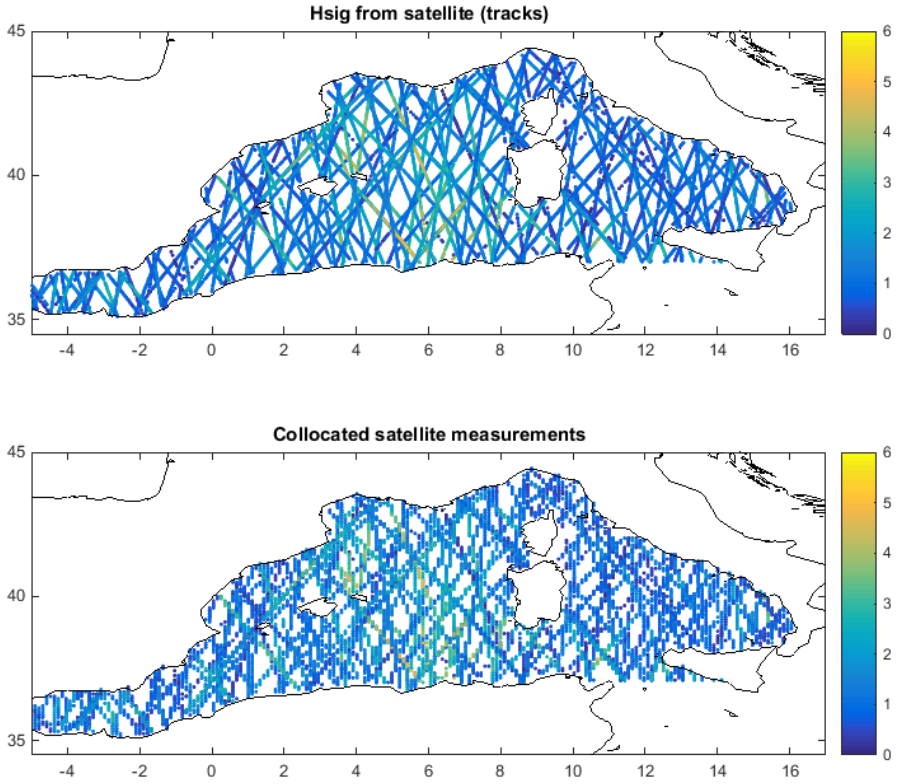

Figure 2.4: Satellite tracks for one month (April 2013) over the Western Mediterranean sea (top) and the space collocated points over a regular grid for the same period (bottom).

Chapter 3

Wave energy balance for semi-enclosed domains

3.1 Introduction

It is widely known that wind and wave predictions are less precise in semi enclosed domains than in the open ocean. Ardhuin et al. (2007) pointed that in the Western Mediterranean Sea, the winds are still the major source of errors for the wave model results. These errors, however, tend to decrease in stormy conditions or, more generally, when the meteorological situation is better defined. However, in coastal areas and enclosed basins, improving the wind quality it is not enough to improve the wave results because of the wave characteristics due to their nearly permanent local generation. Cavaleri and Bertotti (2004) considered the underestimation of wind speed and wave height dependency on fetch, and proved than fetches smaller than 100 km generate larger errors. These errors are more important and persistent in waves than in wind. The boundary layer when the air blows from land to sea and the poor description of the orography are suggested as possible reasons for the underestimation at short fetches.

Previous studies in the Catalan coast describe the wave climate controlled by (1) short fetches, (2) shadow effect for waves from the south and east due to the Balearic islands (figure 3.1), (3) complex bathymetry with deep canyons close to the coast, (4) high wind field variability in time and space, (5) wave calms during the summer and energetic storms from October to May, (6) presence of wind jets canalized by the river valleys and, (7) sea and swell waves combination that generate bimodal spectra (Bolaños, 2004; Sanchez-Arcilla et al., 2008; Alomar, 2012). These characteristics, some of them typical for a semi-enclosed basin, limit the reliability of wave predictions in the area.

More specifically, an underestimation of the significant wave height and wave period has been observed in this area by different authors. Bolaños (2004) considered that part of the error was due to the limited spatial and time scales of the processes to reproduce, around 10 km and 12 hours. The author confirmed that using an atmospheric model nested with enough resolution to reproduce the different phenomena. Alomar (2012) presented two ways to improve the wave predictions. One option consisted in increasing the temporal and spatial resolution of the wave modelling system to capture the wind and wave gradients in the geographic dimension. She proved that using a wind input with better temporal resolution leads to improve the maximum values for a storm event, while a higher wind spatial resolution only improved the timing of the peaks but not the magnitude. The second modification proposed was adjusting the wave growth rate. The author confirms that the observed rate of wave growth in the region of study was faster than the simulations and faster than the rates derived for more homogeneous wind conditions.

Nevertheless, this is not a local effect since in similar locations the same problems have been observed, all of theme using the SWAN third-generation wave model with the exponential wind growth due to Snyder et al. (1981) and rescaled by Komen et al. (1984), and the whitcapping dissipation formulation by Komen et al. (1984).Akpinar et al. (2012) describe an equivalent behaviour, with an under-prediction of the significant wave height and period for the Black Sea. Their results show a clear similarity to the results obtained for the Catalan coast, with an under-prediction of the significant wave height, more important for the maximum values (peaks of the storms) and an important negative bias for the wave periods. Similar results have been obtained also in semi enclosed basins and bays, as Lin et al. (2002) who demonstrate that in Chesapeake Bay (USA) the waves are dominated by locally generated and fetch-limited young seas. The results obtained show significant wave-heights slightly over-predicted, but with an under-prediction of the peak period, with large scatter and a low correlation coefficient. Alari et al. (2008) identify a strong underestimation of the peak-periods for waves locally generated and fetch limited in a small bay called Küdema, in the Baltic Sea. An intensive study on the wave growth and decay characteristics in the SWAN model was performed by Rogers et al. (2003) after observing a similar under-prediction pattern to the one here described in three different locations in the USA. The authors identify the cause as an under-prediction of low and medium frequency energy in the modelled spectra together with an overly strong dissipation of the swell. The solution proposed was to modify the whitecapping term to depend on the wave steepness.

The goal of this study is, thus, to improve the wave forecasting and hindcasting in the Catalan coast, focusing particularly on the under-prediction of period

measurements. These predictions are of major interest for different agents and activities such as coastal management, harbour access, navigation or fisheries, in an area highly dependent on the sea.

To reach this goal two actions are considered. The first one consists in modifying the source terms in the energy balance equation to increase the wave energy for early generated waves. As noted Alomar et al. (2014), the wave growth rates are under-predicted for the wave conditions in the study area. To modify the balance equation two options are available: increase the energy from generation processes or reduce the dissipation. The measure proposed in this paper is based on the second option, and consists in modifying the formulations implemented as previously done by Rogers et al. (2003) to correct the whitecapping dissipation term and its dependence on the wave number and wave steepness for young sea waves. The second action consists in evaluating the methodology to obtain the integral wave parameters from the modelled spectra, considering the frequency integral range measured by the buoys in order to compare the simulations and observations under the same conditions.

3.2 Background: re-evaluation of the energy balance. The whitecapping term

3.2.1 The energy balance

The wave growth in the SWAN model is mainly controlled by the energy input from the wind and the dissipation processes, while the non-linear terms redistribute the energy to higher and lower frequencies. To prescribe the growth rate, three different wind input formulations are available in the model, with an associated dissipation term for each.

The wind input is written in terms of a resonance mechanism Philips (1957) and a feed-back mechanism (Miles, 1957). The first mechanism contributes to the initial stage of wave growth and varies linearly with time, while the second mechanism controls the energy transfer from the atmosphere to the waves, with an exponential behaviour (SWANteam, 2015a). The total wave growth due to wind is then described as the sum of both terms:

$$S_{in}(\sigma,\theta) = A + B \cdot E(\sigma,\theta) \tag{3.1}$$

Where A and B depend on the wave frequency and wind speed; the expression of the A term is that of Cavaleri and Malanotte-Rizzoli (1981) with a filter to avoid growth at frequencies lower than the Pierson-Moskowitz frequency (Tolman, 1992a), and it is commonly smaller than the exponential term. The B term is represented by two different formulations. The first one is the same one used in the WAM Cycle 3 model (WAMDIgroup, 1988), due to Snyder et al. (1981) and rescaled by Komen et al. (1984). The second formulation is from the WAM Cycle 4 model (Komen et al., 1984) and is due to Janssen (1991a). A third wind input formulation is available based on that of Yan (2007).

Three whitecapping formulations are implemented in SWAN, corresponding to each of the growth options. In fact, the total dissipation is obtained from the sum of the three terms mentioned in chapter 2: whitecapping, bottom friction and depth-induced breaking. However, as all the measurement instruments are located geometrically near the coast but in deep or intermediate waters, where the bottom friction and the depth-induced breaking are very small, in our balance we will only consider the wave growth and dissipation due to whitecapping.

For this purpose the first two whitecapping formulations are obtained from the pulse-based model of Hasselmann (1974) reformulated in terms of wave number (WAMDIgroup, 1988):

$$S_{ds,w}(\sigma,\theta) = -\Gamma\hat{\sigma}\frac{k}{\hat{k}}E(\sigma,\theta) \tag{3.2}$$

where $\hat{\sigma}$ and $\hat{k}$ denote the mean frequency and the mean wave number, and the coefficient Γ depends on the wave steepness (Janssen, 1991b):

$$\Gamma = C_{ds}\left((1-\delta)+\delta\frac{k}{\hat{k}}\right)\left(\frac{\hat{s}}{\hat{s}_{PM}}\right)^{p} \tag{3.3}$$

The coefficients C_{ds}, δ, and p can be adapted to the study case,$\hat{s}$ is the overall wave steepness, and $\hat{s}_{PM}$ is the value of $\hat{s}$ for the Pierson and Moskowitz (1964) spectrum.

In SWAN the previously mentioned coefficients are obtained by adjusting the energy balance for idealized wave growth conditions (fully developed wind seas in deep water). Then, depending on the growth formulation used, the coefficients may vary to reach the desired target. For the WAM Cycle 3 formulation $C_{ds} = 2.36\cdot10^{-5}$, $\delta = 0$, and $p = 4$ (Komen et al., 1984); and for the WAM Cycle 4 formulation $C_{ds} = 4.0\cdot10^{-5}$, $\delta = 0.5$, and $p = 4$ (Komen et al., 1994).

The third whitecapping formulation is obtained from a saturation-based model (van der Westhuysen et al., 2007), and it is based on experimental data. The formulation is designed for mixed sea-swell conditions and is not suitable for shallow water.

3.2.2 Application to the Catalan coast

Alomar et al. (2014) studied the wave growth for the Catalan coast, and detected that the growth rates derived from measurements may be larger than the simulated rates obtained with SWAN. Also, they affirm that under variable wind conditions, like the ones observed in the study area, these growth rates are higher than for homogeneous wind conditions. In conclusion, the authors pointed out that the source terms are a potential source of error within wave forecasting, especially in sharp-gradient regions, defined by the presence of submarine canyons near the coast, highly variable wind conditions and an abrupt line coast. Therefore, it becomes important to better understand wave growth and energy dissipation under variable wind geometric conditions, so as to improve the resulting wave simulations.

To deal with the wave under-prediction problem in the Catalan coast we therefore propose to adjust the different terms of the energy balance. As it is well known, the whitecapping term, or dissipation in deep waters, is the least understood part of

wave evolution equation. By combining some intuition with a pragmatic approach, it still is the tuning knob of any wave model (WISEgroup, 2007).

Important previous work has been carried out in this topic. Rogers et al. (2003) execute some simulations in three different locations (all of them with similar properties to as the ones described for the study area), using the SWAN model with the WAM cycle 3 growth formulations and the Hasselmann (1974) whitecapping expression. The author changed the delta coefficient from 0 to 1 without modifying the remaining parameters involved in equation 3.3 and obtained an improvement of the predictions at lower frequencies for short fetch/duration events. However, they clearly demonstrates that with this modification, the energy is over-predicted in fully developed seas. In their work it is shown that for mean fetch and duration smaller than 350 km and 12 h respectively, the model with the increased delta is much closer to the Pierson and Moskowitz (1964) energy level than are the models with lower delta values. Rogers et al. (2003) also pointed out that the model with delta equal to 1 exceeds the Pierson and Moskowitz energy level at larger fetch/durations.

Due to the similarities between the study areas considered by Rogers et al. (2003) and our selected area, with local generated sea and storm events associated with short duration and fetch, a similar experiment, with a modification of the delta parameter, has been carried out for the Catalan coast to adapt the numerical growth rates to the measurements in the area. With this modification we expect an increase of the energy for lower frequencies which will result in a smaller prediction error for the wave period.

However, there are other studies dealing with this same issue and proposing different solutions. Siadatmousavi et al. (2012) realized a similar correction for the Gulf of Mexico, obtaining a worsened fit for the SWAN results. Moreover, they showed that the effect of using different expressions for the parametric high frequency tail added to the spectrum and the reduction of the cut-off frequency from 1 Hz to 0.5 Hz may reduce the under-prediction of the SWAN model under longer fetch and more homogeneous wind conditions. Because of the difference in conditions this approach has not been further pursued in this thesis.

3.3 Methodology

3.3.1 Data available and model setup

In the framework of the European project FIELD AC (contract no. FP7-SPACE-2009-1-242284) two measurement campaigns have been carried out. The FIELD AC project is focused on the meteo-oceanographic forecasting for small regions such a beach, a harbour or the mouth of a river. To reach this goal, it is necessary to simulate with high resolution and in a coupled manner the meteorology, the circulation and wave fields, the land/river discharge and the resulting transport (e.g. for sediment) patterns.

Three of the instruments deployed off the Catalan coast were used to validate the wave model results: two AWAC directional systems located at the seabed and one directional wave buoy. The characteristics of these instruments, together with their location and the data provided can be found in table 3.1. The data was collected during two periods, the first one from the 12th of November 2010 to the 18th of January 2011, and the second campaign going from the 11th of March 2011 to the 18th of April 2011. The campaign was scheduled during these months because, as mentioned in chapter 2, from October to May the more energetic wind and wave events are expected in the area. However, the measurements show that during the first period only one storm from the north-west occurred, while during the second period several energetic episodes from the south and east were captured.

Table 3.1: List of the instruments location and information provided for the Catalan coast.

Institution	Name	Lon	Lat	Depth	Parameters provided
FIELD AC campaign	AWAC Bogatell	2.21º E	41.39º N	24 m	H_s, Dir, Tm_{02}, Tp, Tm_{01}
	AWAC Besos	2.24º E	41.41º N	24 m	H_s, Dir, Tm_{02}, Tp, Tm_{01}
	Buoy Besos	2.26º E	41.40º N	50 m	H_s, Dir, Tm_{02}, Tp, Tm_{01}
XIOM	Blanes	2.28º E	41.65º N	74 m	H_s, Dir, Tm_{02}, Tp, Tm_{01}
	Llobregat	2.14º E	41.28º N	45 m	H_s, Dir, Tm_{02}, Tp, Tm_{01}
	Tortosa	0.98º E	40.72º N	60 m	H_s, Dir, Tm_{02}, Tp, Tm_{01}
Puertos de estado	Barcelona	2.20º E	41.28º N	68 m	H_s, Dir, Tm_{02}, Tp
	Tarragona	1.47º E	40.68º N	688 m	H_s, Dir, Tm_{02}, Tp

Additionally, five more instruments have been considered in the study. The local network XIOM (Xarxa d'Instruments Oceanogràfics i Meteorològics, www.xiom.cat) with four buoys along the coast and time series for more than 25 years has been used to characterize the wave properties in the study area. For this purpose, three of these buoys have been used to validate the obtained results (table 3.1). Complementary to this local network, the general Spanish network of Puertos del Estado (www.puertos.es) presents three buoys in the study area. Two of them have also been used in this study; the first one is located offshore the Barcelona harbour entrance, while the second one is located in the southern part of the domain at about 50km from the coast (Tarragona buoy, in deep water offshore wards the Tarragona harbour entrance).

All the buoy locations used are represented in figure 3.1. Table 3.1 shows that, except for the Tarragona buoy, all the instruments are moored near the coast. However, due to the young wave age conditions prevailing in the area (consequence of the short fetch available and the highly variable wind conditions) all the instrument locations correspond to deep or intermediate water conditions.

The bathymetry used is obtained from GEBCO (General Bathymetric Chart of the Oceans, www.gebco.net) with a grid resolution of 30 arc-second (0.0083º).

The simulations have been structured in three nested domains covering the Western Mediterranean Sea (figure 3.1). The first one is a large domain all over the mentioned area with a grid resolution of 9 kilometres. This domain is used to generate boundary conditions for the smaller domains. The second domain is located in the Balearic Sea, with a mesh size of 3 kilometres and the next one is a domain following the Catalan coast and shelf domains, represented by a curvilinear grid with a mean cell size of 1 kilometre. The grid dimensions and resolutions are presented in table 3.2.

Table 3.2: Description of the grids implemented in SWAN for the Catalan coast.

	Western Mediterranean Sea	Balearic Sea	Catalan Coast
Longitudes	4.90º W - 16.05º E	0.45º W - 5.26º E	0.17º E-3.591 E
Latitudes	35.00º N - 44.52º N	39.00º N - 43.66º N	39.63º N - 41.83 ºN
Mesh size	196 x 119	160 x 174	208 x 106
Grid resolution	9km (0.107º x 0.081º)	3km (0.035ºx0.027º)	1km (mean value)

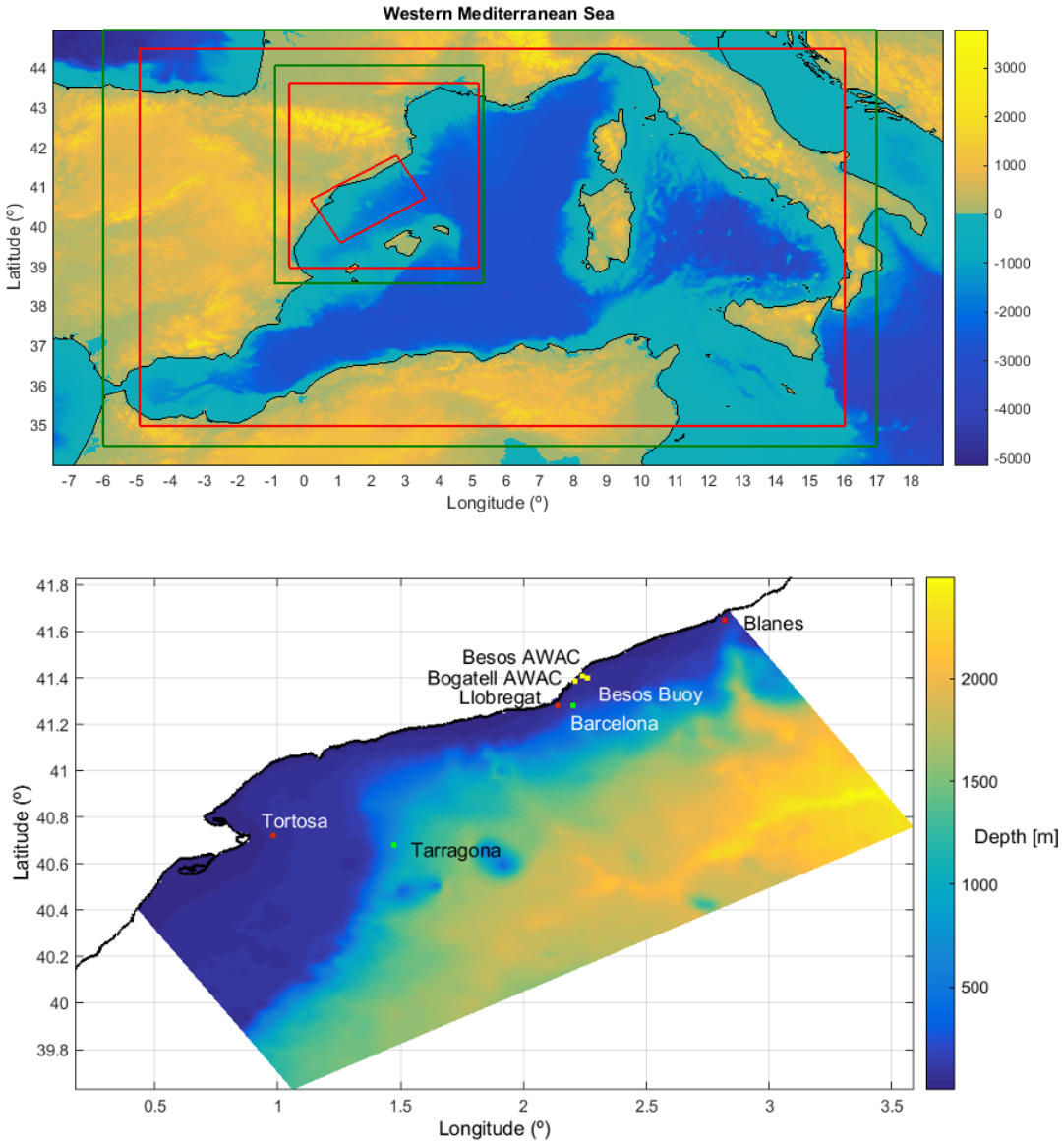

Figure 3.1: On top: The Western Mediterranean Sea. Represented the local distribution of the computational grids implemented in SWAN (in red) and the two atmospheric domains used as a forcing (in green). At the bottom: a detailed bathymetry for the finest grid (1km grid size in average) is presented. The dots represent the measurement locations.

The initial conditions for each domain have been obtained running the SWAN model in a stationary mode while the boundary conditions for the medium and small domains are generated by the enveloping larger domain. The largest grid covers almost the whole Western Mediterranean Sea which can be considered as a semi-enclosed basin. As the boundaries of this grid are far away from the area of interest, we do not expect that omitting the influx of energy along these boundaries will affect our model results near the Catalan coast.

Two periods are considered in the present study, corresponding to the measurement campaigns mentioned before. These periods have been selected because of the different processes represented in each one such as offshore wind conditions; long fetch storm events and calm periods, all of them typical processes for the study area. During these dates two high resolution campaigns were carried out within the European project FIELD AC and there are available high resolution wind fields and a variety of observations. The selected wind field domains are represented in figure 3.1, and have been provided by the Barcelona Supercomputing Centre (BSC, www.bsc.es) using the Weather Research and Forecasting (WRF) Model (Skamarock et al., 2005). The first wind domain covers the full Western Mediterranean Sea, with a spatial resolution of 12 km and a temporal resolution of 1 hour and it is used for the Western Mediterranean Sea grid. The two smaller wave grids are forced by the second wind field provided by BSC, with a spatial resolution of 4 km and a time resolution of 1 hour. As presented by Alomar et al. (2014) this resolution is considered enough to capture the wind space and time gradients in the studied coastal area. A more extensive validation of the wind patterns against remote-sensing measurements and a comparison to other wind options is presented by Bertotti et al. (2014), where the WRF model is considered to perform reasonably well, with a correlation coefficient for the study period around 0.83, a bias of 0.56 m/s and a RMSE = 1.98 m/s, quite high. The high-resolution wind field is also analysed with practically identical results, presenting some minor differences only very close to the coast.

3.3.2 Whitecapping dissipation for early wave growth

As mentioned before, an assessment and subsequent modification of the whitecapping formulation (equations 3.2 and 3.3) has been performed. The delta (δ) values considered are: 0, 0.5, 0.75, 1, always keeping the coefficient $C_{ds} = 2.36 \cdot 10^{-5}$ and $p = 4$. Rogers et al. (2003) demonstrate that an increase of the delta value causes a decrease in the lower frequency energy dissipation, and consequently, an increase of the peak period and mean period (Tm_{02}). However, this increase of the delta parameter without modifying C_{ds} leads to an overestimation of the total energy for fully developed sea conditions.

In the study area, the wave growth rates for the typical conditions are proven to be larger than the ones obtained from the SWAN model, as previously, so the delta modification may be a good correction to this problem, always keeping in mind that an over-prediction will occur for waves with longer fetch and/or duration. Since we do not observe fully developed sea conditions in the area the overestimation is acceptable.

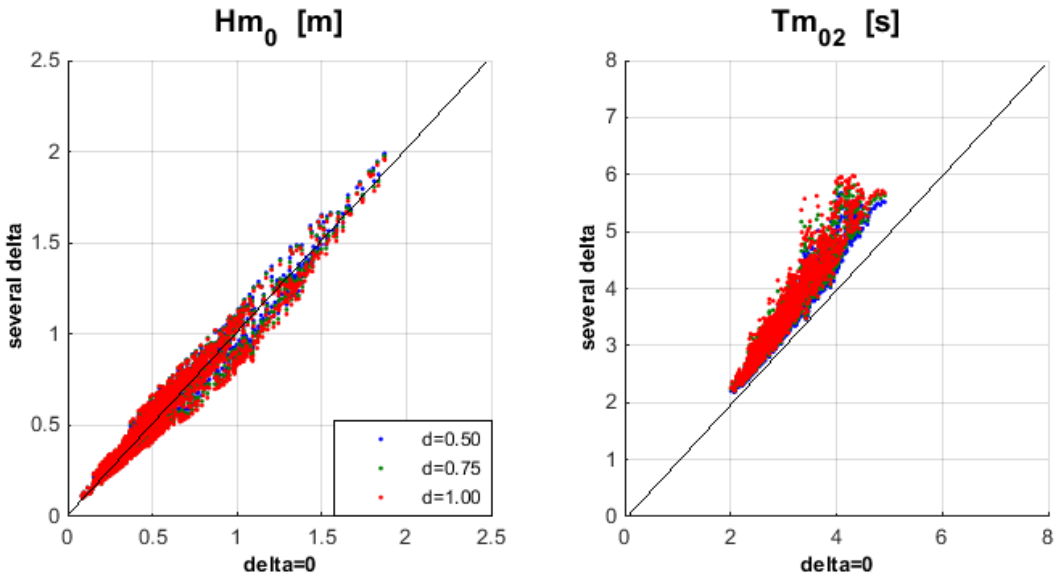

Figure 3.2: Scatter plots for the Hs and Tm_{02}, showing the effect of modifying the whitecapping term for three different delta values. Results from the finest grid, for the first study period in the Besos buoy location.

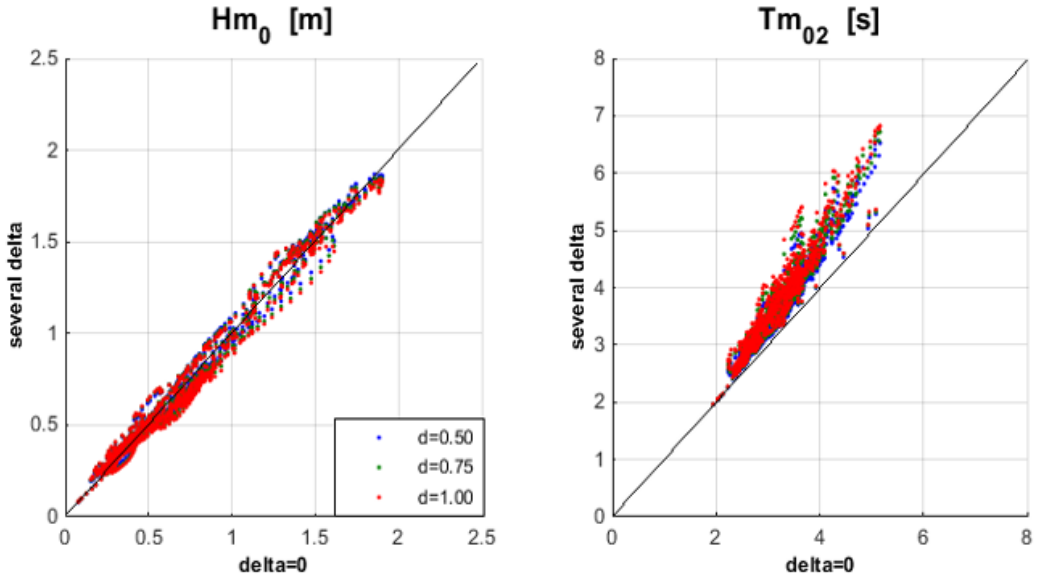

Figure 3.3: Scatter plots for the Hs and Tm_{02}, showing the effect of modifying the whitecapping term for three different delta values. Results from the finest grid, for the second study period in the Barcelona buoy location.

The results of a sensitivity analysis are shown in figures 3.2 and 3.3. The two temporal periods previously chosen have been included in the comparison, and the eight buoys have been used to validate the results, but only the results for two different locations, each one for one period and representative of the whole set, are

presented. The graphics, supported by tables 3.3 and 3.4, show that a modification of the delta parameter hardly affects the significant wave height, while the effect is more noticeable for Tm_{02}. The increase of the delta parameter causes an important increase in the period values because it augments the dissipation for higher frequencies. The increase of the period is, thus, also important for the smaller frequencies in their relative weight within the spectrum.

In order to better evaluate the sensitivity of the two variables to different delta values, a linear regression fitting, with formulation $a \cdot x + b$, is computed comparing the results using delta values higher than zero with the default value (delta = 0). The coefficients of the linear fitting corresponding to the figures 3.2 and 3.3 are presented in tables 3.3 and 3.4, respectively.

Table 3.3: Linear regression line coefficients for the data presented in figure 3.2.

Besos buoy	Variable	a	b
$\delta = 0.5$	Hsig	0.975	0.041
	Tm_{02}	1.276	-0.434
$\delta = 0.75$	Hsig	0.955	0.047
	Tm_{02}	1.335	-0.523
$\delta = 1$	Hsig	0.937	0.051
	Tm_{02}	1.378	-0.591

Table 3.4: Linear regression line coefficients for the data presented in figure 3.3.

Barcelona buoy	Variable	a	b
$\delta = 0.5$	Hsig	0.996	0.015
	Tm_{02}	1.278	-0.498
$\delta = 0.75$	Hsig	0.985	0.015
	Tm_{02}	1.328	-0.566
$\delta = 1$	Hsig	0.974	0.014
	Tm_{02}	1.364	-0.618

In fact, there are not so many differences in using delta values between 0.5 and 1, although it seems, from the performed computations, that the best option is delta equal to 1 in almost all the locations for the two periods . However, in some locations with more energetic situations and a smaller under-prediction, normally when there

is a longer fetch, a delta equal to 0.75 or event 0.5 could be more appropriate according to the observations.

3.3.3 Adjusting the frequency interval to the measurements

In wave modelling it is common to compare some integrated parameters obtained from a numerical model with measured data, but it is not so common to determine how these bulk parameters have been obtained from the model and the wave buoy and to confirm that the comparison is being done under precisely the same terms, as noted by Akpinar et al. (2012).

Third-generation wave prediction models represent the wave spectrum over a certain frequency range, called the prognostic range. This range is affected by the source terms and propagation terms. For higher frequencies a parametric tail is used, typically an f^{-5} or, in SWAN, an f^{-4} tail. The wave model computes the bulk parameters integrating the spectra up to a high frequency limit (in SWAN the typical value is 10 Hz). However, the spectra provided by measurement instruments, buoy or pressure gauge, have a limited frequency range, usually between 0.05 and 1 Hz, and often also integrated parameters are obtained over this range (without considering a parametric tail), so one should be careful to ensure that the same quantities are being compared.

Two options are available to modify the integral frequency range used to obtain the bulk parameters. The first one consists in obtaining the spectra from the wave model and as a post process compute the bulk parameters in the range of interest. The second option is to introduce the frequency integration range in SWAN so that the outputs are computed for the desired frequency range.

In our case, the different buoys have different integral ranges (from 0.025 Hz to 0.58 Hz in some locations, and from 0.033 Hz to 0.625 Hz in the others), so the chosen interval goes from 0.03 Hz to 0.6 Hz. This frequency range has been introduced in the SWAN model to integrate the numerical spectrum and obtain the corresponding simulated bulk parameters.

Akpinar et al. (2012) carried out a sensitivity test of the integration range, finding that, depending on the wave conditions, the results may differ noticeably. It was also pointed out that significant wave height is rather insensitive to the integration range while the period (Tm_{02}) is more sensitive to the integration range and the dependence becomes smaller as the waves periods increase.

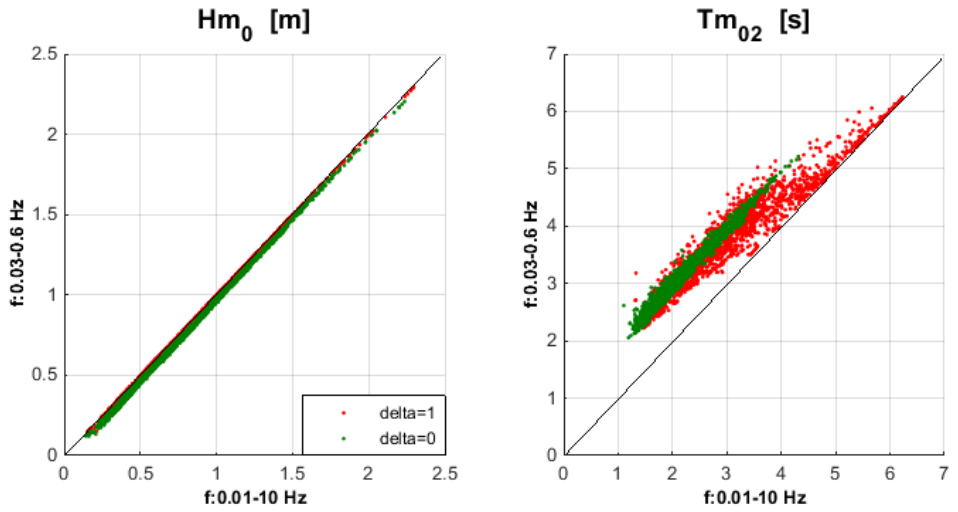

Figure 3.4: Scatter plots for the Hs and Tm_{02}, showing the effect of the adjustment of the frequency integration interval for two different delta values. Results from the finest grid, for the first study period in the Llobregat buoy location.

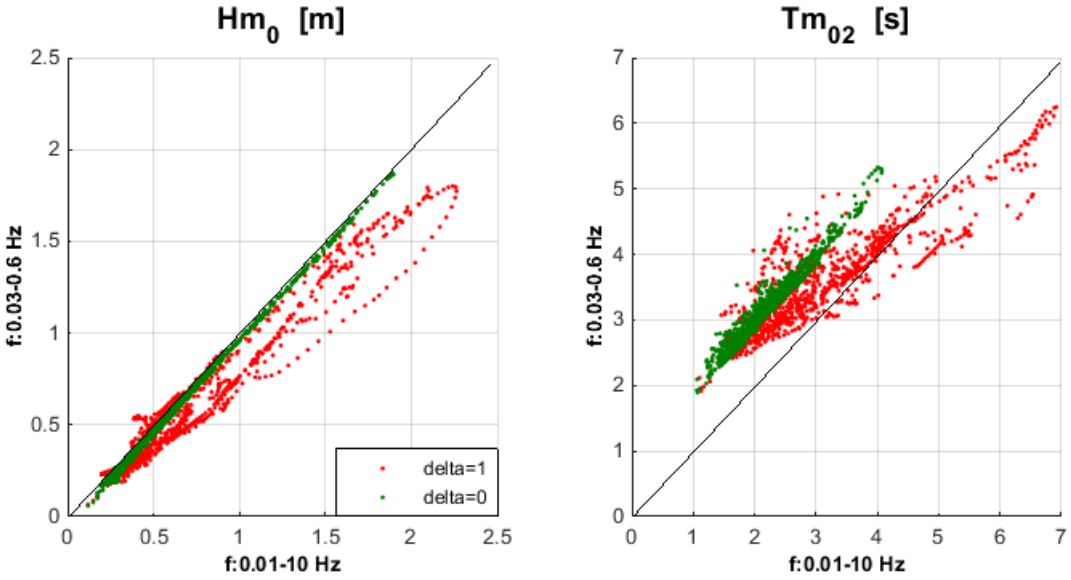

Figure 3.5: Scatter plots for the Hs and Tm_{02}, showing the effect of the adjustment of the frequency integration interval for two different delta values. Results from the finest grid, for the second study period in the Besos buoy location.

In figures 3.4 and 3.5 some representative results of our own sensitivity tests are presented. For the first period studied (figure 3.4), where the wind mainly blows from the coast and the waves are locally generated, the significant wave height is hardly affected by this adjustment. The mean period (Tm_{02}) presents different types of behavior depending on the delta applied; for delta equal to zero (default setting in

SWAN) there is clearly an increase in the mean period, while for delta greater than zero, this enhancement is more important for lower periods, as observed by Akpinar et al. (2012). Similar results are obtained for the second observation period studied, where there are more energetic events. For the several values of delta tested, the effect of adjusting the frequency interval is different. In some locations, as shown in figure 3.5, the significant wave height may suffer a reduction, especially for higher Hs values, and the same situation is observed for the mean period (Tm_{02}). Similar results have been obtained when studying the mean wave period Tm_{01} (not shown).

Our results were as expected. Since with this adjustment we are integrating only one part of the total energy spectrum to obtain the bulk parameters, part of the total energy corresponding to the higher frequencies is not being considered, causing a decrease of the wave momentum and their derived parameters. The effect is more important for spectra with more energy in higher frequencies, where an important part of the energy is located outside the integration range considered for the validation. In our opinion this adjustment of the frequency integral ranges is necessary to compare model results with instrument measurements under the same terms.

3.4 Analysis of the results

Eight simulation series have been run for each study period, adjusting the integration frequency interval and testing four different delta values mentioned in section 3.3.2 for the whitecapping term. The results presented in the following figures and tables correspond to the finest grid (1 km averaged grid size), during both periods considered and validated with the measured data from the eight buoys available in the area. All this work has generated a large volume of information summarized in this section and discussed in the next one.

First campaign

During the first observation period, from the 12th November 2010 to the 18th January 2011, there is a predominance of offshore blowing winds, which generate young sea waves that interact with swell generated in the open sea. This situation is characterized by bimodal spectra, and relatively mild energetic conditions.

Table 3.5: Summarize of the statistical errors for the simulations presented in figure 3.6.

Besos buoy	Variable	RMSE	Bias	SI	R
Delta = 0 f: 0.01 - 10Hz	Hsig	0.25 m	-0.03 m	0.35	0.73
	Dir	73.7º	-	0.52	0.40
	Tm_{02}	2.60 s	-2.37 s	0.56	0.43
	Tp	2.67 s	-1.64 s	0.42	0.29
Delta = 0 f: 0.03 - 0.6Hz	Hsig	0.26 m	-0.07 m	0.37	0.73
	Dir	66.2º	-	0.47	0.44
	Tm_{02}	1.69 s	-1.38 s	0.38	0.45
	Tp	2.67 s	-1.64 s	0.42	0.29
Delta = 1 f: 0.01 - 10Hz	Hsig	0.27 m	-0.04 m	0.37	0.67
	Dir	63.6º	-	0.45	0.47
	Tm_{02}	2.05 s	-1.62 s	0.45	0.36
	Tp	1.95 s	-0.94 s	0.31	0.42
Delta = 1 f: 0.03 - 0.6Hz	Hsig	0.27 m	-0.06 m	0.38	0.68
	Dir	58.4º	-	0.41	0.49
	Tm_{02}	1.27 s	-0.81 s	0.28	0.46
	Tp	1.95 s	-0.94 s	0.31	0.42

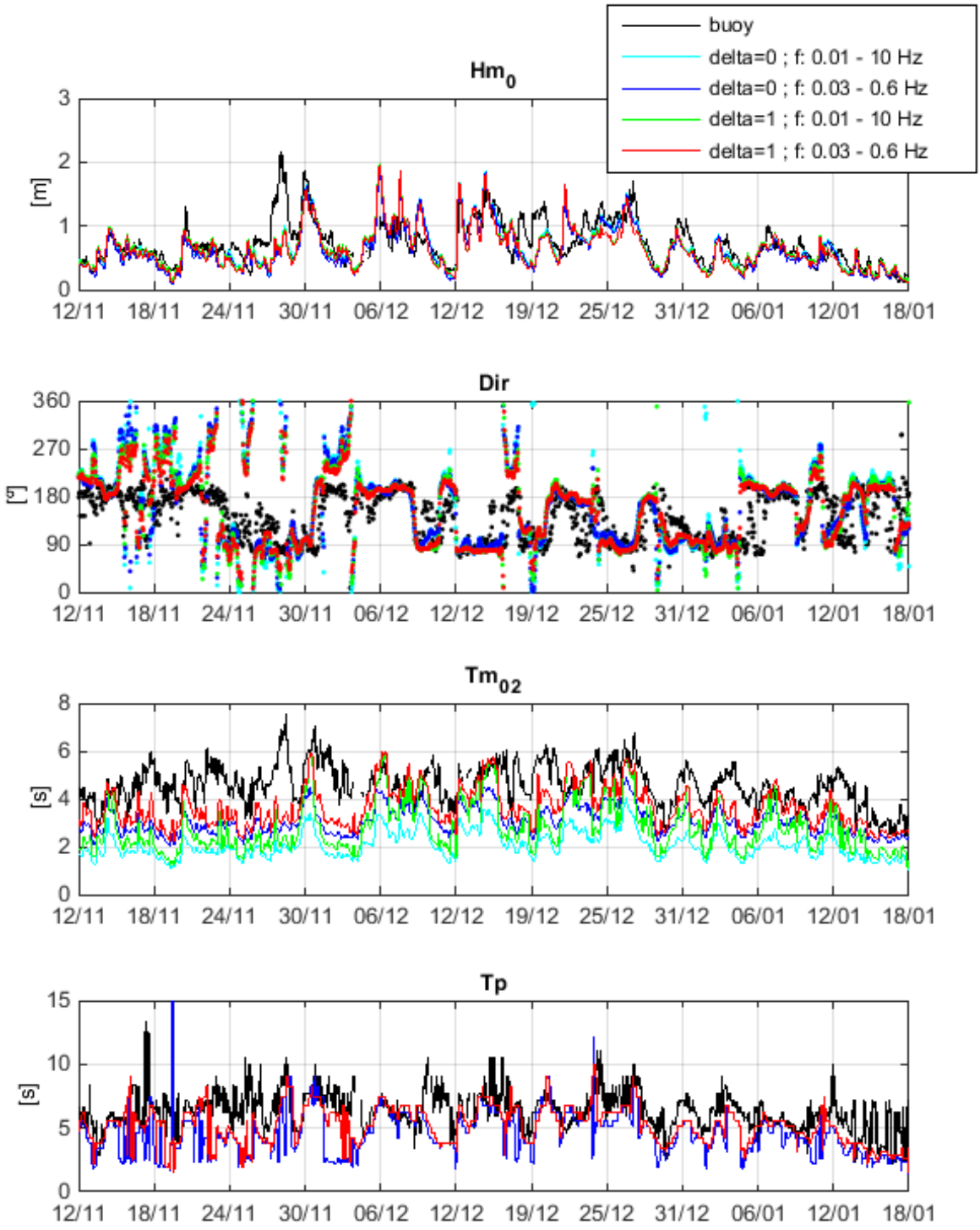

Figure 3.6: Time series for the significant wave height (a), mean wave direction (b), mean wave period (c) and peak wave period (d) comparing the results obtained from the simulations run with the SWAN configuration by default, adjusting the frequency interval to obtain the integration parameters and modifying the whitecapping term. First study period in Besos buoy.

Different time series are compared in figure 3.6 to determine the effect of properly adjusting of the frequency interval for calculating the bulk parameters and the proposed modification of the delta value in the whitecapping formulation. The location corresponds to the Besos buoy, moored just in front of the Besos river mouth and affected by the offshore winds. The corresponding errors are presented in table 3.5.

Figure 3.7 presents a comparison between the results without modifications (i.e. SWAN model using the whole prognostic range to integrate the bulk parameters and using a delta value of 0 in the whitecapping term) and the improved settings (obtained adjusting the frequency range to the one measured by the instruments and correcting the delta value to 1 so that the whitecapping term depends on the square of the wave number). To prove the regional validity of the comparison, figure 3.7 corresponds to another location, Tortosa, also highly affected by the offshore wind conditions. The corresponding errors are presented in table 3.6. Despite testing four delta values, the results show that for this period, in most of the locations the best adjustment corresponds to using delta equal to 1; these are, thus, the results here discussed.

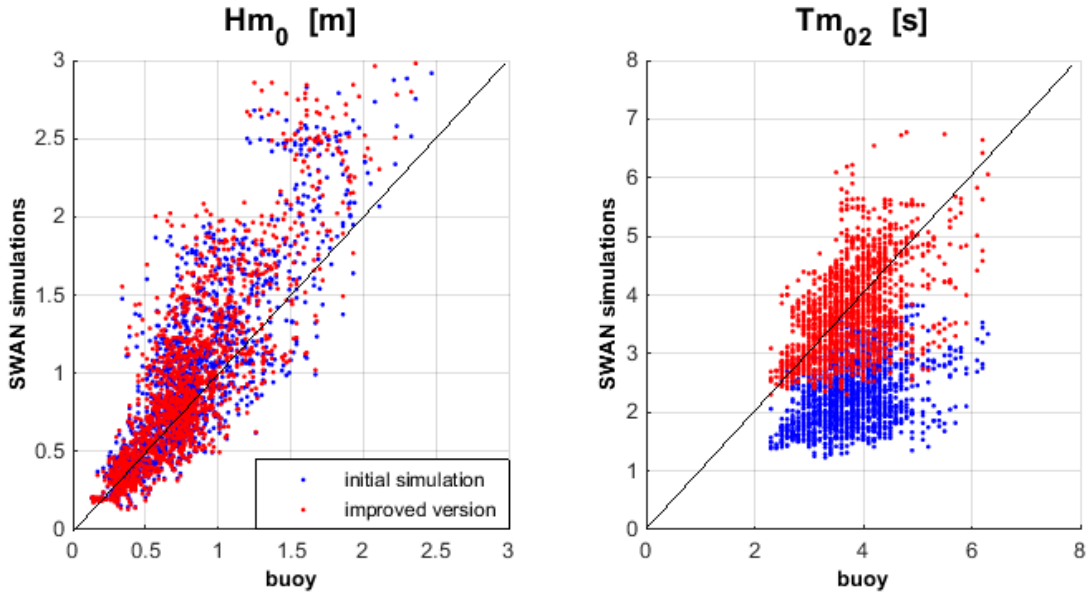

Figure 3.7: Scatter plots for the Hs and Tm_{02}, showing the improvement between the original simulation and the resulting run with both proposed corrections (frequency interval from 0.03 Hz to 0.6 Hz, and delta equal to 1 in the whitecapping term). Results from the finest grid, for the first study period in the Tortosa buoy.

Table 3.6: Summarize of the statistical errors for the simulations presented in figure 3.7.

Barcelona buoy	Variable	RMSE	Bias	SI	R
Delta = 0 f: 0.01 - 10Hz	Hsig	0.35 m	0.20 m	0.42	0.85
	Dir	72.7º	-	0.37	0.45
	Tm_{02}	1.60 s	-1.33 s	0.42	0.38
Delta = 1 f: 0.03 - 0.6Hz	Hsig	0.38 m	-0.22 m	0.46	0.85
	Dir	68.5º	-	0.35	0.48
	Tm_{02}	0.72 s	0.08 s	0.19	0.50

Second campaign

During the second observation period, from 11th March 2011 to 18th April 2011, the situation is quite different, with wind blowing mainly from the east with a much longer fetch and, thus, more energetic and developed wave conditions.

Table 3.7: Summarize of the statistical errors for the simulations presented in figure 3.8.

Besos buoy	Variable	RMSE	Bias	SI	R
Delta = 0 f: 0.01 - 10Hz	Hsig	0.28 m	-0.04 m	0.28	0.88
	Dir	50.6º	-	0.38	0.41
	Tm_{02}	2.24 s	-2.12 s	0.52	0.68
	Tp	2.33 s	-1.69 s	0.38	0.54
Delta = 0 f: 0.03 - 0.6Hz	Hsig	0.29 m	-0.08 m	0.40	0.88
	Dir	47.5º	-	0.35	0.43
	Tm_{02}	1.32 s	-1.12 s	0.31	0.72
	Tp	2.33 s	-1.69 s	0.38	0.54
Delta = 1 f: 0.01 - 10Hz	Hsig	0.24 m	0.05 m	0.33	0.91
	Dir	42.6º	-	0.32	0.56
	Tm_{02}	1.35 s	-0.99 s	0.31	0.73
	Tp	1.57 s	-0.36 s	0.25	0.61
Delta = 1 f: 0.03 - 0.6Hz	Hsig	0.29 m	-0.09 m	0.39	0.89
	Dir	43.9º	-	0.33	0.51
	Tm_{02}	0.88 s	-0.31 s	0.20	0.77
	Tp	1.57 s	-0.36 s	0.25	0.61

In figure 3.8, the different time series are compared to determine the effect of properly adjusting of the frequency interval for calculating the bulk parameters and the proposed modification of the delta value in the whitecapping formulation. The results correspond to the Besos buoy, located just in front of Barcelona, in the central part of the Catalan coast. The respective errors are presented in table 3.7.

In figure 3.9 a comparison is presented between the original SWAN simulations (using the complete prognostic range to integrate the bulk parameters and using a delta value of 0 in the whitecapping term) and the "improved" simulations (obtained adjusting the frequency range to 0.03 Hz to 0.6 Hz and choosing delta = 1). For this period, with more energetic wave conditions, the majority of buoy positions along

the Catalan coast show the best adjustment when using delta equal to 1; only in cases of comparatively higher wind velocities and longer fetch, a smaller delta value (0.75) generates better results. The respective errors are presented in table 3.8.

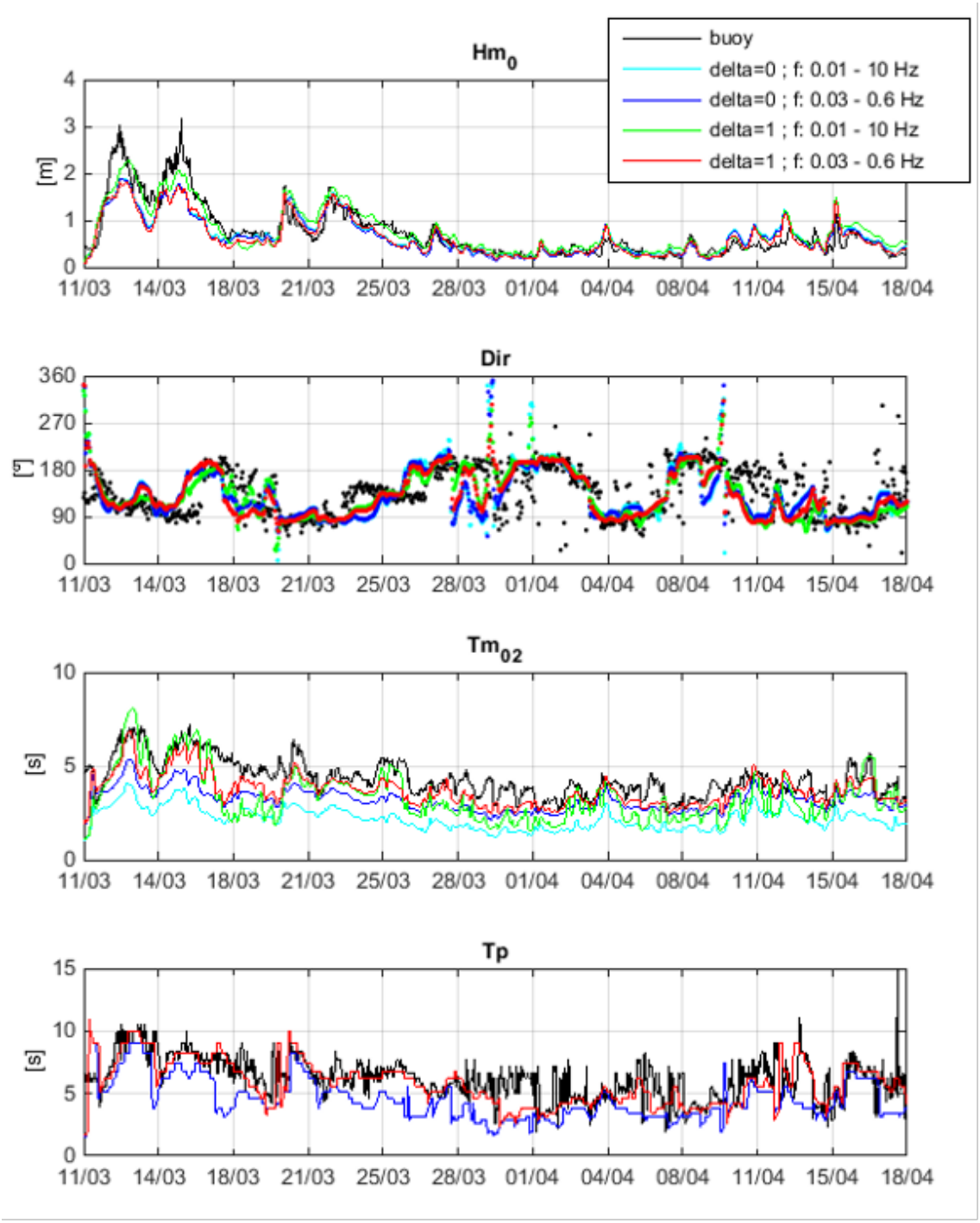

Figure 3.8: Time series for the significant wave height (a), mean wave direction (b), mean wave period (c) and peak wave period (d) comparing the results obtained from the simulations run with the SWAN configuration by default, adjusting the frequency interval to obtain the integration parameters and modifying the whitecapping term. Second study period in Besos buoy.

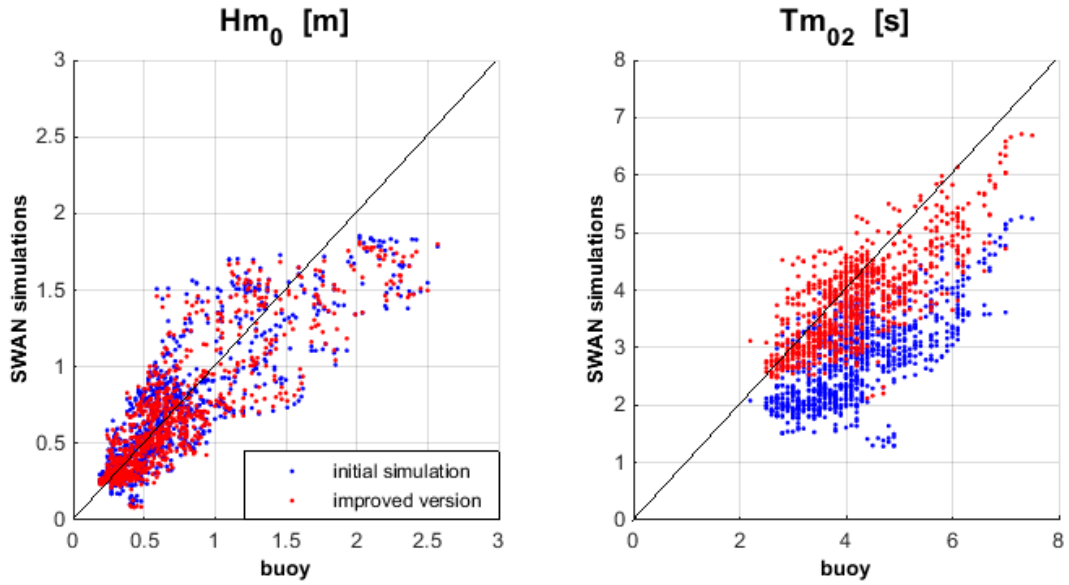

Figure 3.9: Scatter plots for the Hs and Tm_{02}, showing the improvement between the original simulation and the resulting run with both proposed corrections (frequency interval from 0.03Hz to 0.6 Hz, and delta equal to 1 in the whitecapping term). Results from the finest grid, for the second study period in the Llobregat buoy.

Table 3.8: Summarize of the statistical errors for the simulations presented in figure 3.9.

Llobregat buoy	Variable	RMSE	Bias	SI	R
Delta = 0 f: 0.01 - 10Hz	Hsig	0.2 m	-0.01 m	0.35	0.83
	Dir	49.5º	-	0.35	0.52
	Tm_{02}	1.53 s	-1.25 s	0.37	0.69
Delta = 1 f: 0.03 - 0.6Hz	Hsig	0.26 m	-0.02 m	0.34	0.85
	Dir	38.7º	-	0.28	0.69
	Tm_{02}	0.72 s	-0.25 s	0.17	0.77

3.5 Discussion

It has been proven during the study that the under-prediction of the mean period (Tm_{02}) and peak period in the Catalan coast is a persistent problem (e.g. figures 3.6 and 3.8). As concluded by Alomar et al. (2014), the main reason is that the wave growth rates included in wave models are lower than the measured rates in the area. This is due to the specific features of the Catalan coast: a semi-enclosed domain with transient wind (in strength and direction) and fetch-limited conditions.

In order to correct this systematic error, two modifications have been proposed. The first is a modification of the delta value in the Hasselmann (1974) whitecapping term formulation implemented in SWAN, as previously done by Rogers et al. (2003). This correction introduces a dependence on the squared wave number, improving the prediction of the energy spectra at lower frequencies. In fact, the SWAN team has recently modified the default option of delta for the WAM cycle 3 formulations from 0 to 1 in version 40.91AB. The results obtained in this study support the recent choice of the SWAN team, at least for young or moderate sea wave conditions.

The second modification is an adjustment of the frequency range used to integrate the bulk parameters in the wave model, so that it coincides with the one used by the field instrument; this ensures that the comparison is being made under the same conditions. The first proposed correction is specific for domains with a limited fetch and variable wind conditions, while the second aspect is valid, and necessary, for all cases.

From the results shown in this study, it can be concluded that the behavior of the SWAN model is sensitive to the prevailing conditions and situation; here the proposed modifications will affect differently each type of wave conditions. A general improvement can be observed in all studied cases (not only the results shown here in figures 3.6 and 3.8 but also in the other simulations performed) with the modifications here proposed. They result in a significant wave height and mean wave direction that are slightly modified; however, the mean period (Tm_{02}) and the peak period increased considerably solving largely the well-known under-prediction problem.

In general terms, we may conclude that the corrections here proposed can be valid along the Catalan coast and also for similar environments and wave conditions: young and moderate sea waves with variable wind fields. These conditions are typical of coastal areas within semi-enclosed domains.

With the proposed corrections the significant wave height can become slightly lower within the frequency interval adjustment due to a reduction of the energy considered to calculate the bulk parameters in the validation process. This is a

consequence of not using the parametric tail in the spectrum to compute the integral wave parameters. In the Catalan coast there is a tendency to slightly under-predict the significant wave height, mainly during storm events. This problem may be slightly exacerbated by this correction, but with a limited quantitative relevance, as can be observed in tables 3.5 to 3.8. However, this consideration is necessary to be sure that the comparison between modeled and measured values is done under the same terms.

Due to the young sea wave conditions present in the Catalan coast, the correction of the whitecapping term is essential. However, this modification is less relevant for the significant wave height than for other variables as is mentioned below. The mean wave direction is not so affected by the proposed modifications. They may lead to a slightly smoother behavior when there is an abrupt change of direction. Under other conditions, there is hardly any difference.

The peak period and the mean wave period (Tm_{02}) are the variables most affected by the proposed changes, presenting an important improvement for the Catalan coast. In figures 3.6 and 3.8 we show a comparison between the original results obtained running SWAN, and the improved simulations with a frequency integration range between 0.03 Hz and 0.6 Hz and a correction of the whitecapping term. These results show a great improvement in all locations; the $RMSE$ is reduced and the negative bias is almost corrected. However, the effect is more important in Tm_{02} because the effects of the two corrections are added, while Tp is not affected by the frequency integration range. Similar results to the Tm_{02} have been obtained for the Tm_{01}, although they are not shown in this document.

The present work provides a clear improvement of the wave simulations for the Catalan Coast that could be exported to similar environments, characterized by young/moderate sea wave conditions due to fetch limited and variable wind fields, taking into consideration that depending on the sea state a certain delta would be optimal. However there remains work to be done in the wave modeling physics (e.g. Tolman, 1992a). The actions proposed in this thesis correct part of the problem, but are far from a final solution since better formulations for the energy balance terms are necessary to reproduce the actually occurring growth and dissipation rates in coastal areas within semi-enclosed domains.

3.6 Conclusions

To determine the performance limits for wave forecasting at coastal scales we have looked into the various terms contributing to the wave action balance equation and tested their relevance for a set of observations off the Catalan coast. This represents a particularly demanding situation since the storm duration is limited and the orography affects the wind fields, resulting in the large spatial gradients that compound the problem.

We have focused on the whitecapping term because it is easy to tune it and it is the least well-known term in wave models. Because of that it is often the tuning knob for wave simulations. The results show that, as suggested by other authors, this term should depend more explicitly on the wave characteristics. Moreover we have seen the importance of introducing wave number as a parameter for the closure, which is particularly relevant for the Catalan sea where most of the time there are young seas, actively generated or modified by the acting winds. These young seas are generally steep and the proposed modification works primarily by a different weighting of the mean wave steepness as a function of the wave number so these situations are the most affected by the proposed correction.

Following this argument we have adjusted the present formulation for the whitecapping term in young seas by modifying the delta value of the Hasselmann (1974) expression. It is adapted to the wave – growth and evolution for the Catalan coast but since it is based on the physics of young sea evolution it should be applicable to other similar environments. In fact, the present work supports the choice of the SWAN team to make delta equal to 1 the default value in versions 40.91AB and following. It is however important to notice that the proposed formulation is only suitable for the early stages of generation and should be discontinued after the waves reach a certain maturity, as happens for example in open sea conditions. In this work we have also seen that the integral wave parameters for the simulations and the measurements should be referred to the same frequency interval since otherwise we are introducing into the fit parameters the contribution of high or low frequency bands not present simultaneously in simulations and observations. This refers, more specifically, to the need of adjusting the working frequency interval in the validation process, since now the spectral high frequency tail is present in the simulations but not in the measured data.

It should be finally stressed that the key element in wave models is the balance between input and output terms for the wave action balance. Although we have only considered dissipation due to the deep water breaking, the overall model performance will be the result of combining the various terms contributing to the action balance.

As shown also by previous authors this requires adjusting the growth term, the physical and numerical dissipation and also the nonlinear interactions term (or its approximation) so that the resulting balance conforms to what is happening in nature for the particular studied domain.

Chapter 4

The effect of coupling on the wave modelling in the Catalan Coast

4.1 Introduction

Due to the increased performance of computational resources, the use of numerical models to predict natural events is becoming more prevalent. To accomplish this, numerical models are not only being pushed to increase their spatial resolution but also to increase the complexity of the simulated physics. Coupling of models is one method to allow increase in model complexity (Warner et al., 2010). The coupling of models allows the effects of larger scale processes to directly influence the smaller scale response. Three-dimensional coupled atmosphere–ocean models have been developed and applied to idealized and realistic scenarios to predict the interactions between the atmosphere and the ocean (Warner et al., 2008b; Bolaños et al., 2011; Dietrich et al., 2011b).

It is during the most energetic events when the coupling takes more relevance (Warner et al., 2010; Jorda et al., 2007) due to the intense wind, currents and wave fields involved. The Western Mediterranean sea is an area mainly defined by calm periods most of the year. However, coastal areas are often characterized by highly variable and heterogeneous wind, wave and current conditions, which make the numerical prediction of the meteo-oceanographic processes difficult.

For instance, wind jets induced by orographic effects present strong spatial wind field variability due to the orographic characteristics (e.g. Shimada and Kawamura, 2006; Zhai and Bower, 2013). Instead of the relatively limited fetch in the wind jet region, the wave height can be relevant, interacting with bimodal features (Shimada and Kawamura, 2006). In this sense, several contributions have highlighted the influence of variable wind conditions in relatively small-scale areas (such as wind jet),

influencing wind-wave generation Shimada and Kawamura (2006); Bolaños et al. (2007); Alomar et al. (2014) or modifying ocean circulation patterns (Zhai and Bower, 2013; Schaeffer et al., 2011; Klaic et al., 2011).

The case of the Ebro River shelf (north-western Mediterranean Sea; figure 4.4) is characterized by strong, dry and usually cold wind that blows from the north-west through the Ebro valley, induced by the lee of the Pyrenees Mountains. The westerly wind, greatly affected by the orography, is channelized into a limited band, forming a wind jet (Jansa, 1985). Offshore wind is more usual and intense during autumn and winter, when larger atmospheric pressure gradients take place and cause stronger winds with advection of cold air, but a small atmospheric pressure difference along the Ebro valley is sufficient to initiate wind during any season (Cerralbo et al., 2015).

The current intensifications are another energetic event in which the interaction between the wave field and the current field is relevant. Several authors have studied the interaction between waves and currents using coupled models in different areas of the world (Jorda et al., 2007; Warner et al., 2010; Malhadas et al., 2010; Bolaños et al., 2011).

Intense water flows have been observed along the Catalan coast by several authors (Palanques et al., 2002; Jorda, 2005; Grifoll et al., 2015) associated to strong local winds and with current intensities up to 50 cm/s. According to Mestres et al. (2016) a flow intensification can be defined as an intense water flow lasting more than 12 hours and exceeding a threshold defined as the surface current monthly 95th percentile. With this criteria Mestres et al. (2016) detected up to 14 events in the Catalan coast during a three years period (from June 2008 to July 2011) distributed mainly during spring (6) and summer (5), and less frequently in autumn (1) and winter (2). The mean superficial current for the entire study period in front of the Barcelona harbour was 0.20 m/s, while the events selected reached values around 0.75 m/s and with an extreme of 1.39 m/s during and event occurring in October 2010. As concluded by Mestres et al. (2016) the current intensifications in front of the Barcelona harbour area are mainly induced by locally strong and persistent winds blowing from the northeast to southeast, typically associated to the presence of lows in the southwestern Mediterranean and highs over Central Europe.

In this chapter we present different coupling forms applied to both calm periods and energetic events, as wind jets or current intensifications described before, with the objective to quantify the effect of models coupling on wave fields for the Catalan coast.

4.2 Background: model coupling

4.2.1 One-way and two-way coupling

When working in coastal areas the interaction between the wind, waves and currents fields is not negligible, and therefore it is recommendable to couple the different models. Various types of coupling are available, that will be discussed in this chapter. A one-way coupling (also known as offline coupling) is the simplest option that consists in getting results from one model and introduce them as an input into another model. Additionally, there is the option to execute a two-way coupling (or online coupling), so that for each time step both models run in parallel, and every so often they share physical parameters such as the wave height, the current intensity or the atmospheric pressure, thus being able to reproduce more realistically the physical behaviour in coastal areas.

The last decades, the scientific community has begun to consider the currents fields in the wave modelling. Jorda et al. (2007) quantified the importance of currents fields when modelling the waves in a shelf ocean domain. In this study, he concluded that under storm conditions, a decisive contribution of currents on waves is observed, basically due to the wave refraction. Few years later, Benetazzo et al. (2013) modelled the waves coupled to the circulation model for the semi-enclosed Gulf of Venice, obtaining considerably variations of the significant wave height and an increase/decrease of wave spectral energy in situation of opposite/following currents respectively. Some experimental studies have been carried out by Rusu and Soares (2011), compared to wave simulations under different current conditions.

The interaction between surface winds and waves was studied by Charnock (1995). An estimation of the surface drag created by the waves as a function of the wind speed was proposed. More recent studies have revisited the topic proposing new parameterizations (e.g Johnson et al., 1998). Few years later, studies using atmospheric and wave models have focused on case studies that analyse many aspects of the ocean and atmospheric feedbacks (e.g. Warner et al., 2010), which make difficult to generalize results regarding the potential benefit in the lower level wind simulation and its effect on wave forecast as a result of coupling atmospheric and wave models.

The contributions presented above, although quantifying processes related to the three fields (waves-circulation-atmosphere), treat each phenomena separately (which is usually called one-way coupling). This is performed running the different models sequentially and introducing some of the results as inputs for the other models.

However, the coupling of models can also occur with all the models running

concurrently, using a coupling toolkit to allow the transfer of information between models, which is usually called two-way coupling. Warner et al. (2008a) implemented the SWAN wave model and the circulation model ROMS (Regional Ocean Modelling System; Haidovel et al., 2008; Shchepetkin and Williams, 2005, 2009) coupled in a two-way manner. This coupling was undertaken with the tool Model Coupling Toolkit(MCT; http://www-unix.mcs.anl.gov/mct/ ; Larson et al., 2004; Jacob et al., 2005) and is valid for riverine areas, estuaries, coastal and ocean platform. In this case, the proposed system implements, compiles and executes a parallel models taking into account the influence of currents on waves and waves on currents, but it was not coupled with the atmosphere. The coupling of the three fields at the same time was finally implemented and applied by Warner et al. (2010) under the name of COAWST system (Coupled Ocean-Atmosphere-Wave-Sediment Transport modelling system), which executes a system where the three models run concurrently: the wave model SWAN, the circulation modelling ROMS and the non-hydrostatic meteorological model WRF (Weather Research and Forecasting; Skamarock et al., 2005).

Furthermore, some other models have been coupled in a two-way manner with also good results. Bolaños et al. (2011) improved the coupling between the circulation model POLCOMS (Proudman Oceanographic Laboratory Coastal-Ocean Modelling System; Holt and James, 2001) and the waves model WAM (WAMDI-group, 1988). The previous version (Osuna and Wolf, 2005) worked with a two-way coupled system in two dimensions (with depth-averaged momentum equations) and considered the wave refractions by currents, the bottom friction modification due to wave and current fields, and the increase of the wind stress due to waves. The new version also includes the effects of Stokes drift in the currents and the distribution of the surface tension between the waves and currents. This system was evaluated in the North-western Mediterranean sea and the results conclude that currents, typically small in this region, do not have a great effect on the waves while the currents generated by waves, usually caused by a change in wind stress due to the surface roughness of the sea, are not negligible. Other system that has been used to study the circulation and waves in a coupled manner is formed by the wave model STWAVE (STeady State Spectral WAVE; Smith et al., 2001) and the circulation mode MOHID (Santos, 1995) implemented in a coastal lagoon off the coast of Portugal (Malhadas et al., 2010). In this case performing a one-way coupling in which the STWAVE wave model results are introduced as an input into the MOHID model, where currents are calculated. Dietrich et al. (2011b) have integrated the SWAN model working with unstructured grids with the circulation and storm surge model ADCIRC (Luettich and Westerink, 1994b) for two hurricane events in the Gulf of Mexico, demonstrating the importance of the wave-circulation interactions

under those conditions.

4.2.2 The COAWST system

Since the COAWST system is a free distributed system, easy to implement and suitable for subsequent transfer of the progresses achieved, it has been chosen among the others presented before. The COAWST system uses the SWAN wave model and includes several test cases useful to become familiar with it. Also, the system has shown good and improved results for various different locations.

Besides the SWAN model, defined in chapter 2, the other models used by the COAWST system are described in the following lines:

- *The circulation model ROMS:*

  It is a free-surface, terrain-following numerical model which resolves the three-dimensional Reynolds-averaged Navier-Stokes equations using hydrostatic and Boussinesq approximation. It is a model widely used by the scientific community for a diverse range of applications. ROMS includes accurate and efficient physical and numerical algorithms and several coupled models for biogeochemical, bio-optical, sediment, and sea ice applications. It also includes several vertical mixing schemes, multiple levels of nesting and composed grids.

  ROMS uses finite-difference approximations on a horizontal curvilinear grid and on a vertical stretched terrain-following coordinate. Momentum and scalar advection and diffusive processes are solved using transport equations and an equation of state computes the density field that accounts for temperature, salinity, and suspended-sediment contributions.

- *The atmospheric model WRF (Advanced Research WRF version):*

  It is a non-hydrostatic, quasi-compressible atmospheric model with boundary layer physics schemes and a variety of physical parameterizations of subgrid scale processes for predicting mesoscale and microscales of motion. The model predicts three-dimensional wind momentum components, surface pressure, dew point, precipitation, surface sensible and latent heat fluxes, longwave and shortwave radiative fluxes, relative humidity, and air temperature on a sigma-pressure vertical coordinate grid. WRF has been used extensively for operational forecasts as well as for realistic and idealized research experiments.

- *The coupler Model Coupling Toolkit (MCT; Jacob et al., 2005):*

  To manage the three models running concurrently, and the transfer of information and variables from one to another, the Model Coupling Toolkit coupler

is used (MCT) (Larson et al., 2004; Jacob et al., 2005). MCT is a program written in Fortran90 and works with the MPI parallel communication protocol. During model initialization each model decomposes its own domain into sections that are distributed to processors assigned for that component. Each grid section on each processor initializes into MCT, and the coupler compiles a global map to determine the distribution of model segments. Each segment also initializes an attribute vector that contains the fields to be exchanged and establishes a router to provide an exchange pathway between model components. During the run phase of the simulation the models will reach a predetermined synchronization point, fill the attribute vectors with data, and use MCT send and receive commands to exchange fields. Further details are described in Warner et al. (2008a).

- *The Spherical Remapping Interpolation Package (SCRIP; Jones, 1999):*

  It is used to exchange data fields on different grids computing the interpolation weights.

The variables exchanged between the three models during the coupling process are shown in table 4.1.

4.2.3 Expected improvements

The expected improvements in the wave model due to the coupling process are detailed by analysing the physics behind the coupling. The resulting wave conditions in a local area are a sum of different factors. Under some circumstances, this waves are very sensitive to the current fields and the state of the atmosphere due to interactions between the different fields, and also because the growth of waves is mainly controlled by the wind stress. The main interaction processes affecting the waves are the following:

Wave refraction due to currents

The refraction process is the rotation of the waves approaching to the shore in shallow water due to depth variation. However, it is known that the waves are not only refracted due to bathymetry effects but can also refract in presence of ambient currents distributed no uniformly in space. Then, one section of the wave front is traveling at a higher speed than another. The refraction process causes a change in the direction of the waves and in their frequency, and is strongly linked to the phenomenon of the Doppler Effect.

Table 4.1: Configuration of data fields exchanged between the coupled models.

Source model	Model that adresses	Variables
ROMS	SWAN	Surface currents Free surface elevation Bathymetry
WRF	SWAN	10m surface winds
SWAN	ROMS	Significant wave height Wave length Wave direction Wave period Percent wave breaking Wave energy dissipation Bottom orbital velocity
SWAN	WRF	Significant wave height Wave length
ROMS	WRF	Sea Surface Temperature (SST)
WRF	ROMS	10m surface winds Atmospheric pressure Relative humidity Atmospheric surface temperature Cloud fraction Precipitation Shortwave and longwave net heat fluxes

Wind-stress modifications in presence of currents

Wind is the main wave forcing. When the wind blows, in the boundary layer between the ocean and the atmosphere takes place a process of energy transfer. In the presence of currents the wind tension is altered, since the wind stress is proportional to the squared wind intensity. In a situation with presence of ambient currents, the formula should be modified using the relative wind speed over water instead of the absolute wind speed (equation 4.1).

$$\tau_w = \rho \cdot C_D \cdot (u - u_c)^2 \tag{4.1}$$

Where ρ is the sea water density, C_D is the drag coefficient, u is the wind speed and u_c the current velocity.

Typically, this formulation does not affect too far the result, since in the study area the wind speed is usually of the order of 10 m/s while the currents are two orders of magnitude lower. However, in the Catalan Coast under storm conditions, Jorda et al. (2007) states that the currents near the surface can reach considerable values, thus affecting the wave generation.

Bottom friction

The bottom friction is the main dissipation mechanism in continental shelf areas and sand bottoms. This friction is proportional to the velocity of the water near the bottom (in particular the $U_{rms,bottom}$, the root-mean-square orbital velocity at the bottom). This speed is determined by the presence of currents and waves, and will affect both fields, especially in shallow water areas.

There are several formulations to calculate the bottom friction and the corresponding energy dissipation, depending on the background material, the length of bottom roughness, the presence or absence of ripples and their shape, etc. However, the fact of unknowing too precisely how the bottom is, usually cause more errors than ignore the effect of the currents (Tolman, 1992b).

Wave breaking

When a wave propagates toward the shore, the shoaling phenomenon causes an increase of the wave height. When the ratio of wave height versus depth exceeds a certain limit, the waves start to break quickly, dissipating its energy. In shallow water areas this process becomes dominant over all other processes that affect the

waves (surf zone). In presence of a current field, the wave height is modified so the breaking behaviour changes.

The process of breaking induced by the bathymetry is quite unknown, and therefore little is known of how it affects the wave spectrum (which is the main parameter in the wave models). However, the total dissipation (integrated with the spectral space) has been more studied, and can be modelled approximately as a percentage of the total spectrum energy.

Additionally, in a two-way coupling, the waves also generate modifications in both the current and the wind fields that in the next time steps return to modify again the wave field. From all this process the most important for wave modelling is the wind stress modification due to the sea surface roughness.

Wind stress modification due to sea surface roughness

Waves modulate the surface drag exerted over the surface winds. The stress is a function of the characteristics of the waves and there are several parameterizations to represent it:

The standard sea surface roughness length scale is expressed as a function of the Charnock coefficient (C_a; typical value of 0.016 for young seas) and surface wind stress (u_s):

$$z_0 = C_a \cdot \frac{{u_s}^2}{g} \tag{4.2}$$

where g is the gravity.

Coupling online simulations in COAWST allows three different additional formulations to be chosen to parameterize the sea surface roughness considering the wave effects. The formulation of Taylor and Yelland (2001) considers the wave effects:

$$\frac{z_0}{Hs} = 1200 \cdot \left(\frac{H_s}{L_p}\right)^{4.5} \tag{4.3}$$

where H_s is the significant wave height and L_p is the wavelength at the peak of the wave spectrum.

Drenann et al. (2003) proposed a formulation to estimate z_0 as a function of the phase-wave speed (C_p) and wind friction velocity (u^*):

$$\frac{z_0}{Hs} = 3.35 \cdot \left(\frac{u^*}{C_p}\right)^{3.4} \tag{4.4}$$

Similar to Drennan's formulation, Oost et al. (2002) proposed the following formulation based on an experimental data set:

$$\frac{z_0}{L_p} = \frac{25}{\pi} \cdot \left(\frac{u^*}{C_p}\right)^{4.5} \tag{4.5}$$

Conceptual differences arise from these formulations: Taylor and Yelland (2001) considers the wave steepness, while Drenann et al. (2003) and Oost et al. (2002) are based on the wave age.

Hence, the coupling of WRF with SWAN should allow for a more realistic representation of the wind and wave feedbacks since the waves are explicitly modelled by SWAN and the information is transferred to the atmospheric model every few time steps. An improved simulation of the lower level winds is therefore expected. However, it is necessary to investigate which parameterizations provide a more realistic interaction in order to realistically simulate the lower level wind.

4.3 Methodology

The tests performed in this chapter have been structured in two separate sections: the first one consisting in a one-way coupling, in which the effect of the currents into the wave field is considered, and the second in a two-way coupling, in which the circulation, atmospheric and wave models are coupled.

For each of the mentioned sections two different experiments have been carried out in order to compare the different behaviour during calm periods and local energetic events. In the following lines a description of the different episodes selected for each test are presented.

4.3.1 One-way coupling experiments description

In order to evaluate the one-way coupling effect of the currents on the wave field the episode selected during a calm period goes from 11th March 2011 to 18th April 2011, corresponding to the second period analysed in chapter 3. During this period the wind blows mainly from the east, with long fetches and thus quite developed wave conditions.

In contrast with this first episode, in which the currents are not very intense, a second episode is selected during which a surface current intensification occurred in front of Barcelona harbour. The flow intensification started the 11th of October 2010 around noon, and lasted 48 hours, with a maximum current intensity in the ocean surface of 1.39m/s in north-west direction (figure 4.1). The current intensification is generated by a persistent wind blowing from the east.

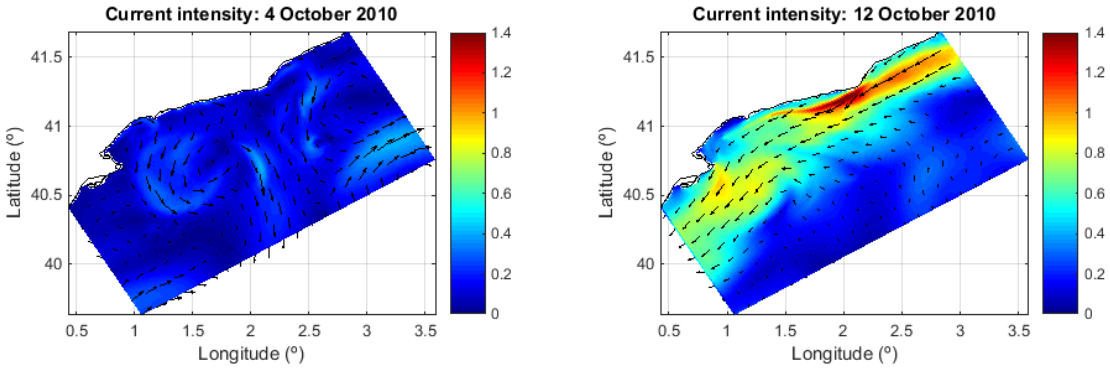

Figure 4.1: Superficial current intensity (in m/s) before the flow intensification (left) and during the peak of the current intensification event (right).

A large set of buoy measurements was available to validate the results for the two episodes selected. However, the Llobregat buoy (defined in table 3.1 and represented

in figure 4.2) was selected due to its location in front of the Barcelona harbour, highly affected during the current intensification event.

The bathymetry used in all the episodes tested is obtained from GEBCO (General Bathymetric Chart of the Oceans, www.gebco.net) with a grid resolution of 30 arc-second (0.0083º).

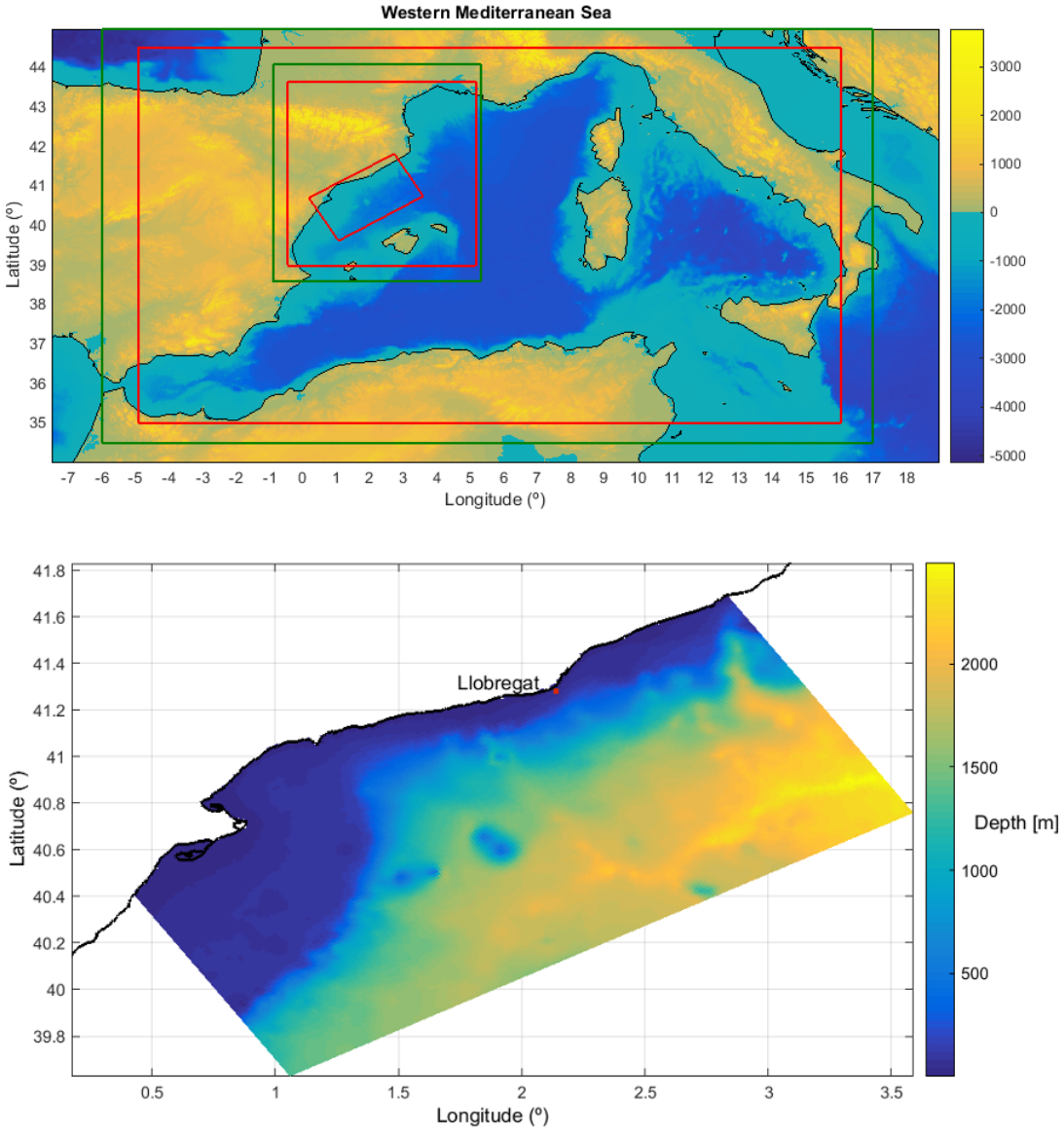

Figure 4.2: Orography and bathymetry of the study area (top). The red boxes represent the SWAN meshes and the green boxes the wind forcing domains for the one-way episodes. In the bottom the Catalan coast domain is represented and the Llobregat buoy location marked with a red dot.

The nesting strategy in both episodes consists of a set of different downscaling meshes (figure 4.2). For the SWAN simulations the grids used are the same ones

described and used in chapter 3. The largest wave domain covers the Western Mediterranean Sea, which is considered enough to capture the wave generation in the study area, so no boundary conditions are needed.

The SWAN model set up used in all the domains is the one described in chapter 2 with the whitecapping term modification proposed in chapter 3.

The set of forcing (including both wind and current fields) used in the two episodes is quite different due to the availability of data sets for each period.

On one hand, for the calm period episode, the wind used is provided by the Barcelona Supercomputing Center (BSC, www.bsc.es) using the WRF model (like in the chapter 3). The resolution of the wind fields provided is 12 km and 1 h for the Western Mediterranean sea domain and 4 km and 1 h for the Balearic Sea domain.

On the other hand, for the current intensification event the only wind available is provided by Meteo-Frace (www.meteofrace.com) using the ALADIN atmospheric model (Radnoti et al., 1995; ALADINteam, 1997) covering the Western Mediterranean Sea domain with a spatial resolution of 0.1º (around 8.5 km) and a temporal resolution of 3 h.

The current field in both episodes was computed with ROMS model for the Catalan coast domain, with a spatial resolution of 1 km and a temporal resolution of 6 h. More information on the ROMS configuration and the validation of the currents fields can be found in Grifoll et al. (2013).

4.3.2 Two-way coupling experiments description

For the evaluation of the two-ways coupling, the entire 2012 year is simulated and analysed. During the full year several north-west wind jet events occurred in the Ebro River shelf, so one of them was selected as the energetic event. The episode lasted from the 19th of May 2012 to the 23rd of May 2012. The sequence of wind field modelled in the Catalan coast mesh during the wind jet period is characterized by a rise of wind intensity during the 20th and 21st of May, leading to a wind jet in the northern margin of the Ebro delta (see daily-averaged wind intensity in figure 4.3). Then, the offshore winds remains strong during the 22nd of May, decreasing during the 23rd of May 2012.

As noted in section 4.2, the air-sea momentum transfer presents high complexity due to the relation of wave characteristics and the sea surface roughness, which in turns affect the wind field. In order to investigate the air-sea momentum transfer in the wind jet, a set of simulations have been designed applying different sea surface roughness formulations included in the COAWST modelling system. The sensitivity

tests pursue an evaluation of the coupling effects on two principal variables involved in the air-sea momentum transfer: wind intensity and significant wave height. In this sense three different formulations have been tested (equations 4.3 to 4.5 described in section 4.2) and compared with the configuration set up by default in WRF.

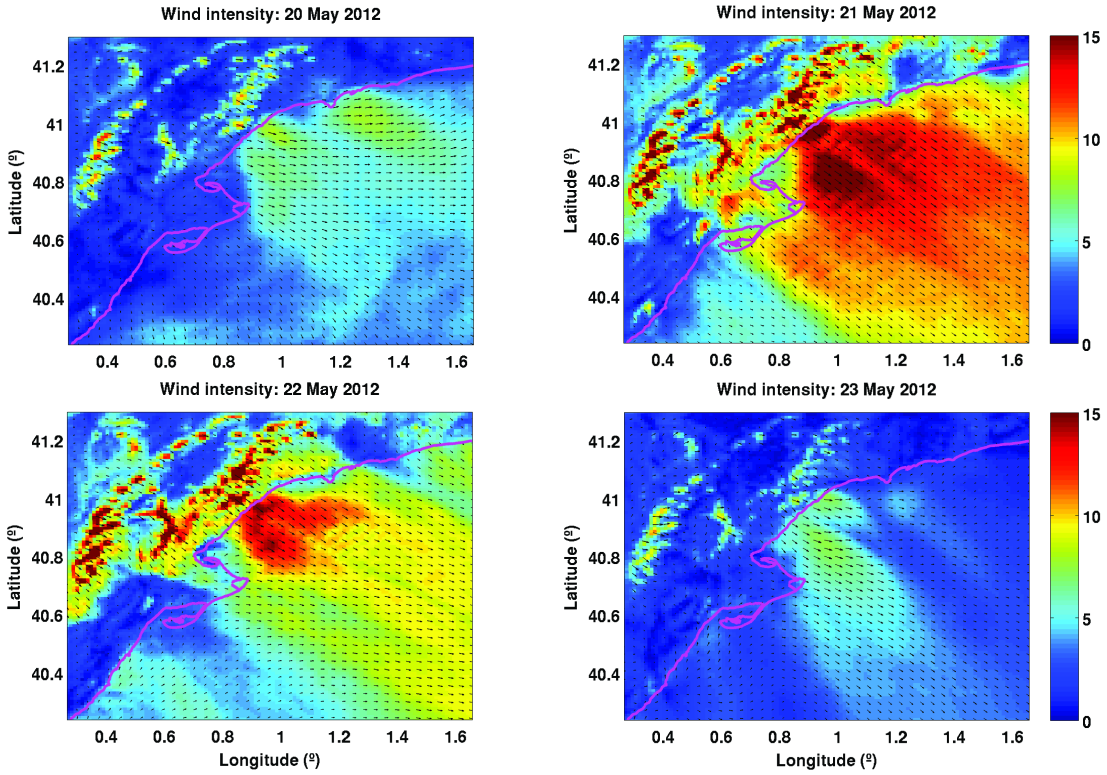

Figure 4.3: Sequence of the wind jet intensity on four days for a wind jet event in the domain of the Catalan coast (in m/s).

In consequence, the coupled results are directly compared with an uncoupled simulation where the sea surface roughness length is only a function of the wind stress. The sensitivity tests are as follows: 'CHK' for the simulation considering the sea surface roughness as a function of the wind stress (uncoupled with the wave sea state) using the Charnock coefficient equal to 0.016 (typical value for young seas), 'T-Y' simulation considering the Taylor and Yelland formulation (Taylor and Yelland, 2001), 'DRE' using the Drennan formulation proposed by Drenann et al. (2003) and 'OOST' simulation considering the formulation introduced by Oost et al. (2002).

As a part of the European project NEPTUNE a buoy was moored in the northern margin of the Ebro shelf where the wind jet develops (figure 4.4) that was used to validate the results for the second section episodes. The buoy was moored 3.1 km from the coast at 43.5 m bottom depth, measuring wind, waves and water currents

for one year (November 2011 to December 2012). A TRIAXYS directional wave sensor mounted on the moored buoy was used to record statistical wave spectral parameters. Wind speed and direction were measured at 4 m height every 10 min using an ultrasonic wind sensor (Gill Instruments), and water currents were measured with a SonTek acoustic Doppler currentmeter profiler (ADCP) at 500 kHz every hour using 20 vertical layers (layer depth was 2m).

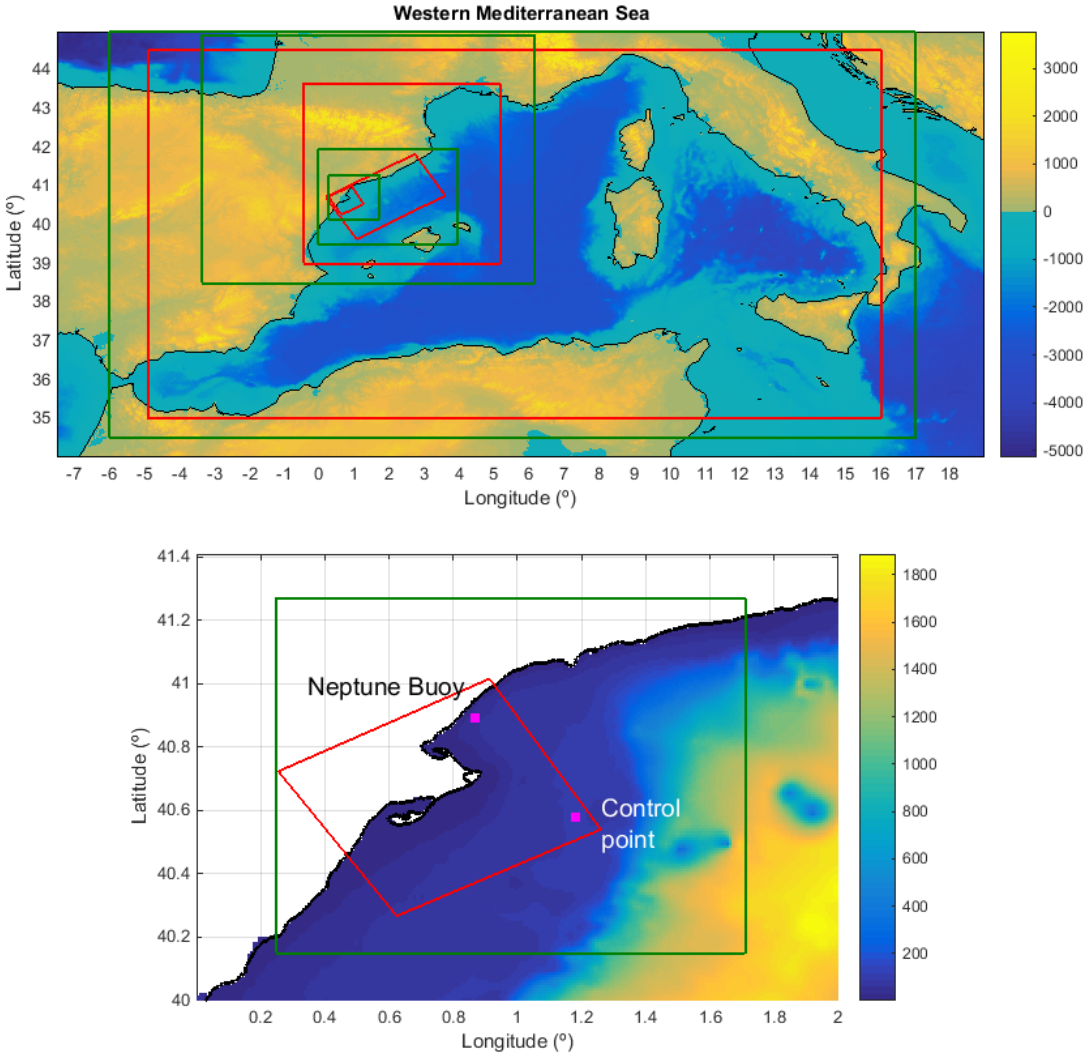

Figure 4.4: Orography and bathymetry of the study area (top). The red boxes represent the SWAN and ROMS meshes and the green boxes the WRF domains for the two-way episodes (resolutions detailed in table 4.3). In the bottom the Ebro delta domain is represented and the Neptune buoy and control point locations marked with pink dots.

During the wind jet event two evaluation locations are considered to compare the results for the sensitivity test simulations. One point corresponds to the Neptune buoy position (where the numerical results are also compared with the measure-

ments) and the second point is located 30 km offshore of the measurement point (see control point in figure 4.4). This point has been chosen in order to capture the wave growth due to off-shore winds and evaluate properly the coupling - uncoupling differences

Additionally satellite-measured winds are used for the numerical model validation. Sea wind intensity and direction were obtained from the National Climatic Data Center (NCDC- NOAA, http://www.ncdc.noaa.gov/oa/rsad/air-sea/seawinds.html). This product is the result of a spatial and temporal interpolation of the data received from the different satellites passing through the study area during a time interval, with a 6 h time resolution and 15 km spatial resolution.

The bathymetry used in all the episodes tested is obtained from GEBCO (General Bathymetric Chart of the Oceans, www.gebco.net) with a grid resolution of 30 arc-second (0.0083º).

The system strategy in the two-way coupling is very similar to the one presented previously with an extra curvilinear grid located in the Ebro Delta with a spatial resolution of 250 m and nested to the Catalan Coast grid (table 4.2). The main purpose of this local grid is to implement the ocean-atmospheric-wave two-ways coupling because is in the coastal areas where the scale of the coupling process may be more evident in the results.

Table 4.2: Description of the grids implemented in SWAN for the Catalan coast. The Ebro Delta grid is only valid for the two-ways coupling episodes.

	Western Mediterranean Sea	Balearic Sea	Catalan Coast	Ebro Delta
Longitudes	4.90º W 16.05º E	0.45º W 5.26º E	0.17º E 3.59º E	0.25º E 1.26º E
Latitudes	35.00º N 44.52º N	39.00º N 43.66º N	39.63º N 41.83º N	40.27º N 41.03º N
Mesh size	196 x 119	160 x 174	208 x 106	253 x 226
Grid Resolution	9 km (0.107º x 0.081º)	3 km (0.035ºx0.027º)	1km (mean value)	250m (mean value)

In the two-way coupling exercises the WRF atmospheric model and the ROMS circulation models run simultaneously to the SWAN model, providing the forcing for the wave model. In table 4.3 a description of the downscaling system of meshes used in the two-ways coupling episodes is presented.

Table 4.3: Resolution of the different domains used in the two-ways coupled system as a function of each model and regional scale.

Model	Western Mediterranean Sea	Balearic Sea	Catalan Coast	Ebro Delta
WRF	27 km	9 km	3 km	1 km
SWAN	9 km	3 km	1 km	250 m
ROMS	-	-	1 km	250 m

The water circulation system for the study area consist of two domains, matching the Catalan Coast and Ebro Delta wave domains (table 4.2). The largest oceanic domain is nested into the daily MyOcean-MEDSEA product (Tonani et al., 2014), with a horizontal resolution of 1/16 º x 1/16 º and 72 unevenly spaced vertical levels, in order to provide suitable boundary conditions for the oceanographic variables in terms of water velocity, sea level, temperature and salinity.

The Western Mediterranean Sea atmospheric model is nested into the ECMWF ERA-Interim reanalysis product (www.ecmwf.int) considering four downscaling meshes, with resolutions of 27km, 9km, 3km and 1km respectively, to obtain suitable grid resolution for the complex orography of the region (figure 4.4).

In the COAWST system designed for the Ebro delta domain the information between models is exchanged every 10 min of simulated time. The computer used to run the coupled simulations belongs to the Centro de Investigaciones Energéticas, Medioambientales y Tecnológicas from the Spanish Government (CIEMAT, www .ciemat.es) and has 48 processors available that were distributed as follow: 32 processors to run the WRF meteorological model, 8 processors to run the ROMS circulation model and 8 processors to run the SWAN wave model. The distribution was designed to minimize the waiting time between the different models on the instant when the information is exchanged.

4.4 Analysis of the results

As previously mentioned, the chapter is divided in two sections. In the first one the effects of the currents on the wave modelling are considered while in the second one a two-way coupling between the wave model and the circulation and atmospheric model is performed.

The results are presented following the same structure, including two episodes, a calm period and an intensification event, for each section.

4.4.1 One-way coupling: The effect of the currents on wave simulation

Calm period

A period longer than 5 weeks is simulated with the SWAN model in the Catalan coast domain using the configuration defined in chapter 3 and compared with measurements from a buoy moored in front of Barcelona Harbour (Llobregat buoy from table 3.1). Additional simulations are carried out in which the effect of the ambient currents is considered in the wave generation and propagation. The time series resulting from this comparison are presented in figure 4.5, where the significant wave heigh, the mean wave period (Tm_{02}), and the mean wave directions are shown. In order to perform a cuantitative comparison several stadistical parameters are computed for the same variables and displayed in table 4.4.

During the study period the waves mainly come from east and south directions, with relatively small significant wave height except from the first week when a storm hit the coast reaching up to 2.5 m significant wave height. At the same time, the surface currents during the period are not very important (figure 4.6), travelling in southwest direction and showing a maximum intensity of 40 cm/s, so the interaction between the two fields can be disregarded as observed from figure 4.5 and table 4.4.

In fact, from the statistics shown in table 4.4 it seems that the coupled system could be performing slightly worse than the SWAN model, mainly for the mean wave period and the mean wave direction. This difference may be due to the accuracy of the current fields, not easy to predict due to their low intensity. The current fields for the selected period are validated in Grifoll et al. (2013) in two different locations near our buoy, showing an acceptable agreement with the observations in the prevalent along-shelf direction, with correlation coefficients between 0.5 and 0.7, but more discrepancies in the across-shelf direction, with correlation coefficients

between 0.4 and 0.6. Nevertheless, these current fields are the best among availabe to us.

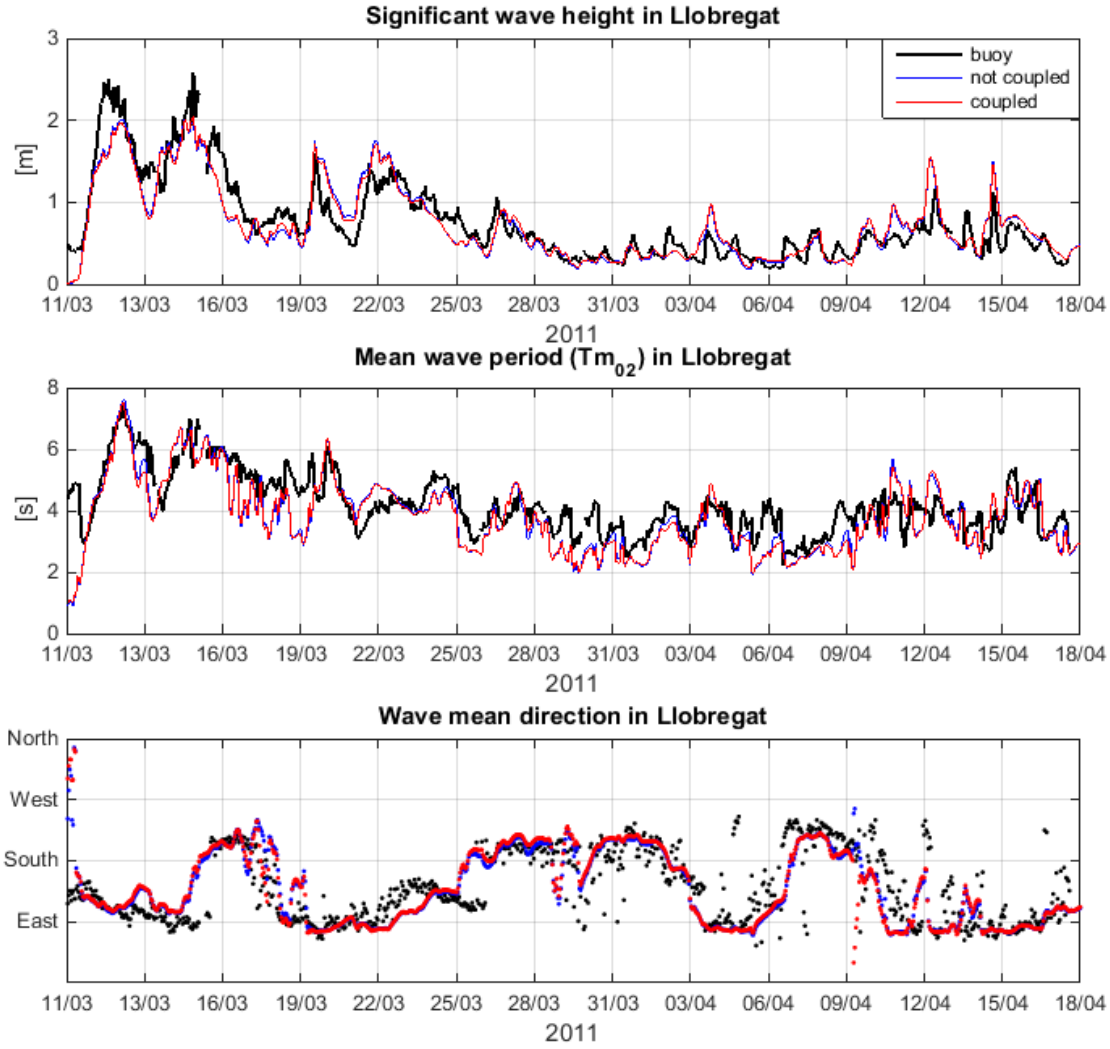

Figure 4.5: Time series of the significant wave height, the mean wave period (Tm_{02}) and the mean wave direction for the 11th of March to the 18th of April 2011. In black the buoy measurement is represented, in blue the results of the not coupled SWAN model in the buoy location and in red the results of the one-way coupled system.

Table 4.4: Statistics for the comparison between buoy measurements and model outputs.

	RMSE	Bias	R
Hs (no coupled)	0.24 m	-0.01 m	0.85
Hs (coupled)	0.24 m	-0.01 m	0.85
Tm_{02} (no coupled)	0.84 s	0.22 s	0.73
Tm_{02} (coupled)	0.85 s	0.25 s	0.72
Dir (no coupled)	39.95 º	-	0.67
Dir (coupled)	41.77 º	-	0.64

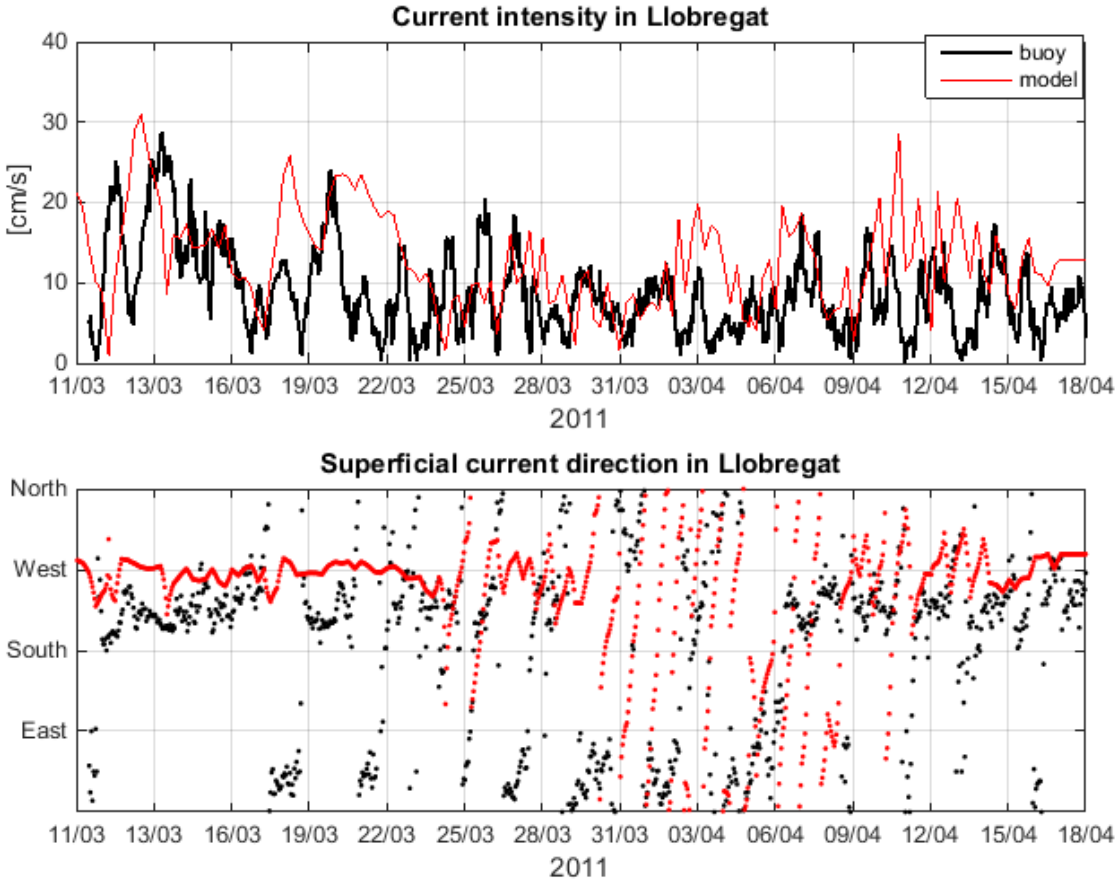

Figure 4.6: Time series of the surface current intensity and the current direction for the 11th of March to the 18th of April 2011. In black the buoy measurement is represented and in red the model results used as forcing for SWAN in the one-way coupling exercise in the buoy location.

Energetic event - current intensification

A current intensification event is studied in order to analyse the effect of the unusual superficial currents in the area on wave modelling. The results for an entire month are presented in figure 4.7, where a comparison between the SWAN simulations, the buoy measurements in a buoy located in front of Barcelona Harbour, and the one-way coupling SWAN simulation are presented. The variables represented are the significant wave height, the mean wave period (Tm_{02}) and the mean wave direction, and the energetic event is identified by the shaded area.

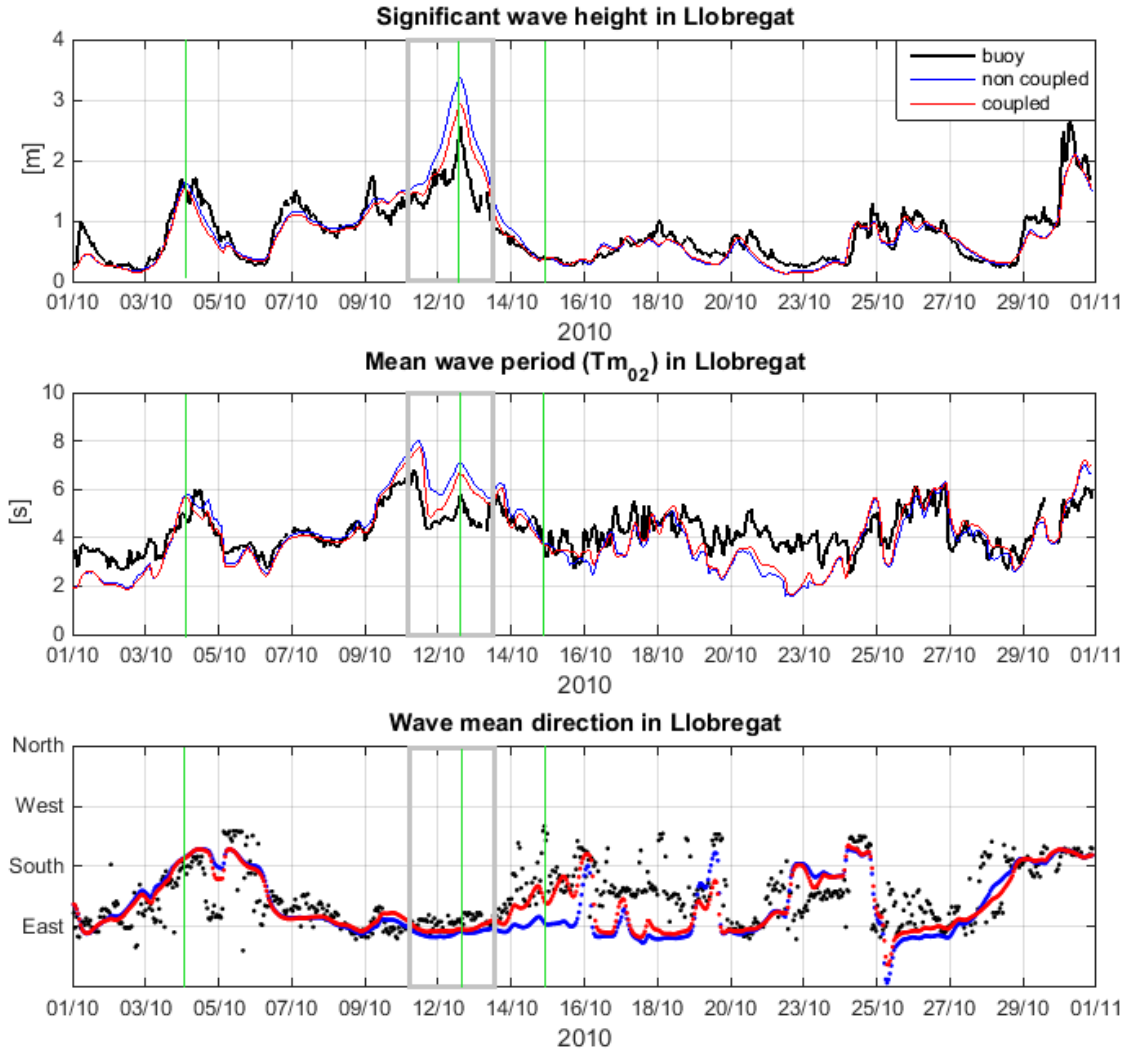

Figure 4.7: Time series of the significant wave height, the mean wave period (Tm_{02}) and the mean wave direction for October 2010. In black the buoy measurement is represented, in blue the results of the not coupled SWAN model in the buoy location and in red the results of the one-way coupled system.

During the event considerable differences can be seen between the uncoupled

SWAN simulation and the one-way coupled SWAN simulation. The significant wave height presents a decrease up to 0.5 m with the coupling, obtaining better adjustments with the buoy measurements. A similar behaviour is detected on the mean wave period (Tm_{02}), where reductions of more than one second are observed, and on the mean wave direction during the current intensification event.

The superficial currents used for the one-way coupling during the entire event are presented in figure 4.8 and compared with the buoy measurements available in both current intensity and direction. From the graphics it can be observed that the time variability of the model data is lower than the buoy measurements, with a temporal resolution of 6 h in comparison with the hourly information from the buoy measurements. Additionally, the current intensification seems to be quite well captured in time but not in magnitude, with a maximum current intensity of 104 cm/s instead of the 139cm/s recorded by the buoy. Despite the poor accuracy of the current field, the results of the one-way coupling are considerably better than those corresponding to the non-coupled simulations, as shown in figure 4.8.

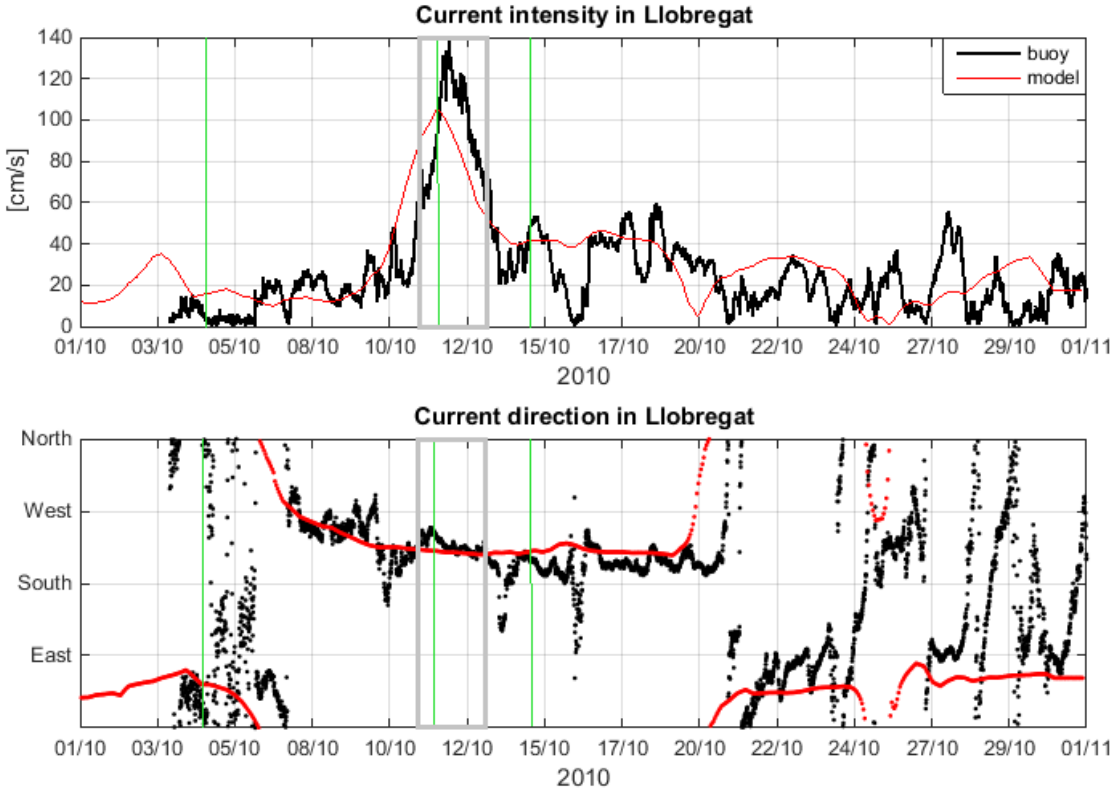

Figure 4.8: Time series of the surface current intensity and the current direction for October 2010. In black the buoy measurement is represented and in red the model results used as forcing for SWAN in the one-way coupling exercise for the Llobregat buoy location.

In order to analyse the effect of the coupling during the current intensification,

not only in one point but in all the study area, several snapshots corresponding to instants previous to the event (figure 4.9), during the energetic event (figure 4.10) and after the event (figure 4.11) are presented, and marked in figures 4.7 and 4.8 with a green vertical line. The significant wave height distribution from the uncoupled model is compared with the one-way coupled model in the top graphics, while in the bottom graphics the current intensity on that moment is represented together with the difference between the not coupled modelled significant wave height field minus the coupled modelled significant wave height field.

The first instant selected, represented in figure 4.9, corresponds to a situation with a relatively high significant wave height (1.7 m) but with currents within the usual magnitude, while the second instant (figure 4.10) represents the specific situation during the maximum current intensification.

Just after the current intensification event a refraction process due to the currents seems to occur. In figure 4.11 the significant wave height comparison between the one-way coupled model and the SWAN results is performed, with almost no differences between the two fields. In contrast, figure 4.12 shows the comparison between the mean wave direction, showing important variations due to the wave refraction. The current field is represented in the lower-left box, not as intense as in figure 4.10 but still presenting higher superficial current intensities than usual, and the wind field is represented in the lower-right box, showing a not very intense wind jet event.

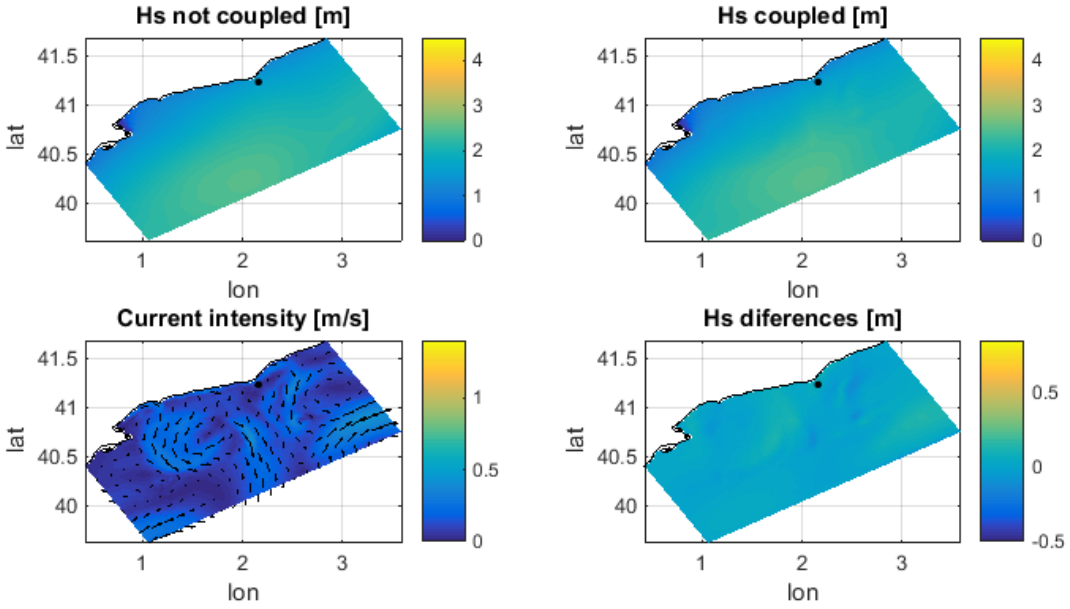

Figure 4.9: Surface current intensity (bottom-left), significant wave height distribution from the SWAN model (top-left) and the one-way coupled SWAN (top-right) and the difference between them (bottom-right) for a time step before the flow intensification: 4th of October 2010 - 06:00h. The Llobregat buoy location is represented with the black dot.

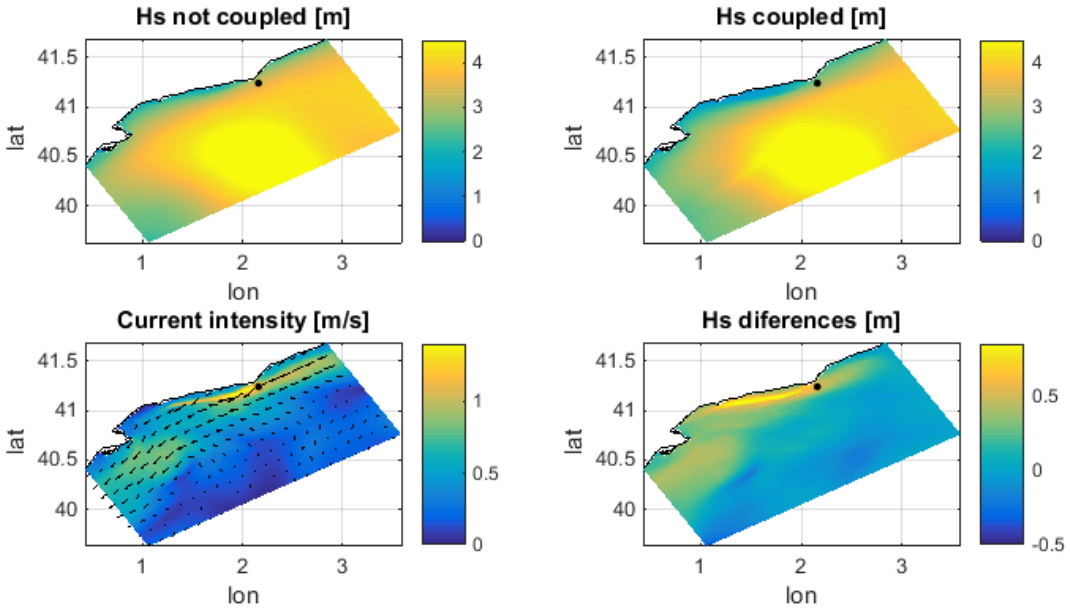

Figure 4.10: Surface current intensity (bottom-left), significant wave height distribution from the SWAN model (top-left) and the one-way coupled SWAN (top-right) and the difference between them (bottom-right) for the peak of flow intensification: 12th of October 2010 - 12:00h. The Llobregat buoy location is represented with the black dot.

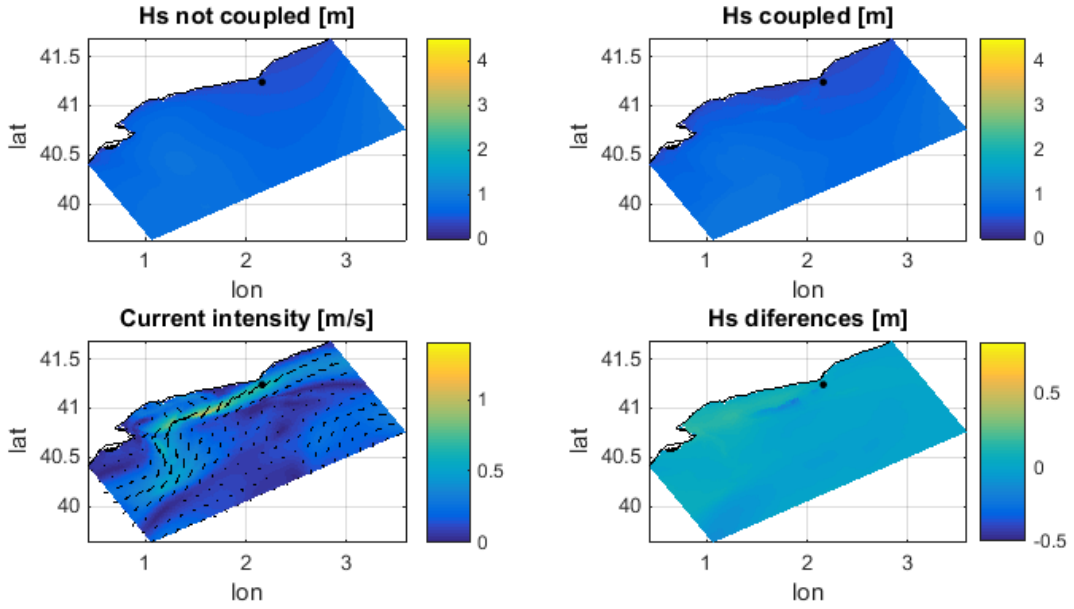

Figure 4.11: Surface current intensity (bottom-left), significant wave height distribution from the SWAN model (top-left) and the one-way coupled SWAN (top-right) and the difference between them (bottom-right) for a time step after the flow intensification, when a refraction process due to currents took place: 15th of October 2010 - 00:00h. The Llobregat buoy location is represented with the black dot.

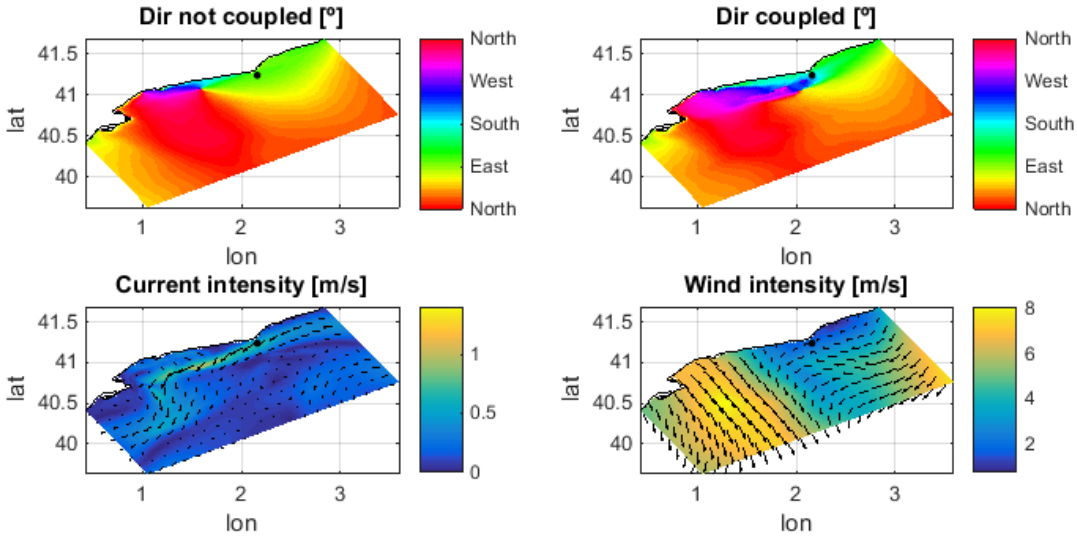

Figure 4.12: Mean wave direction distribution from the SWAN model (top-left) and the one-way coupled SWAN (top-right), surface current intensity (bottol-left) and wind intensity (bottom-right) for a time step after the flow intensification, when a refraction process due to currents took place: 15th of October 2010 - 00:00h. The Llobregat buoy location is represented with the black dot.

4.4.2 Two-ways coupling: Ocean-Atmosphere-Wave characterization

Yearly results

In figure 4.13, three time series comparing the results obtained from the coupled SWAN model (for the Catalan coast domain) and the no coupled SWAN model on the NEPTUNE buoy measurements (see position in figure 4.4) are shown, for a period of three months, between the 1st of January 2012 to the 31st of March 2012. The time series comparison corresponds to the significant wave height, the mean wave period (Tm_{01}) and the mean wave direction. In general, the model reproduces the observations in terms of mean behaviour and variability.

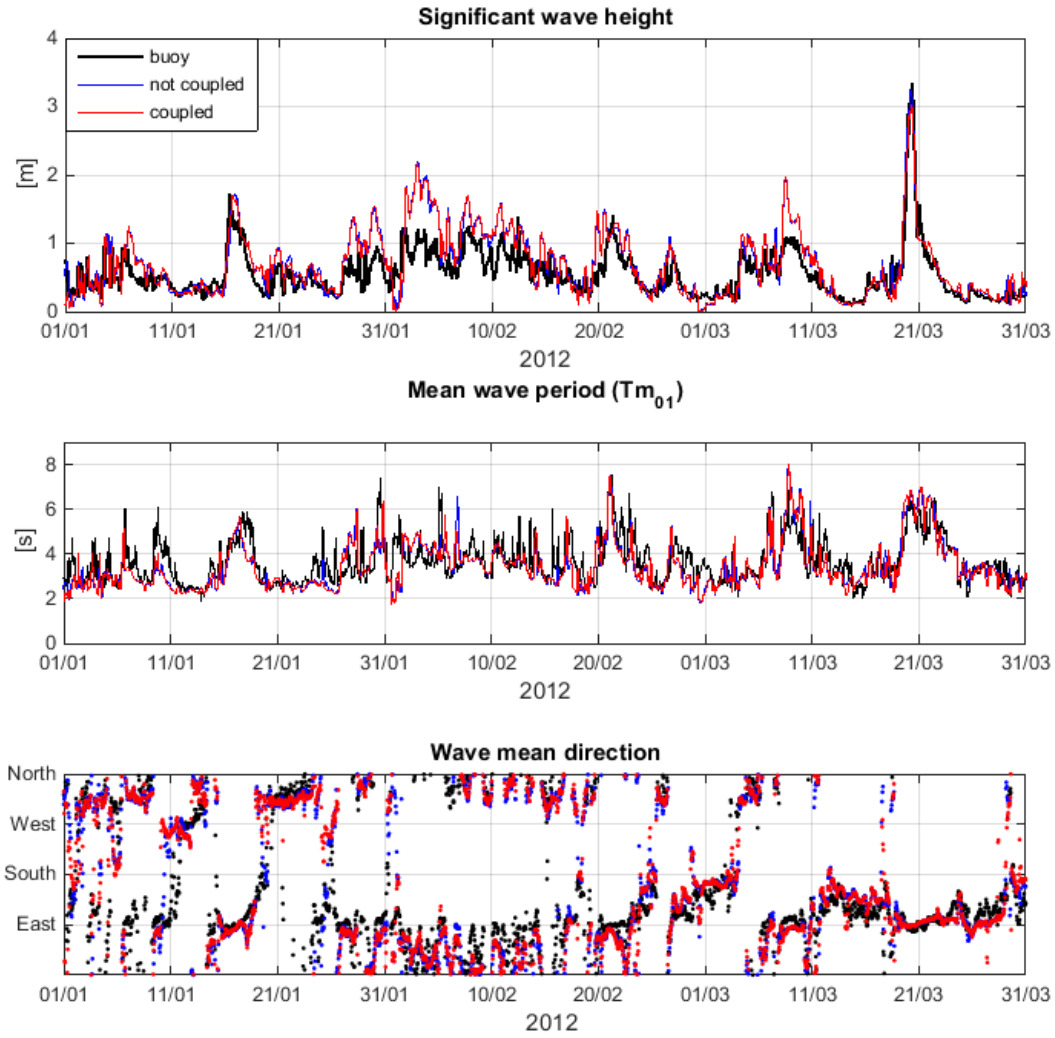

Figure 4.13: Time series of the significant wave height (m), the mean wave period Tm_{01} (s) and the mean wave direction for the first trimester of 2012. In black the buoy measurement is represented, in blue the results of the not coupled SWAN model in the buoy location and in red the results of the coupled system.

Table 4.5 presents the error statistics for the whole year for mesh Catalan coast domain in terms of significant wave height, mean wave period (Tm_{01}) and mean wave direction

Table 4.5: Statistics for the comparison between buoy measurements and model outputs for the two-way coupling exercise.

	RMSE	Bias	R
Hs (no coupled)	0.28 m	0.07 m	0.76
Hs (coupled)	0.29 m	0.09 m	0.75
Tm_{01} (no coupled)	0.84 s	-0.05 s	0.58
Tm_{01} (coupled)	0.83 s	-0.06 s	0.57
Dir (no coupled)	48.99 º	-	0.47
Dir (coupled)	47.60 º	-	0.51

Since the coupling is performed in a two-way manner, also the wind fields and the currents are modified and thus shown.

Modelled winds during the simulation period reproduce the main wind directions previously reported in the study area. The representation of the yearly wind time series in a histogram and the adjustment of these into a Weibull distribution is used to evaluate the statistical inter-comparison between wind observations (measured from the buoy and satellite) and the 3km WRF model results (Catalan coast domain). Blended Sea Winds are used from the NCDC-NOAS SeaWinds project which contain 6-hourly globally gridded, high-resolution ocean surface vector winds and wind stresses on a global 0.25º grid. Figure 4.14 shows the histograms and the Weibull distributions considering the wind intensity time series.

A snapshot of the SeaWinds product is compared with the numerical outputs in figure 4.15. Wind patterns from both products present a significant level of agreement in both components assuming the coarser resolution of the SeaWinds. Additional verification is presented in table 4.6 using model- observation statistics in terms of wind intensity for the whole year of 2012. In summary, modelled winds show an acceptable level of agreement with the observations. Small differences can be observed between the coupled and the not coupled systems, as physically expected since most of the time the annual wave conditions are not significant enough to modify the wind stress due to variations in the sea surface roughness.

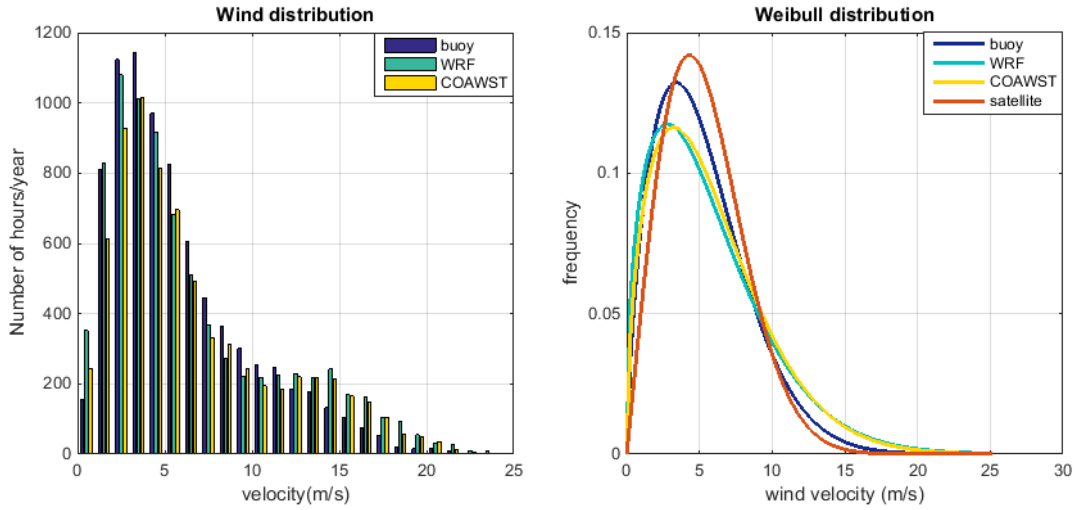

Figure 4.14: Weibull distribution adjustment for the wind velocities regarding the duration for the 12 months analysed.

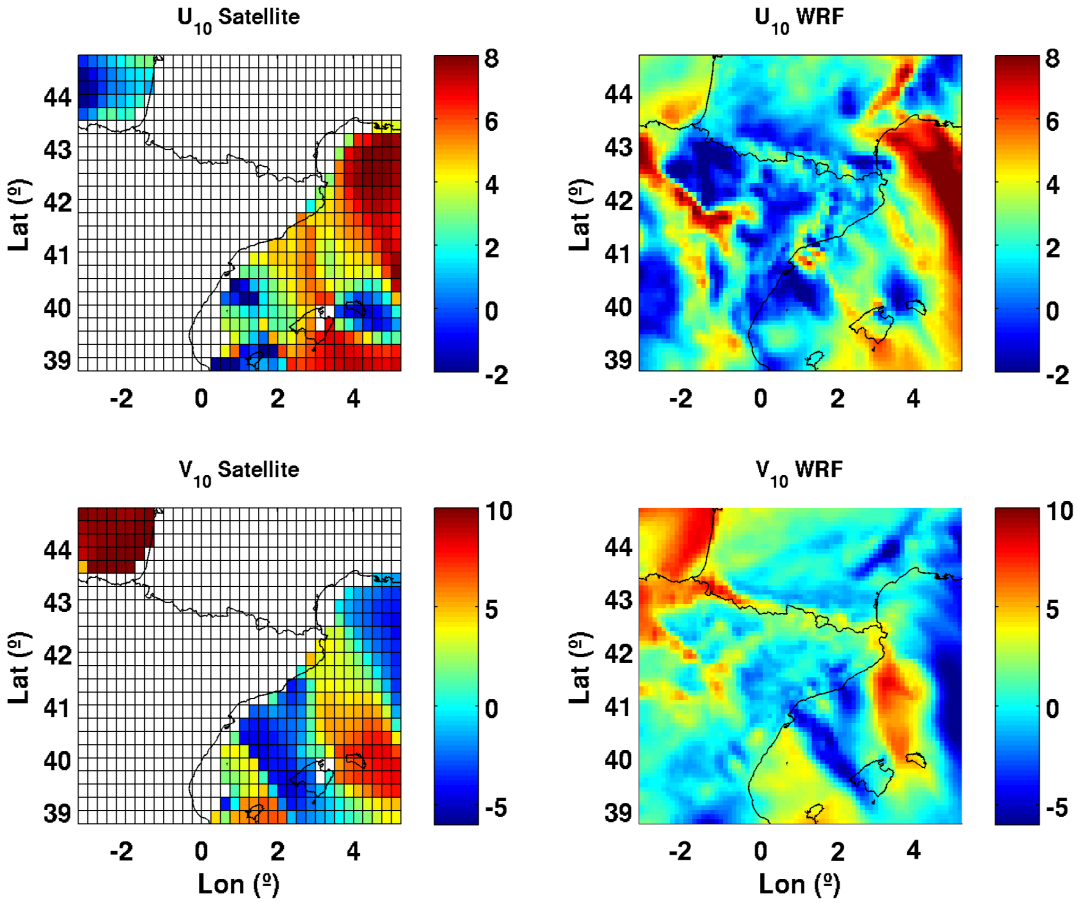

Figure 4.15: Wind components (top: east—west; bottom: north—south) from the satellite gridded product for the study area (left) and from the results of the meteorological model (right). The figure corresponds to 1st of January 2012 at 12:00 UTC.

Table 4.6: Statistics for the comparison between buoy measurements and model outputs. W is the wind intensity.

	Mean	RMSE	Bias	R
W (no coupled)	6.60 m/s	3.20 m/s	0.69 m/s	0.78
W (coupled)	6.59 m/s	2.70 m/s	0.68 m/s	0.79

Table 4.7: Statistics for the comparison between buoy measurements and model outputs. C is the depth-averaged along-shelf currents.

	Mean	RMSE	Bias	R
C (no coupled)	-4.60 cm/s	3.07 cm/s	2.14 cm/s	0.82
C (coupled)	-4.32 cm/s	2.98 cm/s	3.56 cm/s	0.85

The skill assessment of the numerical results in terms of current intensity was carried out following a similar scheme to the one used for winds and waves. The velocity field in the area of study tends to polarize following the along-shelf and cross-shelf direction. In consequence, the comparison of the water velocity measured and modelled is carried out considering the along-shelf and cross-shelf velocity. The numerical model validation with ADCP observations shows an acceptable level of agreement according to the comparison for the entire 2012. Table 4.7 presents the error statistics for the depth-averaged velocity measurements compared with the numerical model results.

Energetic event - wind jet

The two-way coupling yearly results show minimum differences with the not coupled simulations. To evaluate the two-way coupling during energetic events the wind jet occurring in front of the Ebro Delta from the 20$^{\text{th}}$ of May to the 24$^{\text{th}}$ of May 2012 is analysed.

The wind jet presents a wind intensity up to 20 m/s from the north-west direction. In figure 4.16 the measured wind intensity 10 meters above the sea surface and the mean wind direction are represented and compared with the model results (both the WRF results and the two-way coupling COAWST results). From the graphics it is easy to state that an important improvement is observed for the coupled system in comparison with the original wind fields, mainly for the wind intensity. So it can be stated that is for energetic enough events when the coupling improves the results.

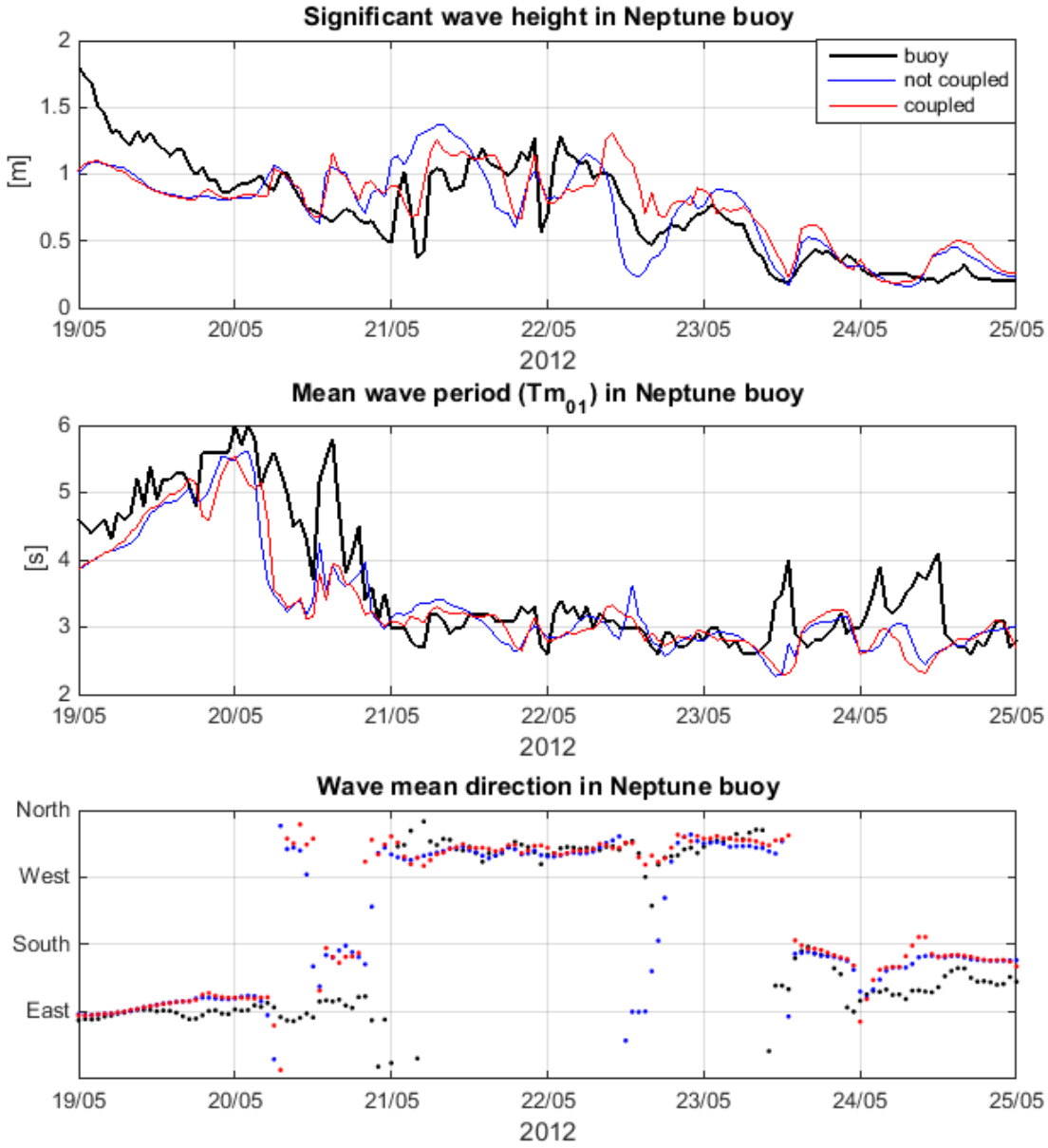

Figure 4.16: Time series of the wind intensity at 10 m above the sea surface and the wind direction for the wind jet event. In black the buoy measurement is represented, in blue the results of the not coupled WRF meteorological model in the buoy location and in red the results of the coupled system.

In the figure 4.16 the time evolution of the measured significant wave height, mean wave period (Tm_{01}) and mean wave direction during the wind jet event are represented and compared with the results from the SWAN model (in blue) and the coupled COAWST system (in red) during the wind jet event. It is interesting to remark that due to the wind intensity the waves generated by the offshore wind change the direction to match the wind direction.

In contrast with the results obtained in section 4.4.2, in which the coupling

showed almost no effect, during the wind jet event some differences can be noticed between the SWAN and the two-way coupling results, with variations of the significant wave height up to half meter. During the calm period (at the beginning and the end of the wind jet event) the differences are not appreciable.

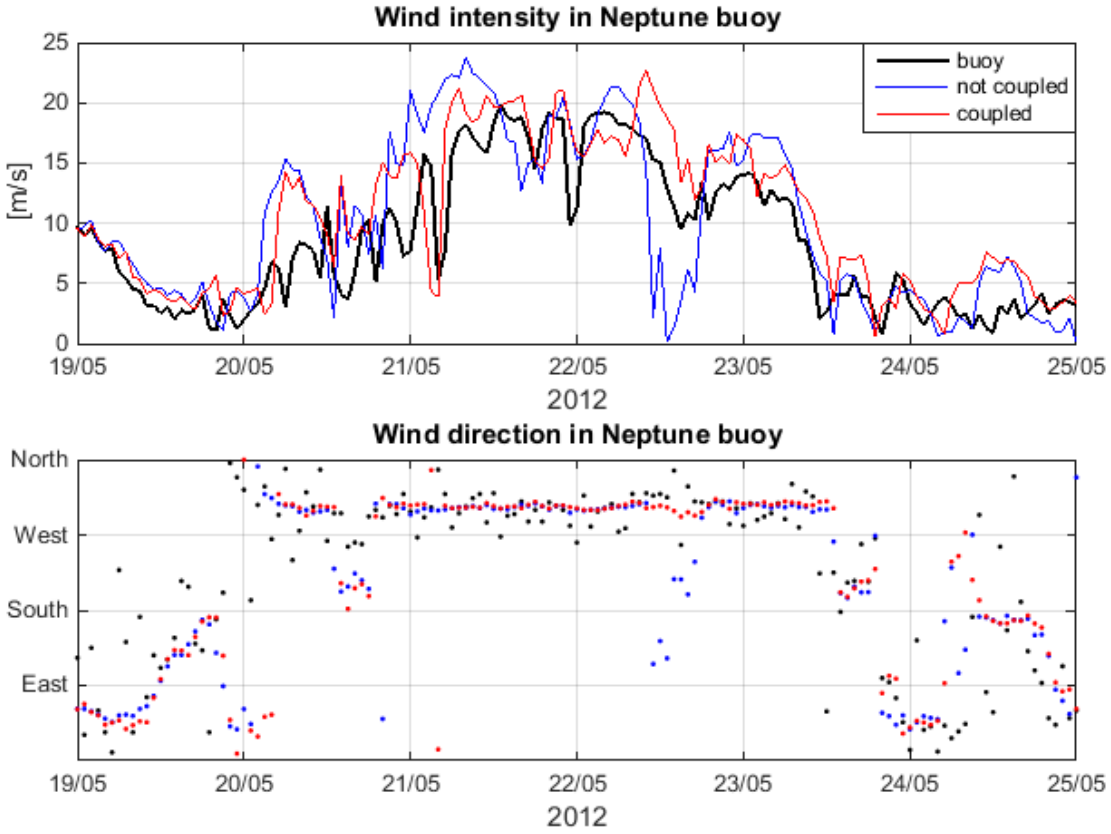

Figure 4.17: Time series of the significant wave height (m), the mean wave period Tm_{01} (s) and the mean wave direction for the wind jet event. In black the buoy measurement is represented, in blue the results of the not coupled SWAN model in the buoy location and in red the results of the coupled system.

The figure 4.18 (right) show a snapshot of the wave's directional spectrum from the two-way coupling system during the wind jet period at the Neptune buoy location; the results reveal the tendency to develop bimodal directional spectrum due to the co-existence of sea and swell waves. Directional spectrum presents a peak around 315º (waves from north-west) associated with the growing wave due to the wind jet and another peak around 135º (waves from south-east) associated with the swell. In figure 4.18 (left) the directional spectrum for a period without wind jet is also shown for comparison.

In summary, the high-resolution mesh (Ebro Delta domain) is able to capture the bimodal spectrum during wind jet. Unfortunately, only the statistical spectral

parameters were recorded in the buoy measurements, so full spectrum comparison is not possible.

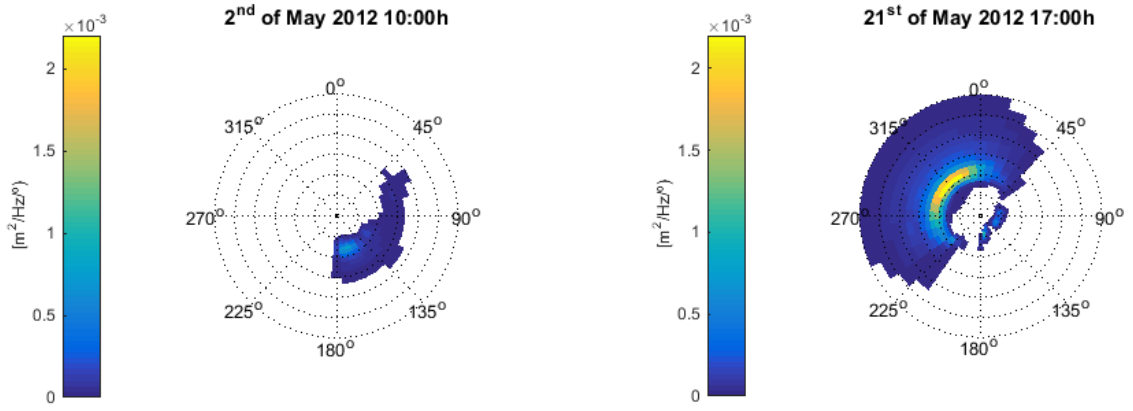

Figure 4.18: Numerical wave spectrum for two different instants at the observation point: before the wind jet event (left; 2nd of March 2012) and during the wind jet (right; 21st of March 2012). The radius represent the frequencies: 0.01-0.18-0.34-0.5-0.67-0.84-1.0 Hz.

Additionally, for the wind jet energetic event a sensitivity test is carried out in order to better understand the air-sea momentum transfer between the wind and the waves in the boundary layer. The study is carried out in two different locations, the Neptune buoy point and a control point located offshore, as previously mentioned.

The wind intensity and the significant wave height from the four simulations, for both the control and buoy points, are compared among them and with observations when available. The results of the numerical simulations (not shown) reproduce the wind intensity and the significant wave height with a similar level of agreement. The not coupled (CHK) and coupled simulations (T-Y, OOST and DRE) only present differences in the numerical outputs during the jointly occurrence of strong winds and wave peaks, being more important for the control point, located further away the coast and so with longer fetch.

Comparing the error statistics for the measurement location among the three coupled numerical simulations it cannot be assured which formulation ensures a better skill assessment (table 4.8). Although DRE sensitivity case presents a slightly better agreement at the buoy location, the relative size of the wind intensity and significant wave height limit the conclusions for the wind jet event. More extensive studies, including similar situations in the area, would be necessary to obtain conclusive findings.

Table 4.8: Statistics for the comparison between buoy measurements and model outputs during the wind jet event, from the 20th to the 24th of May 2012. Hs is the significant waves height and W is the wind intensity.

		Mean	RMSE	Bias	R
Observation	Hs	0.74 m	-	-	-
	W	10.93 m/s	-	-	-
T-Y	Hs	0.72 m	0.26 m	-0.02 m	0.61
	W	11.51 m/s	4.83 m/s	0.58 m/s	0.61
DRE	Hs	0.72 m	0.26 m	-0.02 m	0.62
	W	11.46 m/s	4.79 m/s	0.53 m/s	0.61
OOST	Hs	0.72 m	0.26 m	-0.02 m	0.61
	W	11.47 m/s	4.85 m/s	0.54 m/s	0.60

4.5 Discussion

In the present chapter the effects of the coupling between the wave model and a circulation and an atmospheric model are analysed for the Catalan coast. Two different types of coupling are considered.

On one hand, the one-way coupling (also known as off-line coupling) is carried out. For the one-way coupling only the effect of the ambient currents is introduced into the SWAN wave model. No reference to the atmosphere-wave one-way coupling is made because the only variable obtained from the atmospheric model that can be introduced into the wave mode is the wind intensity, already introduced in SWAN, so there is no option to execute a one-way coupling between the wave model and the atmospheric model.

The results obtained from the first exercises conclude that, during calm periods and even during storm events reaching the coast with significant wave height up to 2.5 m, if the superficial current intensity is not exceptional, there are no appreciable differences between considering or not the current effect on the wave modelling in any of the variables analysed. During the period selected the mean current was around 20 cm/s, a typical value for the area, and the direction was from the east and south-east, matching the direction of the waves, so no refraction occurred.

The behaviour of the two models is statistically quantified in table 4.4, where no differences between the significant wave heights computed considering or not the currents can be noticed, physically expected due to the low current intensity (around 10-20 cm/s) compared with the wind intensity (around 8-10 m/s, two orders of magnitude bigger). For the mean wave period (Tm_{02}) and the mean wave direction slightly differences can be observed between the two models, getting worse results when including the currents effect on the wave modelling. This may be due to the lack of ability of the circulation model to reproduce the currents measured in the area, both in intensity and in direction.

In conclusion, during most of the time, with the conditions typical of the Catalan coast, it is not necessary to introduce the currents field as an input for the wave model. Besides, if one is interested in introducing them anyway it is important to have very accurate currents fields in order not to deteriorate the wave simulation.

In contrast with the previous results, during a current intensification the situation is the opposite. As stated by some other authors in different parts of the world (Jorda et al., 2007; Warner et al., 2008b; Zambon et al., 2014), when the magnitude of the superficial current is more intense than usual, for example due to a flow intensification or during an important storm or hurricane, the effect of the coupling cannot be omitted.

In this sense, the figure 4.9 shows a typical situation, with current intensities around 20 cm/s and significant wave height of 1.7 m in the buoy location. Under these conditions the differences between the SWAN simulations considering or not considering the current field are inappreciable. In contrast, during the peak of the flow intensification analysed, with current fields up to 140 cm/s and significant wave heights around 2.5 m the differences are much more appreciable. The significant wave height variations are located in the current intensification domain (figure 4.10) due to the wind stress modification in this area. Since the direction of wind and waves agree, the relative velocity of the wind to the ocean decrease (see equation 4.1), reducing the wind stress and thus the significant wave height and the wave period.

Another process detected just after the current intensification is a refraction process due to residuary currents in the area and an off-shore wind event. In figure 4.11 the significant wave height for the 15^{th} of October 2010 is represented, both for the SWAN model not considering and considering the current effect, with almost no differences. However, when looking at the wave direction (figure 4.12) it is possible to see some discrepancies between the two model results. The wind pattern for these days presents an off-shore jet affecting the southern part of the Catalan coast domain that tends to modify the angle of the waves in the same direction. The current field is also affected by the off-shore wind, and presents an area between the coast and the current intensification where the direction of the flow turns to the east and south-east. In the not coupled model the mean wave direction in the area is determined by the off-shore wind while in the one-way coupled system the wave field coming from the east is partially refracted by the opposite currents and tends to turn to the south, in accordance to the buoy measurements represented in figure 4.11.

In conclusion, introducing the current fields into the wave model (in a one-way coupling way) is only interesting when the magnitude of the current is one order of magnitude higher than usual (around 100 cm/s in the study area). Even when a storm event is reaching the coast the effect of the coupling is not important unless the current magnitude is also intensified.

For the Catalan coast the current intensifications take place in delimited areas (e.g. southerly of the Barcelona harbour due to the local stretch of the shelf and a persistent wind blowing from the east). As detailed in Mestres et al. (2016), the flow intensifications take place around four or five times a year with a duration between 24 h and 48 h. During these specific events is when the one-way coupling between the wave model and the current field will be very beneficing for the wave simulation. During the rest of the year the effects of the currents can be omitted.

On the other hand, the two-way coupling is considered. In this type of coupling

the wave, circulation and atmospheric model are involved, running in parallel and sharing information (variables mentioned in table 4.1) between models every several time steps.

The wave simulation results from the yearly analyse, resumed in table 4.5, support the conclusions previously obtained. The differences between the coupled COAWST system and the SWAN model are almost inexistent for the significant wave height, the mean wave period and the mean wave direction. Similar deductions are obtained for the wind field (table 4.6) and the current field (table 4.7), also analysed due to their relevance in the coupling. For both variables a slightly improvement of the statistical parameters is obtained with the coupling, but almost negligible.

During the wind jet event the wave model is able to reproduce the bimodal spectrum (figure 4.18) despite there are no spectra measurements in the area to validate the results. The shape of the wind jet modelled is benefited by the high resolution meshes used. According to the results obtained from both the coupled and the not coupled systems, the wind jet approximately covers an area of 50 km width offshore. In this sense, high-resolution meshes used in this investigations are suitable for an accurate wind jet modelling.

Several investigations have found the importance of the sea state in the impact on the air-sea momentum flux mainly during energetic events; in particular the calculations based on the Charnock constant underestimated the air-sea momentum transfer (e.g Janssen, 1989; Janssen and Viterbo, 1996; Drenann et al., 2003) which can be significant under mixed seas (Sanchez-Arcilla et al., 2008). In the northern margin of the Ebro delta and during the wind jet, minor differences were found when comparing the significant wave height and the wind intensity between numerical model and observations.

The detailed analysis of the event showed that when the coupled results (T-Y, OOST and DRE) are compared versus the CHK results (table 4.8), the wind intensity at the measurement location is affected by the sea state during the jointly occurrence of strong winds and wave peaks. For the coupled simulations the wind intensity is reduced due to wave-induced sea surface roughness increasing (figure 4.16). This behaviour is consistent with other coupling atmosphere-ocean investigations under a high level of meteorological energy (e.g Olabarrieta et al., 2012). In parallel, the wave field is modified by the feedback between wave and wind stress, reducing the significant wave height (figure 4.17).

4.6 Conclusions

The coupling between waves, ocean and atmospheric models has been one of the main topics in the scientific community for the last decade. The effect of this coupling on the wave simulation is analysed in this chapter for the Catalan coast area.

Two different types of coupling are considered, the first is the simplest one, a one-way coupling consisting in introducing the current field as an input for the SWAN wave model, and the second one consist in running in parallel the ROMS circulation model, the WRF atmospheric model and the SWAN wave model. This second option requires an important computational capacities, not always available.

From the four different situations studied the main conclusion extracted is that during most of the time, with the calm conditions typical of the Catalan coast, it is not necessary to consider the coupling in any of its forms to provide accurate wave simulations. Even when a storm event is reaching the coast the effect of the coupling is not important unless the current magnitude is also intensified.

Then, the coupling is only interesting during specific energetic local events like wind jet events or current intensifications.

During the wind jets events the numerical results from sensitivity tests have shown the relative relevance of air-sea transfer formulations considering the significant wave height for the sea surface roughness estimation during the wind jet. While for the current intensifications the wind-stress modification and the wave refraction due to the ambient currents are the more significant interactions.

However, both processes are local and punctual in time. For example, the flow intensifications appear four or five times a year, with a maximum duration of 48 hours, that represents around the 2% of the year. Also it is important to remark that, if one is interested in introducing the current effect on the wave simulation anyway it is essential to dispose of very accurate currents fields in order not to deteriorate the previous results.

Chapter 5

Unstructured grids design and validation for wave modelling in semi-enclosed domains

5.1 Introduction

Traditionally, the methodology to improve the resolution of wave forecasting near the coast consists of a downscaling process with a system of nested domains, each with a smaller resolution and covering a smaller area than the previous one (e.g Sanchez-Arcilla et al., 2014; Alomar et al., 2014; Alari et al., 2008), where the required boundary conditions are provided by the coarser mesh.

An alternative to this methodology consists in using an unstructured grid. The main advantage of using an unstructured grid for wave modelling is that it allows working with a single grid with different resolutions at each sub-domain, thus improving the resolution in coastal areas, and therefore the nesting is not needed. Another advantage is that the unstructured grid is able to reproduce the sharp coastline and the areas around islands more accurately than regular meshes (Zijlema, 2010). Finally, unstructured grids allow indirectly what is known as two-way nesting, where information is transferred not only from the coarser to the finer domain but also in the other direction – a process especially interesting in situations with inland winds, such as the case of the Mistral (nort-west wind) on the Mediterranean coast.

Generating a simple unstructured grid for wave modeling is not a difficult process; just the contour of the study domain and a mesh generator (e.g Bilgili et al., 2006; Shewchuk, 2002) are needed. Nevertheless, special attention should be payed to the grid design in order to optimize the triangle's size and its distribution in the study area. For this purpose two different criteria to design an unstructured grid efficiently

are presented, reducing the cell size only when necessary. The first one considers the distance to the coast, where more accuracy is required and hig- resolution winds are provided. The second criterion considers the effect of the bottom on the waves, including the depth, the bathymetric gradient and the level of bottom influence (in terms of a classification into deep, intermediate or shallow waters). Both criteria try to infer/predict where gradients in the wave field are likely to occur.

Once the unstructured grids are designed, sensitivity tests are performed to study the effects of using different spatial resolutions in the wind field for the entire domain. The code used for wave modelling is SWAN, for which the numerical settings also require attention (Zijlema, 2010; Dietrich et al., 2013).

The SWAN model has previously been used to simulate the wave field with unstructured grids (Hsu et al., 2005), mainly coupled with the ADCIRC oceanic model (Dietrich et al., 2011b,a) since it is prepared to work with both types of grids, nested regular systems and unstructured grids, using exactly the same physics. Zijlema (2010) presents and validates the numerical scheme adapted for unstructured grids, consisting of a vertex-based, fully implicit, finite-differences method that requires several sweeps through the grid.

In previous works the unstructured grids for wave simulation have been mainly applied to small domains nested to regional or global grids (Siadatmousavi et al., 2015; Zijlema, 2010; Hsu et al., 2005). In the present study an unstructured grid for a semi-enclosed domain such the Western Mediterranean Sea is designed and compared with a regional unstructured grid nested to a coarser model. The results of the different simulations are validated with measurements from buoys located near the Catalan coast and satellite data for the Western Mediterranean Sea during a one-year period.

5.2 Background: unstructured grids for wave modelling

The use of unstructured grids offers a good alternative to nested models because with them an improvement of the grid resolution near the coast is possible while also removing the internal boundaries and thus the associated complications, both numerical and physical.

In the past decades several studies have been carried out in order to introduce unstructured grids into spectral wave models, most of the time simultaneously to the coupling with a circulation model, since those models have been using unstructured grids for a longer time.

The first spectral wave model that introduced unstructured grids was TOMAWAC (Benoit et al., 1996). TOMAWAC is a third-generation wave model dedicated both to deep water and nearshore applications that uses a finite-elements technique for the spatial discretization in order to better represent complex bottom topographies and irregular shorelines (Benoit et al., 1996). The model was validated during a storm event in the French Atlantic using an unstructured grid varying from 40 km in open seas to 5km in the English Chanel. A few years thereafter Sorensen et al. (2004) created a new Eulerian spectral wave model based on unstructured meshes, the MIKE 21 SW. Using an unstructured finite-volume method for the spatial discretization, the MIKE 21 wave model was validated for a storm event in the North Sea, with grid elements size varying from 15 km^2 to 800 km^2, with very good results (Sorensen et al., 2004).

Roland et al. (2006) and Zanke et al. (2006) presented the Wind Wave Model (WWM) for unstructured grids and validated it for deep and shallow waters, respectively. The WWM model is based on the SWAN wave model, with similar physical formulations but a different numerical scheme, and was verified versus measurement data at the Sargasso Sea, the Baltic Sea and the Pacific Ocean around Taiwan (Hsu et al., 2005) with good results. A few years later the WWM model was coupled to a circulation model developed at the ISMAR-CNR and validated in the Venetian Lagoon (Ferrarin et al., 2008), focused on sediment dynamics, and in the US east coast and the Gulf of Mexico (Roland et al., 2009) during Hurricane Ivan. At the same time, Qi et al. (2009) implemented an unstructured mesh spectral wave model using finite volumes, named FVCOM-SWAVE, and validate it in the Gulf of Maine.

One year later Zijlema (2010) finally implemented a new numerical scheme in the SWAN wave model in order to introduce the usage of unstructured grids, consisting of a vertex-based, fully implicit, finite-differences method. This variant retains the

physics and the numeric as well as the code structure of the regular SWAN model, but it is able to run on unstructured meshes. This model was validated in the Dutch coast by Zijlema (2010) and in the northern Gulf of Mexico by Siadatmousavi et al. (2012); subsequently the unstructured version of SWAN was coupled to the ADCIRC circulation model by Dietrich et al. (2011b, 2012) and validated during several hurricanes in southern Louisiana in an unstructured grid varying from 4-6 km in open waters to 200 m in surf zone zones and 20-50 m in small-scale channels. It was in these works where some instabilities that arise in SWAN when using unstructured grids were detected, but it was not until a few years later that some corrections were proposed by Dietrich et al. (2013).

It is important to highlight that little attention is generally paid to the unstructured grid design for wave models. All the studies presented until now have applied unstructured grids to regional domains, in most of the cases nested to other coarser models. In general, unstructured grids are designed by correlating the size of the elements with the bathymetry (Zijlema, 2010), by determining the grid size as a function of the coastline (Roland et al., 2009) or by improving the grid resolution in some areas as if it were a nesting procedure (Benoit et al., 1996; Hsu et al., 2005). However, no detailed information about the grid design is presented in any of the works.

When focusing on SWAN, the only criteria that an unstructured grid should fulfil in order to be introduced in the model include, firstly, that the number of triangles that meet at each vertex inside the mesh should not be smaller than 4 or larger than 10 and, secondly, that the angles inside each triangle should not be higher than 143º (SWANteam, 2015b), so the Delaunay triangulation is not an indispensable condition. These loose restrictions leave the pressure of a good design of the unstructured grid to the modeller.

Although only limited work has been published about the design of unstructured grids for wave modelling, similar procedures to the one presented here have been generated and applied to generate unstructured grids for circulation models. In this sense Legrand et al. (2000) created a pioneer method to generate global unstructured grids for a circulation model using such criteria as the curvature of the Earth to determine the size of the triangles, thereby properly addressing the coastline boundaries. A few years later the same author improved the method for regional domains, adding some strategies to increase the mesh resolution considering the bathymetric field, an approximated distance to the islands or the tidal wave propagation. The new strategies were applied to the Great Barrier Reef in Australia (Legrand et al., 2006) and to the north-western European continental shelf (Legrand et al., 2007) with good results.

5.3 Methodology

5.3.1 Data available and model set-up

The main data necessary to generate an unstructured grid are the bathymetry and the coastline (also used as the contour of the domain). For the present study the bathymetry has been obtained from GEBCO (General Bathymetric Chart of the Oceans, www.gebco.net) with a grid resolution of 30 arc seconds (0.0083º), and the coast line has been extracted from the National Geographycal Data Center (www.ngdc.noaa.gov/mgg/shoreline).

In order to test the designed unstructured grids, simulations with the SWAN wave model were carried out for a period of one year, corresponding to 2013. For the present study the wind fields have been provided by the Spanish Meteorological Agency (AEMet, www.aemet.es) and include a coarser wind field that provides the wind conditions 10 m above sea level, with a spatial resolution of 0.16 degrees for the entire Western Mediterranean Sea, and a better-resolution wind field that covers only the Catalan coast area, with a spatial resolution of 0.05 degrees (figure 5.1). Both wind fields are obtained using the High Resolution Limited Area Model (HIRLAM; et al., 2002) and have a temporal resolution of 1 h and a forecast horizon of 72 h. In the present study analysed winds have been used for the two resolutions available, herein named HIRLAM 0.16º and HIRLAM 0.05º.

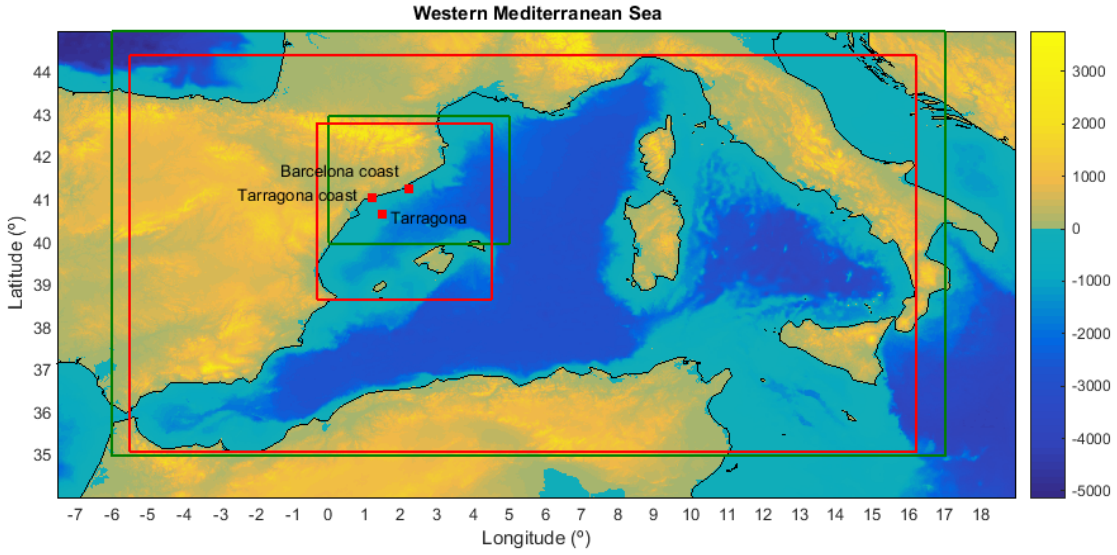

Figure 5.1: Orography, bathymetry and coast line of the study area. The green boxes represent the wind forcing domains, the red boxes the unstructured mesh limits, and the red dots the buoys measurement locations.

The bad accuracy of the winds, especially when the resolution is low, is com-

monly reported as one of the main causes of poor results of wave models near the coast (Ardhuin et al., 2007), so a validation of the wind fields over the sea has been performed for a one-year period. Since it has not been possible to find other wind measurements on the sea for the selected period, only one validation location is presented, corresponding to the Tarragona buoy described in table 5.2 and represented in figure 5.1.

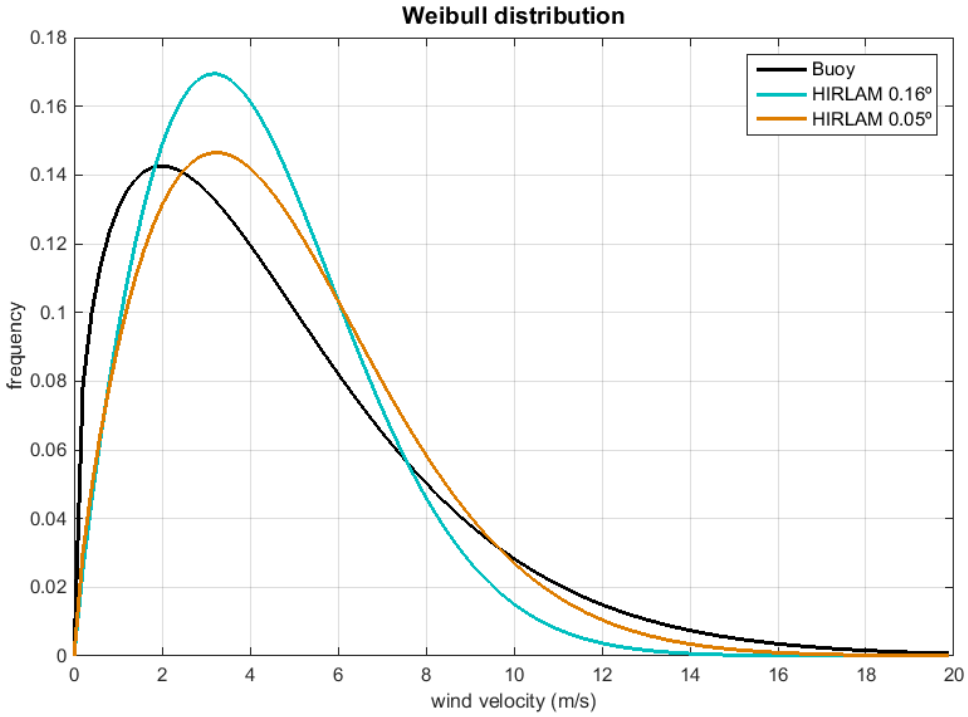

Figure 5.2: Weibull distribution of the wind intensity (m/s) for the buoy measurements (black), the HIRLAM 0.16º wind model (blue) and the HIRLAM 0.05º high resolution wind model (yellow) for the 2013.

The results of the calibration process are shown in figure 5.2, where the histograms obtained as the distribution of the different winds during the whole period are presented using a range of 1 m/s and adjusted to a Weibull distribution. Additionally, some statistics have been calculated and are shown in table 5.1. From the validation process it can be stated that the general quality of the wind is acceptable, with correlation coefficients around 0.85 in intensity and slightly lower, around 0.67, in direction for the two models, although both of them tend to slightly overestimate the intensity of the wind fields.

It can be observed that at the validation location there are no important differences between the accuracy of the two models despite the different resolution (table 5.1), so one cannot be considered to work better than the other. However,

as Alomar et al. (2014) concluded, the wave conditions tend to improve considerably when they are obtained from winds with better resolution in space and time. For this reason, since only one wind field can be used as a forcing in unstructured grids, to take advantage of the high-resolution information a merging process has been performed to combine both existing wind fields into a new one. Since both wind fields proceed from the same source and the continuity is assured, the merging process consisted in interpolating the boundaries. In the results section a sensitivity test is performed for the Western Mediterranean Sea domain in order to determine the effect of adding high-resolution winds in one part of the unstructured grid.

Table 5.1: Results of the validation of the two wind models including the wind intensity (m/s) and wind direction (degrees) for the 2013 year in Tarragona buoy location.

Model	Wind intensity				Wind direction		
	RMSE [m/s]	Bias [m/s]	Si	R	RMSE [º]	Si	R
HIRLAM 0.16º	1.89	0.54	0.40	0.84	77.45	0.37	0.67
HIRLAM 0.05º	2.02	0.92	0.42	0.86	77.08	0.21	0.67

The validation of the numerical results is performed in two different ways. On the one hand, for coastal areas a direct validation with the buoy measurements is performed. The buoy data available for the study period are provided by the Spanish harbour agency, Puertos del Estado (www.puertos.es), at three different locations: the Barcelona coast and Tarragona coast, moored near the coast, and Tarragona, moored in deep waters (figure 5.1, table 5.2).

Table 5.2: List of the instruments location and the information provided by each of them for the Catalan coast.

Name	Lon	Lat	Depth	Parameters provided
Barcelona coast	2.20º E	41.28º N	68 m	Hs, Dir Tp
Tarragona	1.47º E	40.68º N	688 m	Hs, Dir, Tm_{02}, Tp, Wind
Tarragona coast	1.19º E	41.07º N	15 m	Hs, Dir, Tp

On the other hand, for the open-sea conditions the validation is realized by comparing the model results with altimetry wave height measurements for the entirety of 2013. The remote-sensing data used come from several satellite missions (Jason-1, Jason-2, Cryosat-2 and SARAL) and are obtained from the IFREMER ftp

(ftp://ftp.ifremer.fr/ifremer/cersat/products/swath/altimeters/waves), where altimeter significant wave height measurements from nine missions over a 23-year time period are provided in a unified format (Queffeulou and Croize-Fillon, 2016).

Biases and trends are commonly observed in altimeter significant wave height measurements that need to be corrected (Queffeulou, 2004) using buoy and cross-altimeter data comparisons. Ona study (Queffeulou, 2004) illustrates the particular significant wave height variability over the Western Mediterranean Sea, in which the satellite measurements are compared to three buoys located in the area, obtaining generally good agreement and low scatter. However, the results vary depending on the buoy location, mainly due to the particular characteristics of the area, such short fetch, high wind variability and swell predominance.

For this reason a preliminary validation of the satellite measurements in the study areas was performed, comparing the satellite significant wave height with the measurements provided by the buoys presented in table 5.2. The statistics of the validation for the three locations are presented in table 5.3 and represented in a scatter plot (figures 5.3). The collocation is performed using a radius of 50 km and a time threshold of 30 min, as initially suggested by Monaldo (1988) and subsequently reaffirmed by Queffeulou (2004).

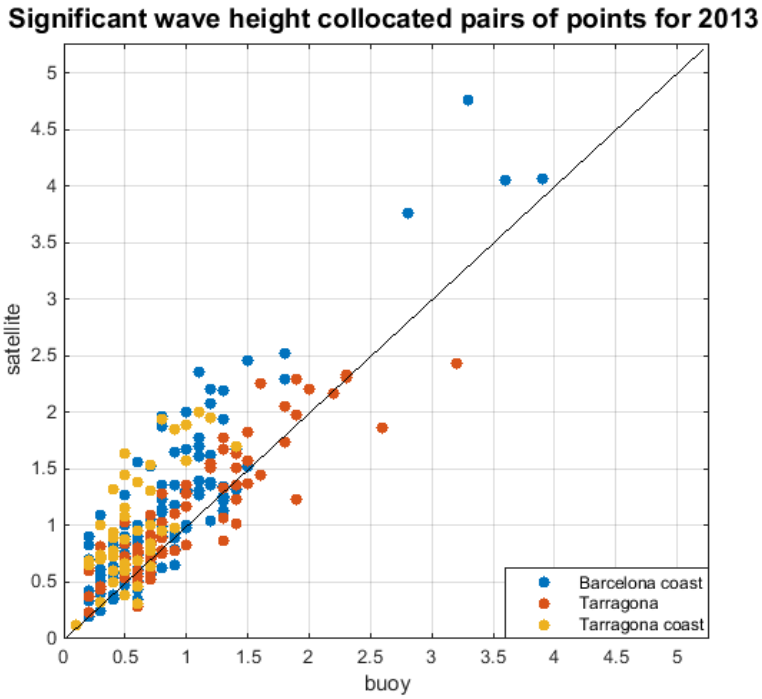

Figure 5.3: Scatter plot of the collocated pairs of point for the significant wave height. The Barcelona coast (blue), Tarragona (orange) and Tarragona coast (yellow) buoys are included in the comparison for the entire 2013.

Table 5.3: Results of the validation of the collocation between satellite measurements and the buoy data for the significant wave height [m] for the entire 2013. The Values column shows the number of collocated pairs of data used to obtain the statistics.

Buoy location	RMSE [m]	Bias [m]	SI	R	Values
Barcelona coast	0.45	0.30	0.54	0.900	126
Tarragona	0.28	0.09	0.29	0.902	80
Tarragona coast	0.54	0.41	0.95	0.709	47

From table 5.3 one can see that the best statistics correspond to the Tarragona buoy, located 50 km offshore, showing a good correlation coefficient and a relatively small RMSE if we consider that only 80 values are available for all the 2013. For the Tarragona coast buoy, located really near the coastline, the statistics are much worse, as expected, due to the known satellite measurement errors nearshore. This behaviour is also appreciable in figure 5.3, where for the coastal buoys a clear overestimation of the satellite measurements is observed in comparison to the buoy data. In conclusion, analysing our results together with the ones presented by Queffeulou et al. (2004) for three other buoy locations in the Western Mediterranean Sea, the altimeter significant wave height measurements are considered acceptable for the validation of the model results in deep waters but not for coastal areas.

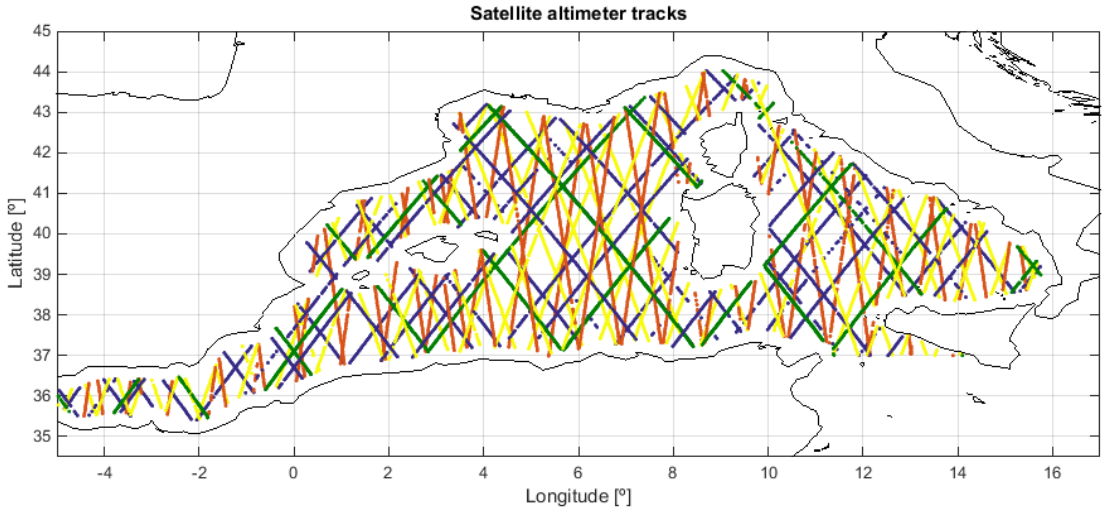

Figure 5.4: Satellite tracks coverage for the four satellite missions during April 2013. The different colours correspond to different satellite missions.

In figure 5.4 the satellite tracks used in the present chapter for the Western Mediterranean Sea domain are represented. For the model validation the satellite data are collocated against numerical results from the unstructured grid. To obtain

the collocated pairs of significant wave height, several processes are necessary: first a time collocation of the satellite data is performed with a 1 h interval, coinciding with the model temporal resolution, after a space collocation is performed with a radius of 25 km, followed by selecting the nearest location and then a linear interpolation in time. The points located at a distance less than 0.3 degrees (roughly 30-35 km) from the coast have been eliminated from the validation process due to the errors associated with the satellite measurements in these nearshore areas. After the collocation process 31,991 pairs of values were obtained for the Western Mediterranean Sea domain and 6,549 pairs for the Balearic Sea domain for the entirety of 2013.

5.3.2 Grid design

The main purpose of an unstructured grid is to provide high resolution in coastal areas and coarser grid size in deep waters, thus requiring a unique mesh. With this methodology the nesting and the corresponding interpolations are avoided. Additionally, these sorts of grids better fit the coastline of the area.

There are plenty of mesh generators able to create an unstructured grid from a closed contour, just considering the resolution of the boundary segments and some size proportion between neighbouring triangles. However, in some of the grid generators, sizing information can be also introduced to control varying levels of mesh resolution within the domain.

The SWAN model accepts three different formats for unstructured grids that correspond to three different sources: (1) the ADCIRC oceanic model (Luettich and Westerink, 1994a), (2) the Triangle grid generator (https://www.cs.cmu.edu/quake/triangle.html; Shewchuk, 2002) and (3) the Easymesh grid generator (http://www-dinma.univ.trieste.it/nirftc/research/easymesh/ easymesh.html; Rebay, 1993). Regardless of the mesh generator used, the data introduced in SWAN are composed of a list of the vertices' coordinates, including boundary markers, and a connectivity table for the triangles. Thus it is possible to generate a grid using any of the described mesh generators, or any other at one's disposal, and then transform the results into the format of any of the three mentioned before.

The grid generator used in the present study is the MESH2D – Automatic Mesh Generation for Matlab (http://es.mathworks.com/matlabcentral/fileexchange/25555-mesh2d-automatic-mesh-generation), a toolbox for 2D meshing in which a size function can be included together with a maximum grid size and the maximum size proportion between neighbouring cells.

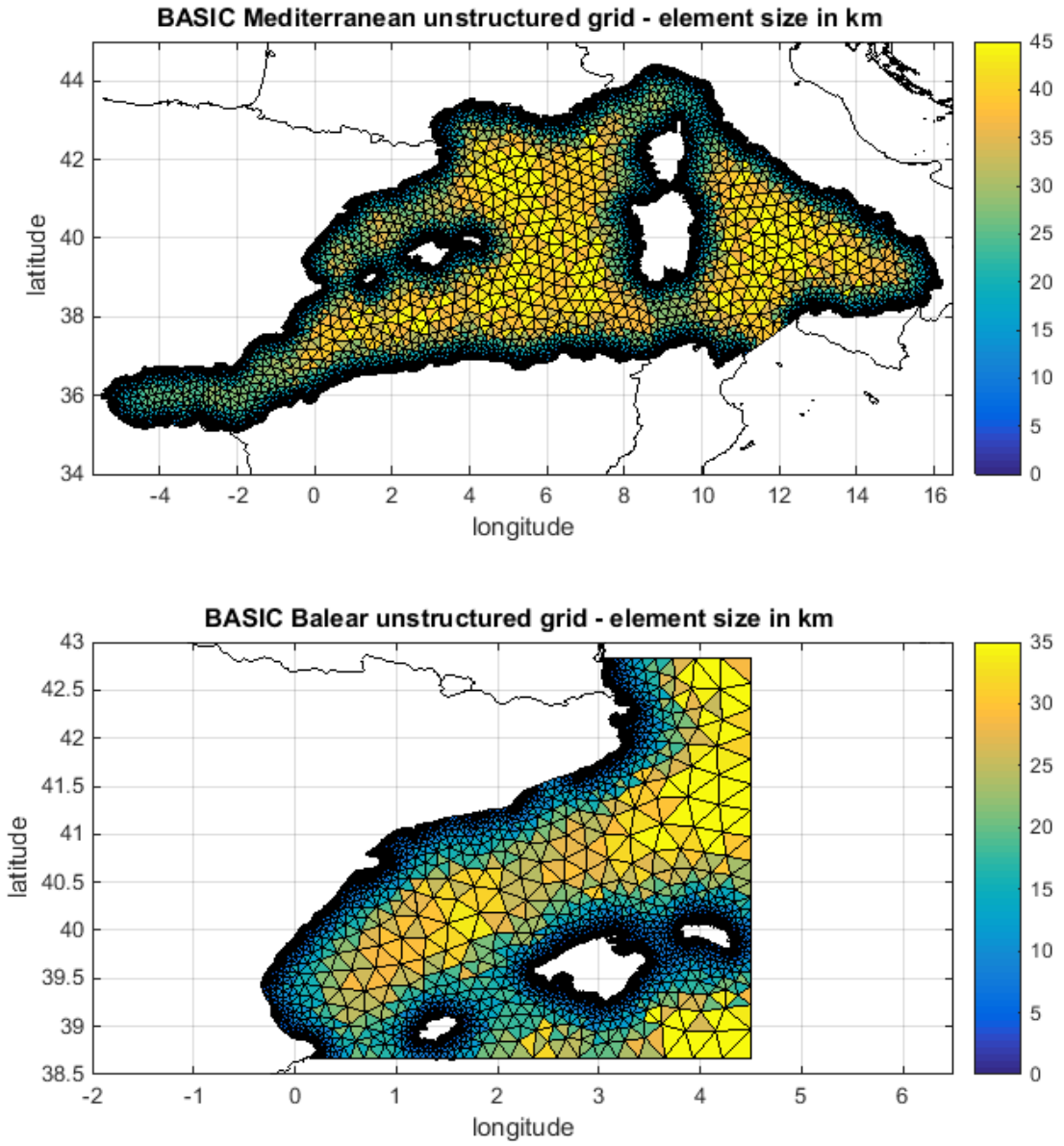

Figure 5.5: Detail of the BASIC unstructured grids designed for the Western Mediterranean sea grid (top) and the Balear Sea (bottom). The colour scale represents the grid size in km as the medium length of the sides of each triangle.

The coastline information is used to generate the contour of the study domain. In the present study two different domains are tested, corresponding to the Western Mediterranean Sea (from the Strait of Gibraltar to the Strait of Sicily) and the Balear Sea (including the Catalan coast and the Balearic Islands), both represented in figure 5.1. The first step into designing the contour of the grid goes through the coastline softening, because the triangle size in the boundary areas depends on the distance between two consecutive points. Then, depending on the resolution desired in each coastal area, the coastline should be smothered subsequently. The minimum

grid size used for both domains has been established as 800 m for the Catalan coast and the Balearic Islands, and up to few kilometres for the remaining boundaries.

Using the mesh generator MESH2D with the softened contour, and considering a maximum grid size of 0.3 degrees and a maximum size proportion between neighbouring cells of 25%, we can compute the first unstructured grids for the Western Mediterranean Sea and the Balearic Sea. We give the name BASIC to these grids, which are represented in figure 5.5 and described in table 5.4, because any size function is used to generate them.

Table 5.4: Description of the grids obtained without any size function.

Grid	Resolution	Lat - Lon	Grid points
BASIC Western Mediterranean Sea	45 km to 800 m	5.495º W – 16.218º E 35.091º N – 44.424º N	8,412 nodes 14,680 triangles
BASIC Balear Sea	35 km to 800m	0.331º W – 4.500º E 38.670º N – 42.830º N	6,328 nodes 11,019 triangles

Two size functions are defined and used in the present study to improve the BASIC unstructured grids. The idea is to refine the mesh only where this procedure can improve the wave simulation results so a balance can be established between grid resolution and the computational time required to resolve the simulation. The criteria selected for the grid sizing are based on the distance to the coast, where usually better forcings are available, and on the bathymetry and depth gradients, because in some areas the bottom conditions increase the wave field variability.

Distanceto the coast criterion

The first criterion considers the distance to the coast, where more accuracy is required, high-resolution winds are provided and buoy measurements are available. In both domains considered the distance is centred on the Barcelona coast, from 1.5º E to 2.5º E and from 41.15º N to 41.50º N (in red in figure 5.7).

The procedure adopted consists first of all in defining a regular grid covering the entire domain and determining the distance to our reference (in degrees). Then equation 5.1 is applied:

$$size_D = A_D + B_D \cdot tanh(C \cdot distance) \tag{5.1}$$

Where the coefficients A_D and B_D are weights to calibrate the function. If one considers $A_D = 0.01$ as the minimum value for the size function and $B_D = 0.24$,

the maximum value that can be reached by the function becomes 0.25, so these parameters can be calibrated for each problem considered.

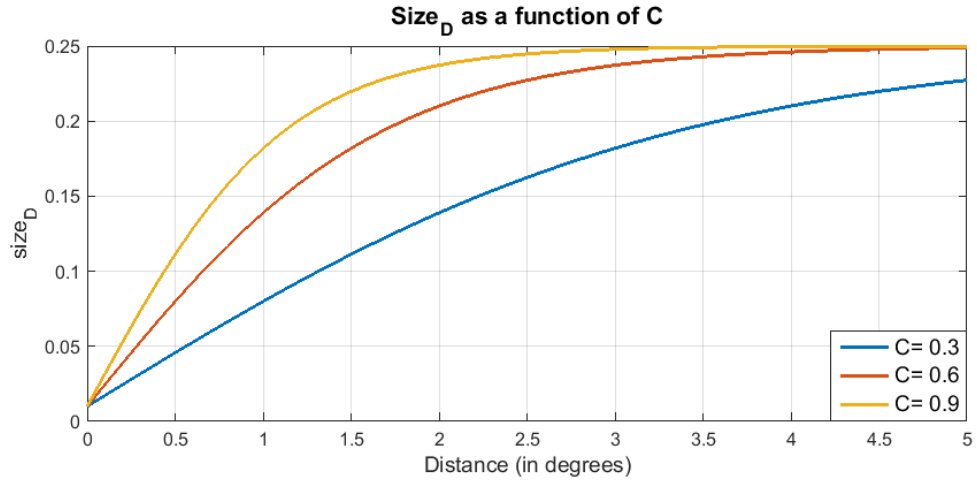

Figure 5.6: $size_D$ function with A_D=0.01, B_D=0.24 and three C values (0.3 – 0.6 – 0.9).

The coefficient C corresponds to the growth velocity of the function, and thus to the spatial distribution of the size function, and can be adjusted to any given problem. In both domains studied we have selected $C = 0.6$, keeping in mind that bigger values make the influence of the size function smaller, and vice versa (figure 5.6). In figure 5.7 the distance to the coast and the $size_D$ function are represented for the Balear Sea domain using the coefficients mentioned above.

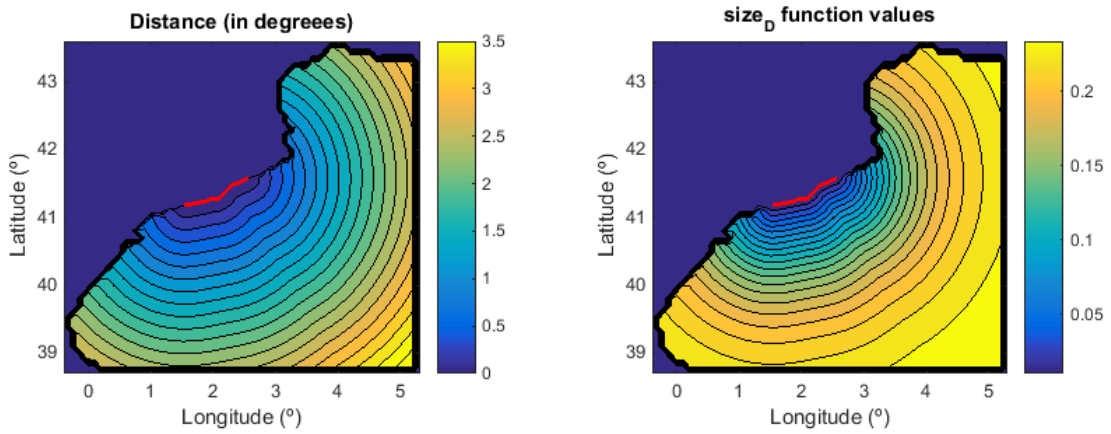

Figure 5.7: Example of the distance to the coast in degrees (left) and the corresponding $size_D$ function values (right) for the Balear Sea domain. In red the coast line from where the distances are calculated is represented.

Depth gradients and bathymetry criterion

The second criterion applied considers the effect of the bottom on the wave propagation, including the water depth, the bathymetric gradient and the level of bottom influence (in terms of classification into deep, intermediate or shallow waters).

A parameter named step is created to include information about the depth and the bathymetric gradient as described in equation 5.2. The step equation is a function of the hyperbolic tangent of the depth (in metres) divided by the bathymetric gradient (both computed in a regular grid covering the entire study area), so when the gradient is big or the depth small the step function gets smaller.

$$step = \frac{tanh(A_S \cdot (depth + B_S))}{min(max(1, gradient), C_S)} \tag{5.2}$$

The coefficient B_S is defined to avoid depths near 0 and is fixed to 10 for our study, while the coefficient A_S is used to scale the effect of the bathymetry. In the present exercise the A_S coefficient has been set to 0.001, so the effect of the depth is considered from 10 up to around 1000 m. The gradient value is also limited between 1 and a maximum value defined by the C_S coefficient. After testing the typical conditions of our study domain, the C_S coefficient was fixed to 100. In table 5.5 some of the values used to calibrate the coefficients A_S, B_S and C_S are presented.

Table 5.5: Description of the grids obtained without any size function.

Depth	Gradient	*step* numerator	*step* denominator	*step* range
Small (<20m)	Important	0.09 – 0.3	80-100	0.001 – 0.0037
Small (<20m)	Small	0.09 – 0.3	1-10	0.01-0.3
Big (>1000m)	Important	0.9	80-100	0.01-0.012
Big (>1000m)	Small	0.9	1-10	0.1-1

Once the step function is calibrated and calculated for the entire study domain, the size function is defined as follows:

$$size_B = A_B + B_B \cdot tanh(C_B \cdot step) \tag{5.3}$$

Where the coefficients A_B and B_B are weights of the function, as used in the

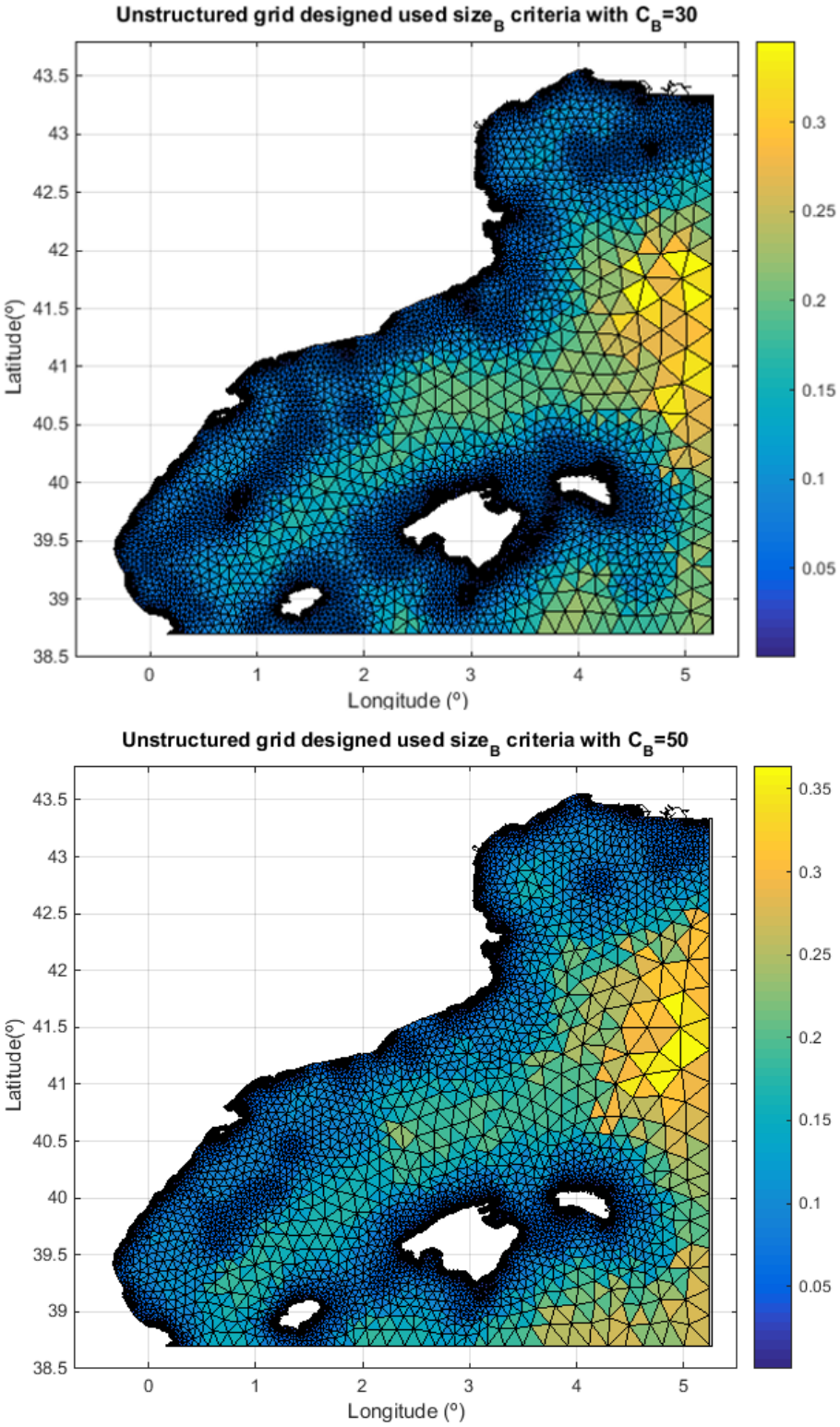

Figure 5.8: Unstructured grids designed using the $size_B$ size function for the Balear Sea domain, using a C_B coefficient of 30 (top) and 50 (bottom).

distance to the coast criterion (equation 5.1), and should be fixed in the same range of values in order to better compare and combine both criteria.

The C_B coefficient needs to be calibrated depending on the step function range of values and the resolution desired in the shallow-water areas or where the bottom gradients are more important (for example in a submarine canyon). In figure 5.8 two different grids are presented, obtained using the $size_B$ size function for two different C_B coefficients.

It is important to remark that the $size_B$ function is based on the water depth and the bathymetric gradient to refine the unstructured grid in some areas. However, the size function described in equation 5.3 does not takes into account the level of bottom influence. The effects of the bathymetry will only be interesting for the wave modelling in situations of shallow or intermediate waters in which the wave conditions depend on the depth (table 5.6), so we should use the $size_B$ criterion under these conditions (equation 5.4).

$$size_B = \begin{cases} A_B + B_B \cdot tanh(C_B \cdot step) & \text{if} \frac{\mathrm{d}}{\mathrm{L}} < 0.5 \\ A_B + B_B & \text{if} \frac{\mathrm{d}}{\mathrm{L}} > 0.5 \end{cases} \tag{5.4}$$

Table 5.6: Classification of the wave conditions depending on the bottom influence. Where d is the water depth (in metres), L the wave length (in metres), T the wave period (in seconds) and g the gravity constant.

Criteria	Classification	Wave length
$\frac{d}{L} < 0.05$	Shallow waters	$L = T \cdot \sqrt{g \cdot d}$
$0.05 < \frac{d}{L} < 0.5$	Intermediate waters	$L = \frac{g \cdot T^2}{2\pi} tanh\left(\frac{2\pi d}{L}\right)$
$\frac{d}{L} > 0.5$	Deep waters	$L = \frac{g \cdot T^2}{2\pi}$

For the purpose of delimiting the areas where the depth affects the wave characterization, three extreme situations for the Catalan coast have been reproduced in SWAN. The stationary simulations are run in the same regular grid covering the entire Western Mediterranean Sea used to calculate the size functions, with the following wind conditions: wind blowing from the east with an intensity of 25 m/s, offshore wind from the north-west with an intensity of 15 m/s and southerly wind with an intensity of 15 m/s. The magnitude and direction of the extreme wind conditions correspond to typical values for the Catalan coast and have been obtained from previous studies (Bolaños et al., 2009; Font, 1990).

Grid design

A combination of both sizing criteria presented before and defined in equations 5.1 and 5.4 is used to generate the unstructured grids for the Balear Sea and the Western Mediterranean Sea domains. The coefficients used, chosen after some testing and adapted to the domain scales and characteristics, are the following: $A_D = A_B = 0.01$; $B_D = B_B = 0.24$; $C = 0.6$; $A_S = 0.001$; $B_S = 10$; $C_S = 100$; and $C_B = 50$.

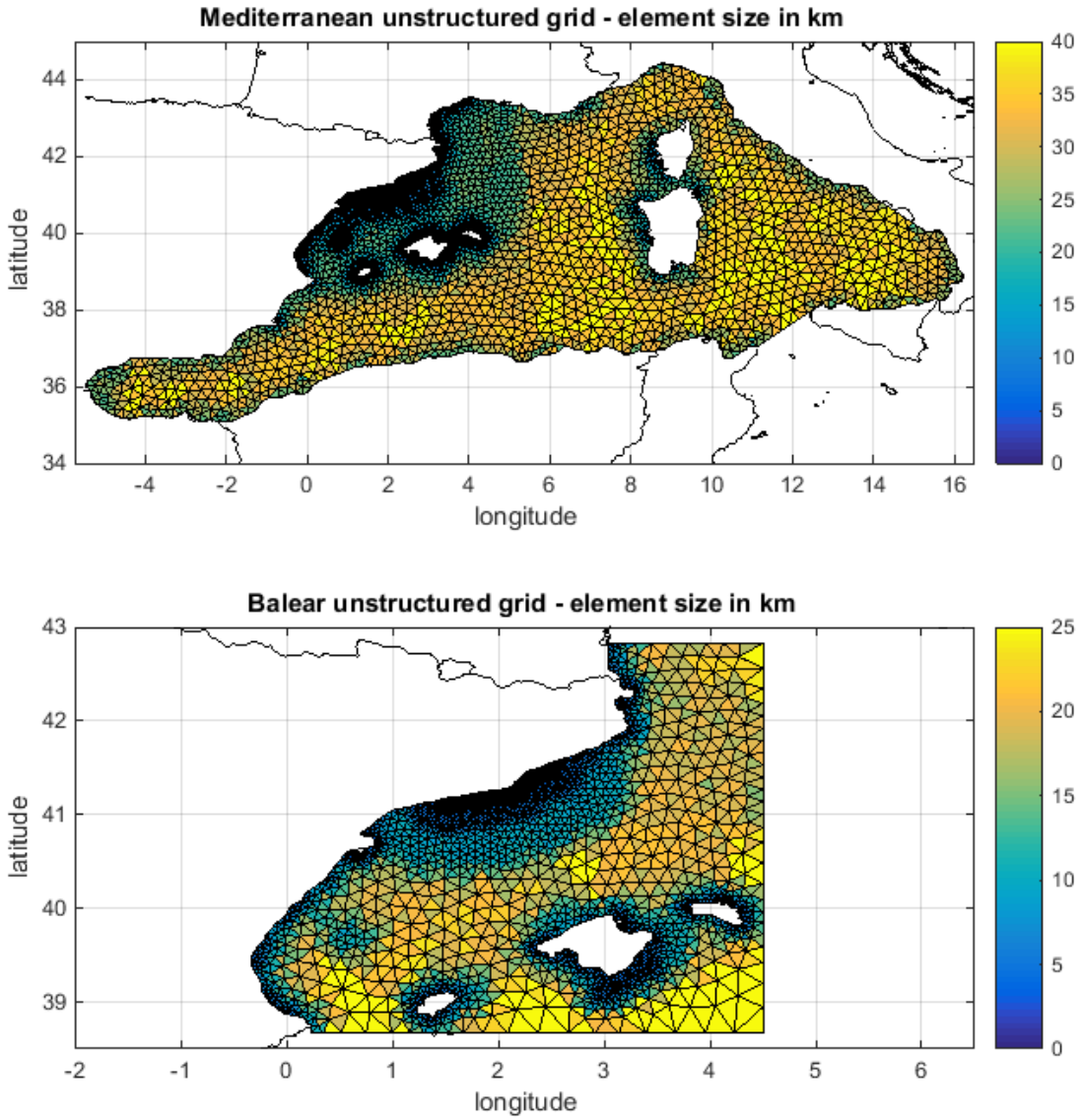

Figure 5.9: Detail of the unstructured grids designed for the Western Mediterranean sea grid (top) and the Balear Sea (bottom). The colour scale represents the grid size in km as the medium length of the sides of each triangle.

The criteria used to combine both size functions have simply consisted in selecting the minimum value for each point (equation 5.5), since both functions are

defined in the same spatial domain, use the same grid and take values from the same interval (from 0.01 to 0.25).

$$size = min(size_D, size_B) \tag{5.5}$$

The mesh generator used is MESH2D for Matlab, using equation 5.5 as a size function, with a maximum grid size of 0.3 and a maximum size ratio between neighbouring cells of 25%. The resulting grids are represented in figure 5.9 and described in table 5.7. In figure 5.10 a zoom from the Mediterranean sea unstructured grid for the Catalan coast region is presented so the resolution of both designed grids can be compared in the coastal areas, presenting almost no difference between them.

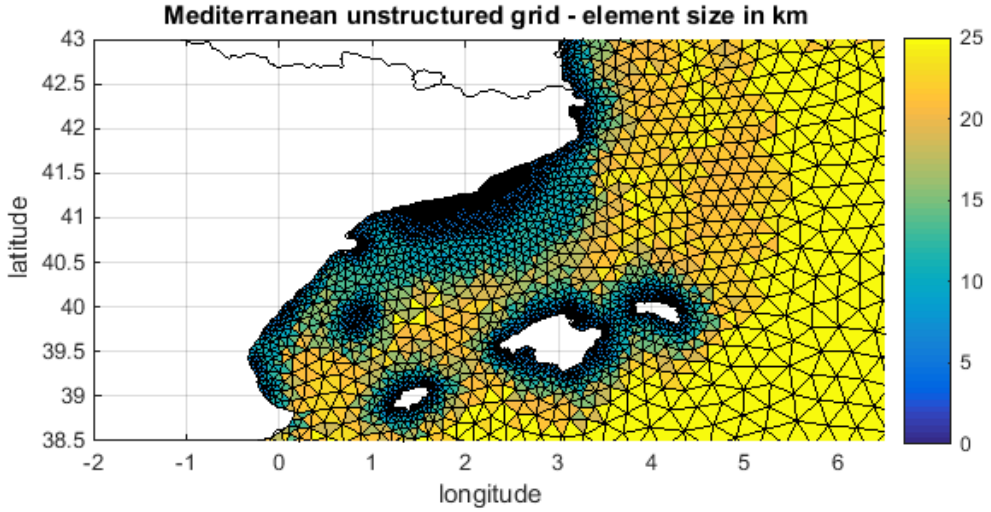

Figure 5.10: Zoom of the Western Mediterranean sea unstructured grid designed. The colour scale represents the grid size in km as the medium length of the sides of each triangle.

Table 5.7: Description of the grids generated, including the mesh resolution, the domain covered and the number of nodes and triangles for both grids.

Grid	Resolution	Lat - Lon	Grid points
Wester Mediterranean Sea	40 km to 800 m	5.495º W – 16.218º E 35.091º N – 44.424º N	4,548 nodes 8,317 triangles
Balear Sea	25 km to 800m	0.331º W – 4.500º E 38.670º N – 42.830º N	2,710 nodes 4,928 triangles

If the resulting grids are compared with the BASIC grids, obtained using the same grid generator without any size function (table 5.4, figure 5.5) but using exactly

the same values for the maximum grid size and the maximum size ratio between neighbouring cells, an important reduction of nodes and triangles can be observed, as well as a better distribution of the cells.

5.3.3 Using unstructured grids in SWAN: the refraction problem

In order to introduce the designed grids into SWAN, small changes in the files format are required. We have decided to use the Tringle grid generator format, consisting of two files with the extensions .node and .ele. The first file (.node) is a table with as many rows as the grid has nodes, and three columns, including the longitude, the latitude and a marker for each node. The marker can take the following values: 0 for an inside point of the computational grid, 1 for land boundary points and 2 for free boundary points, where the boundary conditions should be introduced. The second file (.ele) is the connectivity table, used to generate triangles, and includes for each element the three nodes that generate it in anticlockwise order.

The SWAN configuration is the same one used allthroughout the thesis, described in chapter 2 but using a delta coefficient equal to 1 for the whitecapping term as described in chapter 3. The main difference in the SWAN model when working with unstructured grids is the numerical scheme, which has been adapted from the backward space, backward time (BSBT) first-order upwind SWAN scheme (SWANteam, 2015a) by Zijlema (2010). It consists of a vertex-based, fully implicit, finite-differences method that requires several sweeps through the grid. The parameters used to define the convergence criteria and the maximum number of iterations are set up as suggested in the SWAN manual (SWANteam, 2015b). Another difference that appears in SWAN when working with unstructured grids is that the model is not able to compute the wave setup, which is especially important in shallow waters and in the surf zone, where the set-up induced by the waves may generate variations in the sea level and along-shore currents (SWANteam, 2015a).

It is widely known that the SWAN model may present some refraction problems due to the numerical scheme used to resolve the balance equation, and there is no exception to this when using unstructured grids (Zijlema, 2010). The discretization in geographical space in SWAN is solved with an implicit upwind difference scheme that has one main disadvantage: it is numerically diffusive, which naturally degrades the accuracy of the model. The numerical diffusion is caused by gradients of wave action across geographic space, e.g. due to refraction by bathymetry or currents (Zijlema, 2010). Thus this problem usually appear due to intense local variations in the grid size or the bathymetry, making the unstructured grids more susceptible to

this problem due to the varying mesh size. Some possible solutions to this problem include (1) improving the spatial and spectral resolution of the computational grid, (2) smoothing the bathymetry and (3) activating the spectral propagation velocity limiter included in SWAN and described in detail in Dietrich et al. (2013). Of course another possible solution is to enable selectively some physical processes, e.g. the refraction, depending on the region studied as performed in Dietrich et al. (2011b,a, 2012). However, this last option is not acceptable in this study since the refraction is considered crucial in coastal areas.

The most convenient solution for our domain consists in activating some of the mentioned limiters. They are based on the Courant-Friedrichs-Lewy (CFL) criteria for the spectral propagation (refraction and frequency shifting) velocities in SWAN. These limiters are not required for model stability, but they improve accuracy by reducing local errors that would otherwise spread throughout the computational domain (Dietrich et al., 2013).

After analysing the first results obtained from SWAN simulations, few refraction errors were detected in some local areas, where due to refraction excessive wave energy was focused at a single point, causing the computer solution to be infeasible. Since the errors appear only locally, the refraction limiter was considered the most robust solution and then switched on. Several values for the limiter were tested: 0.5, 1.0, 1.5 and 2.0, as suggested in Dietrich et al. (2013). It was set to 1.5, so it was the bigger value that solved the refraction problems without limiting the natural wave refraction.

5.4 Analysis of the results

In the present section a validation of the wave simulations obtained using the designed unstructured grids is performed. In fact, two different validations are presented:in the first one the model results are compared with the buoy measurements near the coast, and in the second one all model results are compared with satellite measurements. The validation period is the entire year of 2013.

The SWAN wave simulations included in the comparison are the following: the Western Mediterranean Sea unstructured grid designed in section 5.3.2 forced with the coarser wind field (named MED) in comparison with the same grid forced with the merged wind field defined in section 5.3.1, and a combination of HIRLAM 0.16 and HIRLAM 0.05 performed to include the high-resolution wind fields in a common grid (named MED-wind).

The results from the Balear Sea unstructured grid are also included in the validation, hereby named BAL-wind. This grid is forced with the merged wind and uses boundary conditions obtained from a coarser domain covering the Western Mediterranean Sea with a spatial resolution of 9 km forced with the coarser wind field.

5.4.1 Nearshore validation

The validation of the yearly SWAN wave simulations using unstructured grids is performed at three different locations, corresponding to two coastal buoys (Barcelona coast and Tarragona coast) and a deep-water buoy (Tarragona) (table 5.3). The variables analysed are the significant wave height, the mean wave period (Tm_{02}), the peak period (not shown because it presents similar behaviour to the mean wave period) and the mean wave direction.

Figure 5.11 shows a time series representation for the Barcelona coast buoy during autumn 2013, in which no differences between the three configurations compared can be appreciated. In order to present a quantitative comparison, in tables 5.8 and 5.9 the statistical parameters obtained from the validation for the entire year are presented for the coastal buoys, while in table 5.10 the same results are shown for the deep-water Tarragona buoy.

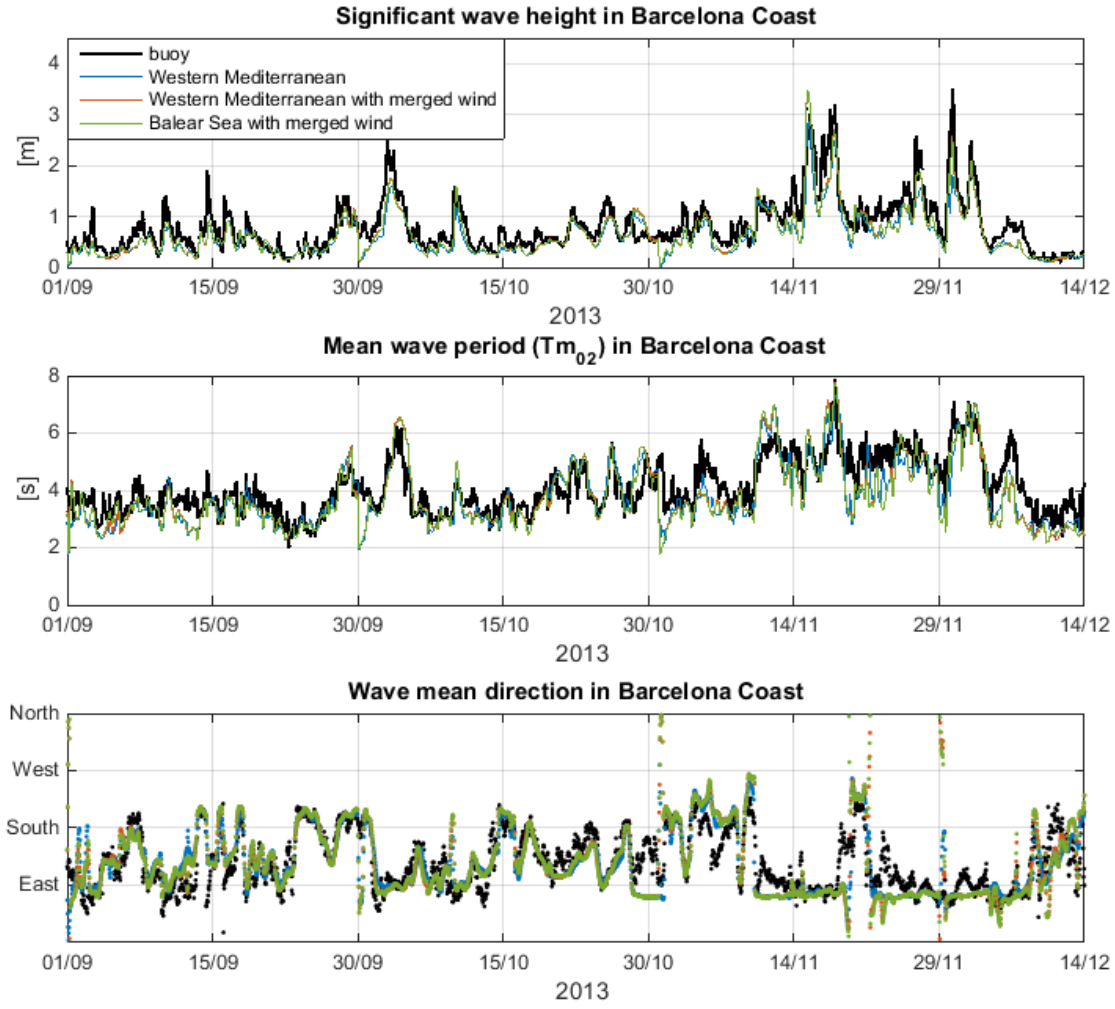

Figure 5.11: Time series of the significant wave height, the mean wave period (Tm_{02}) and the mean wave direction for autumn 2013. In back the Barcelona coast buoy measurement is represented and in colour the three unstructured grid wave simulations.

Table 5.8: Statistics for the comparison between the Barcelona coast buoy measurements and the unstructured grids model outputs, for the significant wave height, the mean wave period and the mean wave direction.

	Hs				Tm_{02}				Dir		
	RMSE [m]	Bias [m]	Si	R	RMSE [s]	Bias [s]	Si	R	RMSE [º]	Si	R
MED	0.26	-0.09	0.35	0.82	0.60	0.12	0.16	0.78	32.8	0.09	0.69
MED-wind	0.22	-0.05	0.30	0.83	0.61	0.09	0.16	0.77	33.7	0.09	0.68
BAL-wind	0.23	-0.05	0.30	0.83	0.62	0.08	0.16	0.77	33.8	0.09	0.68

Table 5.9: Statistics for the comparison between the Tarragona coast buoy measurements and the unstructured grids model outputs, for the significant wave height, the mean wave period and the mean wave direction.

	Hs				Tm_{02}				Dir		
	RMSE [m]	Bias [m]	Si	R	RMSE [s]	Bias [s]	Si	R	RMSE [º]	Si	R
MED	0.19	-0.07	0.38	0.79	0.92	-0.35	0.23	0.63	45.6	0.13	0.44
MED-wind	0.18	-0.04	0.35	0.80	0.88	-0.34	0.22	0.65	46.3	0.13	0.46
BAL-wind	0.19	-0.08	0.38	0.78	0.87	-0.32	0.21	0.64	49.5	0.14	0.46

The results from the Western Mediterranean Sea unstructured grid show similar behaviour in both coastal buoys (tables 5.8 and 5.9). The usage of a better wind field slightly improves the significant wave height and has almost no effect on the wave period and wave direction. Since the depth at the Tarragona coast buoy (15 m) is less than at the Barcelona coast buoy (68 m), the errors are more important at the first one. The increase of the errors at the Tarragona coastal buoy is enhanced when using the Balear Sea unstructured grid with the merged wind field, obtaining a similar accuracy to that obtained when using the Western Mediterranean unstructured grid with the coarser wind forcing, so the effect of improving the wind conditions is not appreciable in the Balear grid for the Tarragona coast buoy location. The differences between the Western Mediterranean Sea domain and the Balear sea grid using the merged wind forcing are inappreciable for the Barcelona coast buoy.

Table 5.10: Statistics for the comparison between the Tarragona buoy measurements and the unstructured grids model outputs, for the significant wave height, the mean wave period and the mean wave direction.

	Hs				Tm_{02}				Dir		
	RMSE [m]	Bias [m]	Si	R	RMSE [s]	Bias [s]	Si	R	RMSE [º]	Si	R
MED	0.24	-0.09	0.27	0.93	0.63	-0.30	0.15	0.85	3.0	0.11	0.65
MED-wind	0.25	-0.03	0.27	0.93	0.61	-0.25	0.15	0.85	36.9	0.10	0.71
BAL-wind	0.25	-0.03	0.27	0.93	0.61	-0.25	0.15	0.84	36.9	0.10	0.71

In general, the statistics present better values for the deep-water Tarragona buoy location (table 5.10), with correlation coefficients of 0.93 for significant wave height (in comparison with 0.83 for the Barcelona coastal buoy) and values of 0.85 for the mean wave period (in comparison with 0.77 for the Barcelona coastal buoy). In contrast, the statistics for the mean wave direction are worst at this location. This is due to the large variability of directions recorded at a more offshore location in comparison with the buoys located near the shore, where the refraction tends to unify the directions. Almost no differences can be appreciated between the three configurations presented.

Despite the little nuances mentioned, the errors, bias, scatter index and correlation coefficient for the unstructured grids present acceptable values for nearshore buoys, of the same order of magnitude as the results presented in previous chapters obtained from regular grids. In conclusion, near the coast the SWAN model using unstructured grids provides good wave simulations and can be a good alternative to the regular grids. An extended comparison between the unstructured grids and the regular nested grids is presented in chapter 6.

5.4.2 Offshore validation

In order to validate the performance of the unstructured grids in open waters, a comparison with satellite measurements is presented in this section. The SWAN configurations used in the validation are the Western Mediterranean Sea unstructured grid and the Balear Sea unstructured grid, both forced with the merged wind fields.

Prior to presenting the results, it is important to keep in mind that the unstructured grids used have been designed to improve the grid resolution in coastal areas, so the resolution in open waters is quite coarse. For the Western Mediterranean Sea grid the maximum cell size is 40 km, and for the Balear Sea grid it is 25 km, in comparison with the resolutions in coastal areas (around 1 km) where the buoys are located, so worst statistics should be expected.

In table 5.11 the statistics obtained from the collocation process for the entire year of 2013 are presented. As expected, the errors and bias are larger than at buoy locations, due to the combination of lower grid resolution and more intense wave conditions. When looking at normalized statistics, such as the scatter index and the correlation coefficients, the values presented are quite similar to those from the buoy measurements, notably in comparison with the Tarragona buoy, located 50 km offshore.

The differences between the two unstructured grids take on more importance in open-sea conditions than in coastal areas, obtaining better results for the Western Mediterranean Sea domain. One probable reason for these differences is the boundary conditions introduced in the Balear Sea domain boundaries that generate an area near the frontiers where interpolations are made and some errors may appear.

Table 5.11: Statistics for the comparison of the collocated pair of points between the satellite measurements and four configurations model outputs, for the significant wave height; coefficients of the linear regression and number of collocated pairs of points.

Configuration	RMSE [m]	Bias [m]	SI	R	a	b	Number of values
MED-wind	0.40	-0.18	0.29	0.94	0.926	-0.078	31,991
BAL-wind	0.41	-0.08	0.30	0.93	1.027	-0.115	6,549

Finally, figure 5.12 shows the comparison of the pairs of collocated points, the observed significant wave height from the altimeters and the model results for both domains: the Western Mediterranean Sea and the Balear Sea. The colour scheme represents the number of values for per 0.10 m box normalized with the maximum number of values in a box. Each figure has two lines: the black line is the line of perfect agreement, and the red line is the linear regression line, with the formulation $a \cdot x + b$ (coefficients presented in table 5.11).

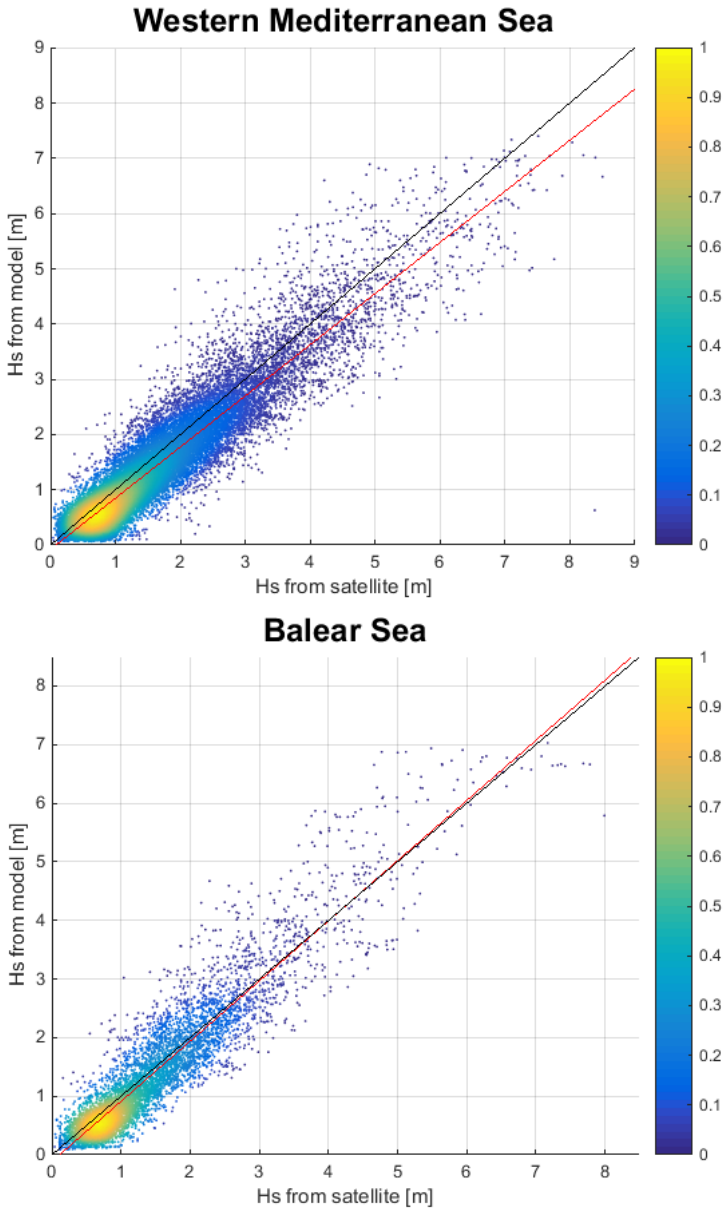

Figure 5.12: Comparison of observed (altimeter) and predicted significant wave height for the 2013. For the two unstructured grids designed. The colours represent the density of points .

5.5 Discussion

The use of unstructured grids for wave modelling is becoming more popular, especially when the unstructured grids cover local domains and are nested to regular grids. As previously mentioned, these types of grids present some advantages, from the use of a unique mesh for different scales with different resolutions to the disposal of boundary conditions and their associated interpolation errors to the better adaptation to the coastline.

The design of the unstructured grid plays an important role in the quality of the results. In this sense, adding some size criteria to the basic distribution of grid sizes is decisive. The first criterion presented here depends on the distance to the coast, because it is in these areas where high-resolution wave conditions are usually required, as well as where more information is available (e.g. better wind forcing). The second criterion proposed increases the grid resolution as a function of the water depth and the bathymetric gradients where the influence of the bottom modifies the wave fields.

Thus, the design of the unstructured grid depends not only on the characteristics of the domain considered but also on the problem that one pretends to reproduce and solve. Unstructured grids are easily adaptable to different situations and scales, and this is probably one of their strengths, but it can be also an inconvenience if the design is not thought through.

Once the unstructured grids are properly designed, and the size and distribution of the cells are optimized, they can be introduced into the wave model. In order to run the simulations, the only factor that needs some especial consideration is the numerical-scheme-associated problems. It is widely known that the SWAN wave model may present some errors due to an excess of refraction that generates an accumulation of energy in some of the cells. This error is more common when using unstructured grids due to the large variability of the grid size. As previously mentioned,there exists the option to activate a refraction limiter to prevent miscalculations. In the present work the refraction limiter has been switched on and calibrated in order to solve the punctual problems, while trying not to affect the natural wave refraction processes that are well represented.

The validation process consisted in comparing the annual results from the SWAN wave model with both buoy measurements and satellite data. The first methodology demonstrates that improving the wind resolution in some areas with better-resolution grids slightly improves the significant wave height statistics in averaged yearly results in those areas and presents fewer effects on the mean wave period and the mean wave direction.

In general, the statistics obtained for the three buoy locations are typical values in wave modelling at the Catalan coast, so the designed unstructured grids are considered a valid alternative to nested regular systems, at least for coastal areas. As expected, the model results show a better agreement with the buoy measurements in deep waters (at the Tarragona buoy, table 5.10), while small problems are detected at the Tarragona coast buoy (table 5.9) located really near the shore, at a depth of only 15 m. These discordances may have several causes: the distance to the coast is really small, so part of the errors may come from the grid resolution and the number of cells between the shore and the comparison point; other reasons may be that the formulations used in the SWAN configuration are selected for intermediate and deep waters, so formulations specific to shallow waters, such as the nonlinear triad wave interaction or bottom friction formulations, are not activated. As will be discussed ater, this is probably the worst disadvantage when using unstructured grids for a regional domain: that one should choose between different scale formulations for a unique mesh.

The results obtained from the satellite measurement validation show the good work of the unstructured grids even in open waters, with correlation coefficients around 0.92 and 0.94 (table 5.11).

Since a collocation process needs to be performed to do the validation, and some data need to be removed (the altimeter measurement points near the coast may present some errors due to the proximity of land), the number of valid points for the entirety of 2013 is not as big as expected. Additionally, the coarse resolution of the unstructured grids in some subdomains is the cause of the decrease in the number of comparison points. The maximum grid resolution, which for the Western Mediterranean Sea grid is around 40 km and for the Balear grid around 25 km, is chosen as part of the grid design and is selected according to the wind resolution and the expected variability of the wave fields in the area. It is therefore important to find an equilibrium between the maximum grid size and the accuracy of the desired results depending on the problem being treated.

To conclude, several benefits of unstructured grids have been mentioned, and the good performance of the designed grids for the Western Mediterranean Sea and the Balear Sea has been praised, but some drawbacks also need to be discussed. The main inconvenience of unstructured grids is exactly the main interest: only one grid with varying mesh size is needed. Using a unique grid involving different scales presents some problems when having to decide which physical process should be switched on and off, or the better formulations or coefficients to use, since usually these decisions depend on the scale represented. This dilemma can be solved using local unstructured grids nested to coarser models instead of using a unique

mesh covering different scales. However, with the proposed solution the boundary conditions are needed again.

5.6 Conclusions

In the present chapter the unstructured grids are proved to be a good alternative to the traditional nested grids for the Western Mediterranean Sea and the Balearic Sea domains.

The design of an unstructured grid is probably the most delicate part ofl the entire simulation process, since to obtain efficient unstructured grids several criteria need to be accounted for. In the present work two different criteria are proposed that decrease the grid size in the areas near the coast and also in intermediate and shallow waters as a function of the depth and the bathymetric gradients. These criteria need to be calibrated depending on the characteristics of the domains to reproduce. The resulting unstructured grids present fewer elements and nodes than the original ones and, what it is probably more important, the triangles are better distributed throughout the domain.

The nearshore validation process, performed for one year and comparing the two unstructured grids using two different wind field (with different resolution), allows us to state that the unstructured grids perform correctly near the coast, especially at the Tarragona buoy location (moored in deep waters) but also at the Barcelona coastal buoy location. The results for the Tarragona coast buoy are not so good due to the closeness of the location to the shore. Some improvements can be appreciated when increasing the wind field resolution, mainly for the significant wave height.

Furthermore, the validation of the significant wave height model results allthroghout the entire domain with altimetry data presents very good results, with correlation coefficients up to 0.94 for the Western Mediterranean Sea.

In conclusion, despite the work associated with a good unstructured grid design, it may be considered a worthy investment due to the good results obtained with the unstructured grids for both cases tested: a semi-enclosed domain such the Western Mediterranean Sea and a local domain like the Balear Sea nested to a coarser model.

Chapter 6

Comparison between nested grids and unstructured grids for a high-resolution wave forecasting system in the Western Mediterranean Sea

6.1 Introduction

Thanks to advances in numerical tools and coastal observations it is now possible to implement operational high-resolution forecast models (waves, oceanic and sediment transport) yielding timely and valuable intervention data to reduce coastal risks due to incoming storms. In this sense, the present chapter proposes a wave forecasting system that might be part of an early-warning system developed to minimize the coastal hazards due to storm events on the Catalan coast, where the SWAN model has been used to provide high-resolution wave conditions in a reduced time frame. This reduction of time is decisive in the period previous to a storm event, when certain decisions need to be made in order to minimize the impacts in coastal areas.

Although nowadays there are several operational systems providing wave forecasts in the study area, all of them use the traditional methodology of nested grids to improve the resolution in some coastal areas. In the present study different grid configurations are tested, including unstructured grids as an alternative to the downscaling process, and considering the use of boundary conditions from an external system, in order to obtain high-resolution wave forecast that are as accurate as possible while reducing the computational time.

6.2 Background: wave forecasting and early warning systems

Sea state information has always been required by the different agents involved on maritime activities, from navigation and offshore activities to local agents concerned about the uses of the coastal areas and the possible damages happening when a storm reach the coast.

During the last two decades great efforts have been carried out with the intention to provide that information with the better accuracy possible, for different locations and with different resolutions. The evolution of the spectral wave models together with the progress of the computational capabilities enabled the development of operational wave forecasting systems. It was during the late 80s and the 90s that many national weather services in Australia, Japan, Europe and North America started using spectral wave models, normally driven by surface-level winds obtained from regional or global weather forecast models (Kandekar and Lalbeharry, 1996).

The first operational global wave model implemented were the U.S. Navy's Global Spectra Ocean Wave Model (GSOWM) in 1985 (Clancy et al., 1986) and the United Kingdom Meteorological Office global wave model (Francis and Stratton, 1990).

The GSOWM model, implemented by the U.S. Navy's Fleet Numerical Meteorology and Oceanography Center (FNMOC) was initially based on the global and regional implementations of the WAM model, including several regional implementations nested to the global run, with a resolution of 1º. In August 2001 the WAM spectral model was changed to the WAVEWATCHIII.

The Met Office global wave model was based on a second-generation model first developed and described by Goldin (1983) and improved by Holt (1994). The operational run consisted of a 12 hours hindcast during which assimilation of ERS-2 altimeter measurements of significant wave height were performed, followed by a five days forecast, with a spatial resolution around 1º.

Another of the first global wave operational systems was developed by the European Centre of Medium Weather Forecast (ECMWF), described in detail and validated against buoy measurements and altimeter data in Janssen et al. (1997). Since November 1991 the new version of WAM model (Komen et al., 1994) was running operationally at ECMWF, implemented on the globe with a resolution of 1.5º and on the Mediterranean and Baltic Sea with a resolution of 0.25º with a forecast horizon up to 10 days. The assimilation of altimetry wave height data from the ERS-1 mission started in 1993, and supposed a beneficial impact on the wave forecast that may last up to 5 days (Komen et al., 1994). At December 1996 the

parallel version of the global model was introduced, with an effective resolution on the order of 55 km (Bidlot and Holt, 1999).

Simultaneously, since early 1991 Kandekar and Lalbeharry (1996) implemented an operational ocean wave model called the Canadian Spectra Ocean Wave Model (CSOWM) for the Canadian Meteorological Center (CMC). The global model was designed to operate over two separate oceanic regions, the northwest Atlantic and the northeast Pacific, with a resolution of 1^{o} and a nested finer grid with resolution 0.36^{o}. The verification results, comparing one year results with buoy measurements located in the Canadian coast, suggested that the CSOWM model was able to provide wave height analysis and forecast out to 36 h with considerable skills. In 1996, the CSOWM model was substituted by the WAM cycle 4 spectral wave model, covering the same domains.

The latest global wave forecast implemented was the National Centres for Environmental Prediction (NCEP) wave model, in October 1994 (Chen, 1995), with a spatial resolution of 2.5^{o}. The model used was WAM cycle 4 until 2000, when the WAVEWATCHIII model with parallel programming was implemented. The initial WAM spectral model was modified to consider the ice edge and to assimilate buoy and ERS-2 altimeter measurements in 1998.

In order to determine the quality of the operational wave forecasting systems, in 1995 a group conformed by the five wave models from different meteorological centres mentioned above (including the ECMWF, the Met Office, the U.S. Navy's GSOWM, the Canadian COSWM and the NCEP) agreed to exchange wave model results and statistical scores at selected locations in where measurements were available. The methodology and results of this program are presented in Bidlot and Holt (1999) and Bidlot et al. (2002). Some of the conclusion obtained from this collaboration included that still some work was needed in order to improve the spectral wave models, since a tendency to under predict some storms in global scales was detected, and that assimilating altimeter wave heights had a positive impact on the model performance (Bidlot et al., 2002).

In the last years the operational wave forecasting systems have been evolving, including some new parametrizations and techniques in order to improve the wave forecast in a global domain but also in coastal areas. The usage of several regional finer grids nested to the global model has been the traditional methodology used by the different meteorological agencies in order to provide information near the coast. Some examples of this are observed in the Netherlands (Sembiring et al., 2015), in the Portuguese continental coast (Soares et al., 2011) or in the east coast of India (Sandhya et al., 2014). The last version of the NCEP wave forecasting system, which uses a mosaic of grids with two-way nesting in a single model (still using

WAVEWATCHIII) to increase the spatial resolution and extend the global domain closer to the North Pole while at the same time optimizes the computational coast is a clear example of this evolution (Chawla et al., 2013).

In this sense, some international projects have appeared in the recent years, like the MyWave EU project. This is an ongoing project, started in 2012, that brings together several major institutions responsible for forecasting, research and observation of ocean waves in Europe, including Meteo-France (France), Helmholtz Zentrum Geesthacht (Germany), Puertos del Estado (Spain), ISMAR (Italy), Deltares and KNMI (The Netherlands) and HRG (Greece). The expected outcome of the project is a unified European system for forecasts and disseminations of wave predictions that includes new and improved wave physics. The equivalent North American project is the National Oceanographic Partnership Program (NOPP) project entitled 'Improving Wind Wave Predictions: Global to Regional Scales' (Tolman et al., 2013) focused on improving the physics and the methodologies to provide wave forecasts.

The information provided by the wave forecasting models can be used in different applications. One of the most recent is the configuration of an early warning system that, using the results of the wave forecasts together with sea level and meteorological forecasts and some information of the area, generates different alarms when a storm event or a hurricane reaches the coast. Some examples of this systems are presented by Alves et al. (2015) applied to the tropical storm sandy, by Souza et al. (2013) where coastal vulnerability early warning system is defined for the Irish Sea and the Liverpool bay, or by Gracia et al. (2014) for the Catalan coast.

6.3 Methodology

6.3.1 Experimental configuration

Four different configurations have been tested to determine which may be the best option, regarding the accuracy of results and the computational time, when designing an operational wave forecasting system (figure 6.1). Different situations are considered: on the one hand, the regular nested grids are compared with a unique unstructured mesh, while, on the other hand, the systems covering the entire Western Mediterranean Sea, a semi-enclosed domain, are compared with local grids nested in actually running regional forecast systems. The aim of this comparison is to provide accurate wave conditions with high resolution in coastal areas in an efficient way.

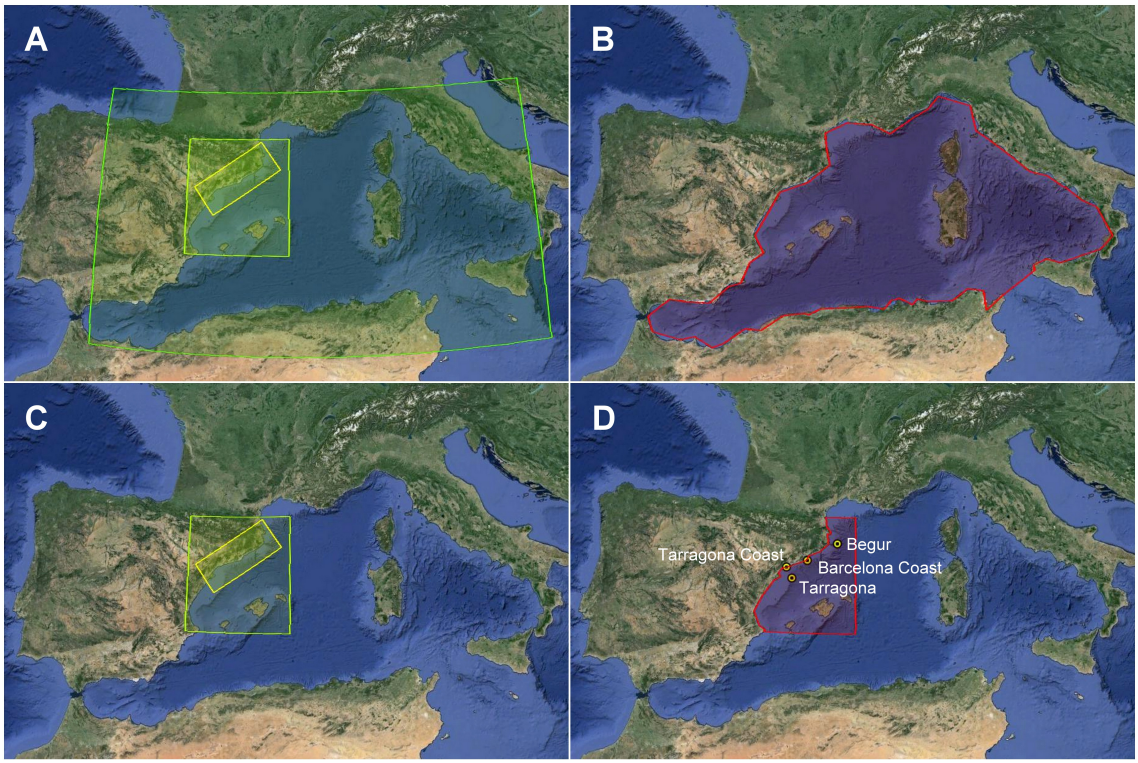

Figure 6.1: Representation of the four configurations tested in the study. The yellow dots in configuration D represent the buoy locations.

Regarding the grids covering the entire semi-enclosed domain, the regular nested system (herein named A) is comprised of three meshes with a spatial resolution of 9km, 3km and 1km, while the regional unstructured mesh for the Western Mediterranean Sea (herein named B) is the one designed in chapter 5, with 8,317 elements and 4,548 nodes, and a resolution from 40 km in open waters to 800 m in shallow waters (figure 5.9). Similar systems to the ones presented previously are considered

in the second alternative, albeit covering a smaller area, the Balear Sea, and nested to an actually running regional operational system. The first one (herein named C) consists of the two smaller regular nested grids (with 3km and 1km spatial resolution), and the second one consists on the local unstructured grid covering the same area (herein named D) designed in the previous chapter, with 4,928 elements and 2,710 nodes and a resolution from 25 km at the boundaries to 800 m in the coastal area (figure 5.9). In table 6.1 and table 6.2 the characteristics of all the meshes used and the configurations considered are presented.

Table 6.1: Description of the grids used in the study, including the mesh resolution, the domain covered, the number of grid points for regular grids and the number of nodes and triangles for unstructured grids and the wind forcing.

Grid	Resolution	Lat-Lon	Grid points	Wind forcing
Mediterranean regular	9 km	4.900 W – 16.048 E 35.000 N – 44.523 N	119 x 196 (23,324 nodes)	HIRLAM 0.16º
Balear regular	3 km	0.470 W – 4.500 E 38.670 N – 42.830 N	155 x 139 (21,545 nodes)	HIRLAM 0.16 º
Local regular	1 km	0.145 E – 3.291 E 40.083 N – 42.787 N	136 x 332 (45,152 nodes)	HIRLAM 0.05º
Mediterranean unstructured	40 km to 800 m	5.495 W – 16.218 E 35.091 N – 44.424 N	4,548 nodes 8,317 triangles	Merged wind
Balear unstructured	25 km to 800m	0.331 W – 4.500 E 38.670 N – 42.830 N	2,710 nodes 4,928 triangles	Merged wind

Table 6.2: Description of the four configurations considered in the present study, named A to D and formed by one or several grids. The need of boundary conditions is resumed in the third column.

Configuration	Grids used	Boundary conditions
A	Mediterranean regular Balear regular Local regular	No
B	Mediterranean unstrcutured	No
C	Balear regular Local regular	Yes
D	Balear unstructured	Yes

The SWAN model is implemented using the four configurations mentioned above,

using the formulations and parameters defined in chapter 2 but for the whitecapping term that has been calibrated in chapter 3. For the regular grids, SWAN provides several numerical schemes; however, among them the one that was used for this exercise is the backward space and backward time (BSBT), a first-order upwind scheme (SWANteam, 2015a), since it is the equivalent to the numerical scheme available for the unstructured grids. As mentioned by Zijlema (2010), in most of the situations the CPU cost per grid point is higher for the unstructured meshes; however, the reduction of the number of grid points in this type of meshes offsets the total time.

In order to provide some general results and conclusions, avoiding the seasonal effects, one year of simulations is performed, corresponding to 2013. Additionally, a storm event is also analysed in detail, since during these periods the information provided by the model forecast needs to be more accurate, mainly for coastal early-warning systems as mentioned previously.

6.3.2 Data available

Three buoys located along the Catalan coast and operated by the Spanish harbour agency Puertos del Estado (www.puertos.es) were considered for the validation process. Two of the buoys, Barcelona coast and Tarragona coast, are moored near the coast; the other buoy, Tarragona, is moored in deep waters (figure 5.1, table 5.2). In order to evaluate the performance of the models in open water a validation with altimetry data is carried out. The remote sensing data used comes from several satellite missions: Jason-1, Jason-2, Cryosat-2 and SARAL, and is obtained from the IFREMER ftp (ftp://ftp.ifremer.fr/ifremer/cersat/products/swath/altimeters /waves). A validation of the satellite measurements in a semi-enclosed domain like the Western Mediterranean Sea is developed in chapter 5, where also the collocation process and the selection of the valid measurements is detailed.

The bathymetry used for the simulations is obtained from GEBCO (General Bathymetric Chart of the Oceans, www.gebco.net) with a grid resolution of 30 arc-seconds (0.0083º).

The winds for the present study are the same ones used in chapter 5. It have been provided by the Spanish Meteorological Agency (AEMet, www.aemet.es) and include a coarser wind field that provides the wind conditions 10 m above the sea level, with a spatial resolution of 0.16 degrees for the entire Western Mediterranean Sea, and a better resolution wind field that covers only the Catalan coast area, with a spatial resolution of 0.05 degrees. In the present study analysed winds have been used for the two resolutions available, herein named HIRLAM 0.16º and HIRLAM

0.05º. The validation of the wind fields is detailed in section 5.3.1. From the validation results it can be noted that there are no important differences in the accuracy of the two models despite the different resolution, so one cannot be considered to work better than the other. However, from the results obtained in chapter 5 it is stated that increasing the wind field resolution improves the results mainly for the significant wave height, so when possible the high-resolution wind field will be used instead of the coarser one. As previously mentioned, for both unstructured grids a unique wind field can be used, so a merging process has been performed to combine both existing wind fields into a new one. In table 6.1 the wind forcing used for each of the SWAN configurations is detailed.

For the Balear Sea configurations, in order to avoid some computational time when running the coarser wave domain, a consideration has been to nest our system to an actually working operational service. The boundary conditions necessary for running configurations C and D are initially obtained from the wave forecast system of the Spanish harbour agency, Puertos del Estado, using the significant wave height, the mean wave period, the mean wave direction and the wave spread coefficient to generate a theoretical spectrum at the boundaries. The operational forecast system, described in Gomez and Carretero (2005), consists of an application of the WAM model (WAMDIgroup, 1988) for the Spanish Mediterranean coast, with two nested domains with a spatial resolution from 5 to 10 minutes and a temporal resolution of 1 h that are operated on a twice-a-day cycle and provide a forecast horizon of 72 h. However, analysed wave fields have been used in the present study.

6.3.3 Computational structure

The computations were performed in a small cluster named 'Alien' belonging to the computational centre of the civil engineering school of Barcelona, BarcelonaTech. The machine is made up of Dell computers and a Red Hat Linux operating system, including four nodes with Intel processors and two nodes with AMD processors. Each of the four Dell PowerEdge R900 nodes has four quad-core Intel Xeon processors with 2.4GHz, 16 MB of L3 cache per processor and 128 GB of RAM, while the two Dell PowerEdge R805 nodes have quad-core AMD Opteron processors with 2.5 GHZ, 6MB of cache per processor and 32GB of RAM.

An initial test was performed to determine the time requirements for running the SWAN model depending on the number of CPUs used. The Western Mediterranean Sea domain was chosen for the exercise, forced with the HIRLAM 0.16º wind field, for a period of three days. Only the Intel nodes were considered, and the parallelization was carried out through the OpenMP protocol.

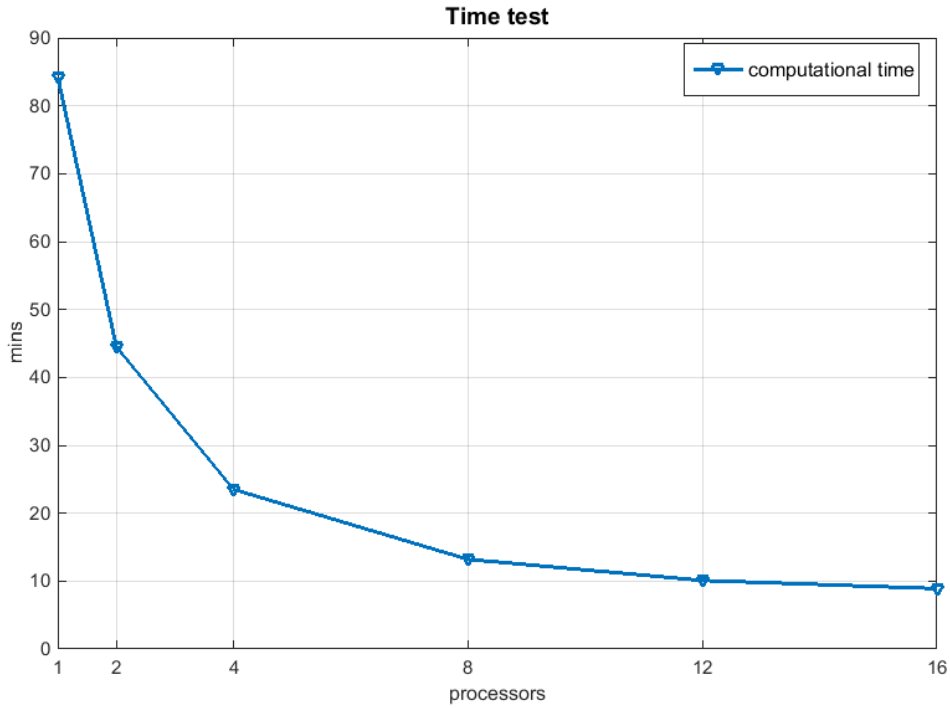

Figure 6.2: Time requirement in minutes necessary to run the test case using from one up to sixteen processors.

The results presented in figure 6.2 show an exponential decrease of the computational time required to run the model when increasing the CPUs. The reduction of time is especially significant from one to eight processors, while adding more processors does not result in an appreciable time savings. It can be concluded that, for the machine used, the optimal situation would be to work with eight or more processors. However, the machine available is shared with other users, so only one core can be guaranteed per jobs (equivalent to four processors). For this reason it was decided herein to use four processors to run the SWAN model.

6.4 Analysis of the results

6.4.1 Yearly analysis in coastal areas

Four different configurations have been tested for a one-year period and validated in three different locations. In these sections only the most representative results are presented. That implies that two unique locations will be shown: the Tarragona deep water buoy, since it is the only one located in the open sea, and the Barcelona coast buoy. The results obtained from the Tarragona coast buoy present similar behaviour to the Barcelona coast buoy (with some additional errors as mentioned in chapter 5) and the observed differences will be mentioned in the discussion but not shown in detail.

A comparison between the results from the different configurations and the Barcelona coast buoy measurements are represented in the Taylor diagrams in figure 6.3 for the significant wave height and the mean wave period, respectively. The results for the peak period are not presented but have behaviour very similar to the Tm_{02}. From the graphics it is straightforward to declare that configurations A and B have almost the same statistics, while configuration C is slightly further from the buoy point and configuration D presents the worst results.

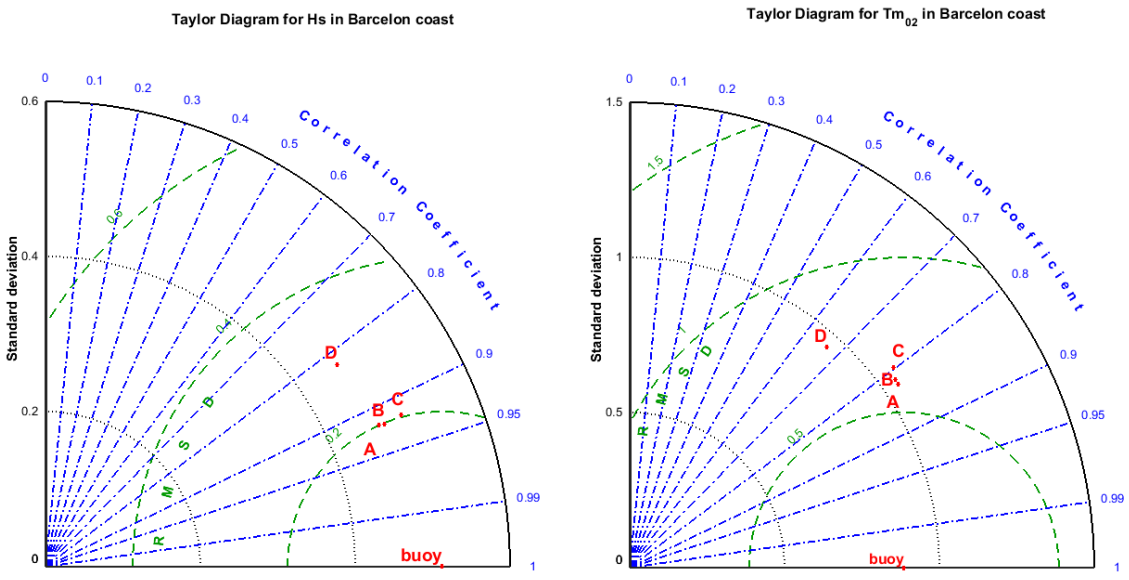

Figure 6.3: Taylor diagram of the significant wave height (left) and the mean wave period (right) for the annual analyse in the Barcelona coast location. The letters correspond to the configurations tested.

In the first columns of table 6.3 the statistic for the significant wave height

are shown, with a RMSE around 22 cm and a negative bias of 5 cm in all the configurations except D. The correlation coefficient is very good for configurations A, B and C, with values around 0.92, but the scatter index is slightly high, around 0.30. Configuration D is the only one presenting a positive bias.

Table 6.3: Results of the validation of the four configurations including the significant wave height (m), the mean wave period (s) and the wave direction (degrees) for the 2013 year in Barcelona coast buoy location.

	Hs				Tm_{02}				Dir		
	RMSE [m]	Bias [m]	Si	R	RMSE [s]	Bias [s]	Si	R	RMSE [º]	Si	R
A	0.23	-0.05	0.30	0.92	0.60	0.08	0.16	0.83	33.93	0.09	0.69
B	0.22	-0.05	0.30	0.92	0.61	0.09	0.16	0.82	33.69	0.09	0.68
C	0.23	-0.05	0.30	0.92	0.65	0.08	0.17	0.80	36.25	0.10	0.67
D	0.30	0.16	0.40	0.82	0.85	0.72	0.22	0.67	54.35	0.15	0.53

Also in table 6.3 the results for the mean period are presented. The RMSE is around 0.6 s for configurations A, B and C, and the bias is not very important except for configuration D, where a clear overestimation is present. The correlation coefficients take values around 0.80, and the scatter index has values around 0.16.

The wave direction is validated with RMSE around 36 degrees, a very low scatter index and a correlation coefficient of 0.68 in the best situations.

In summary, configurations A, B and C have a similar quality for the significant wave height, while configurations A and B work slightly better than C for the mean period and the wave direction. For the three wave parameters considered, configuration D is clearly the one presenting the worst results, showing an overestimation of the significant wave height and the mean wave period not present in the other alternatives.

Almost the same conclusions may be extracted from the comparison between the four configurations and the measurements of the Tarragona coast buoy (not shown). The main differences derive from the fact that the mean values of the variables are smaller, so the RMSEs are also smaller, and the correlation coefficients slightly worse (e.g. around 0.86 for the significant wave height or 0.68 for the mean period).

The results from the validation process for the deep-water Tarragon buoy are presented in figure 6.4, where the Taylor diagrams for the significant wave height and the mean wave period are shown. From the diagrams it can be declared that there

are no important differences between configurations A, B and C, while configuration D tends to work slightly worse mainly for the mean wave period.

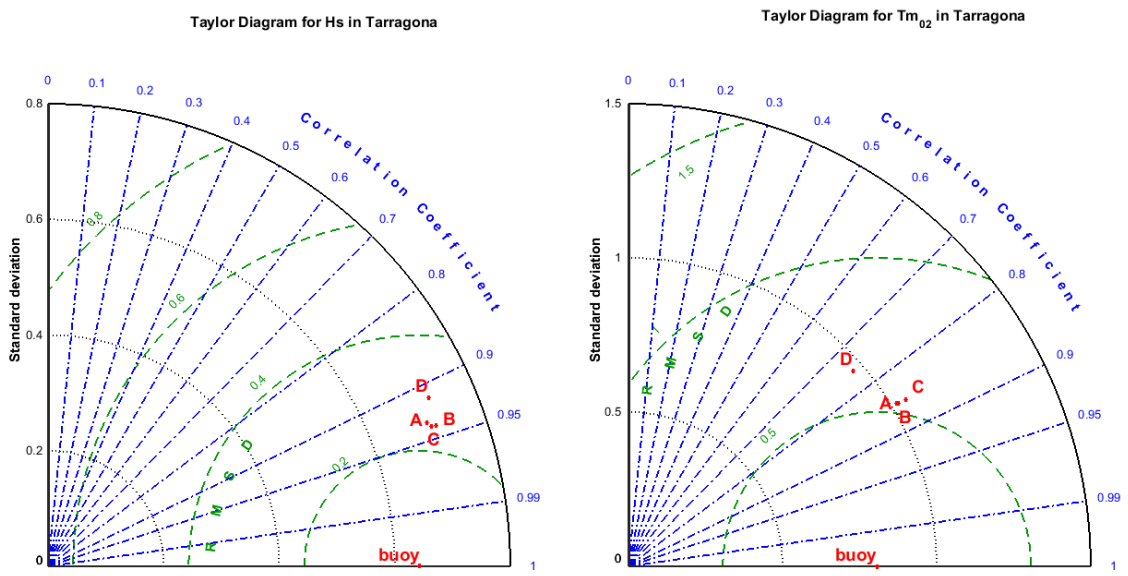

Figure 6.4: Taylor diagram of the significant wave height (left) and the mean wave period (right) for the annual analyse in the Tarragona location. The letters correspond to the configurations tested.

Table 6.4: Results of the validation of the four configurations including the significant wave height (m), the mean wave period (s) and the wave direction (degrees) for the 2013 year in Barcelona coast buoy locationResults of the validation of the four configurations including the significant wave height (m), the mean wave period (s) and the wave direction (degrees) for the 2013 year in Tarragona buoy location.

	Hs				Tm_{02}				Dir		
	RMSE [m]	Bias [m]	Si	R	RMSE [s]	Bias [s]	Si	R	RMSE [º]	Si	R
A	0.25	-0.03	0.28	0.94	0.61	-0.26	0.15	0.86	37.83	0.11	0.69
B	0.25	-0.03	0.27	0.94	0.61	-0.25	0.15	0.86	36.89	0.10	0.71
C	0.24	-0.0	0.27	0.94	0.60	-0.21	0.15	0.86	37.71	0.11	0.70
D	0.32	0.15	0.36	0.91	0.68	0.32	0.17	0.76	48.43	0.14	0.61

The results in table 6.4 show that, in contrast with the previous case, configuration D does not present results very different from the others for the significant wave height in terms of correlation coefficient. At this point located in deep water the RMSEs are around 25 cm; the bias is negative in all the configurations except

D, as was happening in coastal waters; and the correlation coefficients tend to be higher than in coastal zones, between 0.91 and 0.94.

Similar behaviour is identified when looking at the mean wave period in table 6.4. The RMSE is around 0.60 s, there is an underestimation of the Tm_{02} in all the configurations except D, and the correlation coefficients and scatter index are better than in coastal areas.

The wave direction is analysed in the last columns of table 6.4. In deep water the RMSE is slightly higher, around 37 degrees, for configurations A, B and C, while for configuration D the RMSE is smaller than in coastal areas. In general the correlation coefficients are better, with values around 0.70 for configurations A, B and C, and 0.6 for configuration D (still better than in coastal areas).

In summary, the four configurations have good accuracy for the significant wave height, but D is the worst among them. For the mean wave period the bad behaviour of configuration D is enhanced. However, in general all the configurations work better in deep water than in coastal areas.

6.4.2 Yearly analysis in the Western Mediterranean Sea

In order to evaluate the performance of the four configurations in open waters a validation with altimetry measurements has been carried out for both domains, the Western Mediterranean Sea and the Balear Sea. Since the area covered by configurations A and B is larger than the one covered by configurations C and D, two different comparisons are presented. The first one corresponds to the Western Mediterranean Sea domain, including all the values obtained from configurations A and B, and the second comparison corresponds to the Balear Sea domain, so results from configurations A and B have been limited to this region and compared with configurations C and D. Additionally, the resolution in open waters is quite different between the regular grids and the unstructured grids. For the Western Mediterranean Sea domain, the regular grid presents a spatial resolution of 9 km while the unstructured grid has a maximum grid size of 40 km. A similar situation is reproduced in the Balear Sea domain, with a regular grid presenting a resolution of 3 km and an unstructured grid with a maximum grid size of 25 km. This resolution differences also generate an important reduction of the collocated pairs of points used in the validation. The number of collocated pairs for each configuration for the entire study period are presented in the last column of the table 6.5. It is important to remember that the points located within a distance of 30 km from the coast have been omitted in the validation process due to the common altimeter measurement errors in that area.

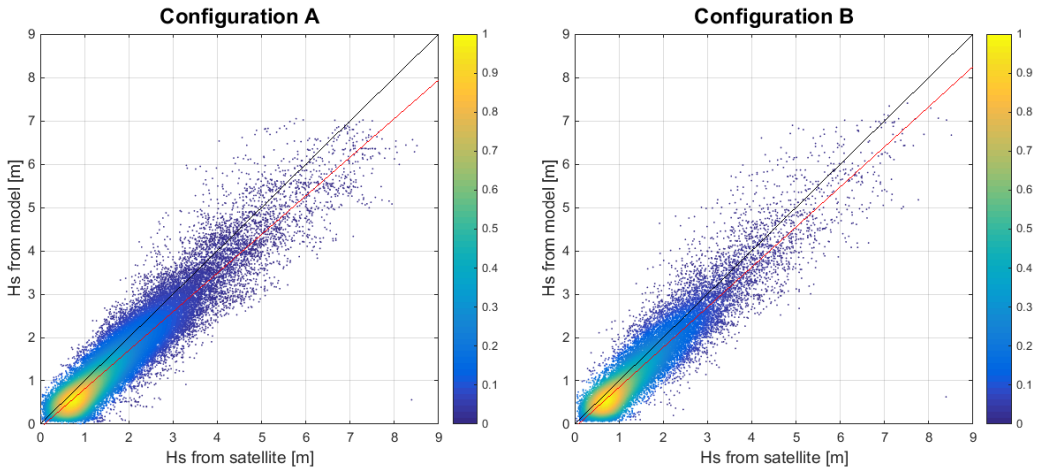

Figure 6.5: Comparison of observed (altimeter) and predicted significant wave height for the 2013, for the Western Mediterranean Sea region. The colours represent the density of points.

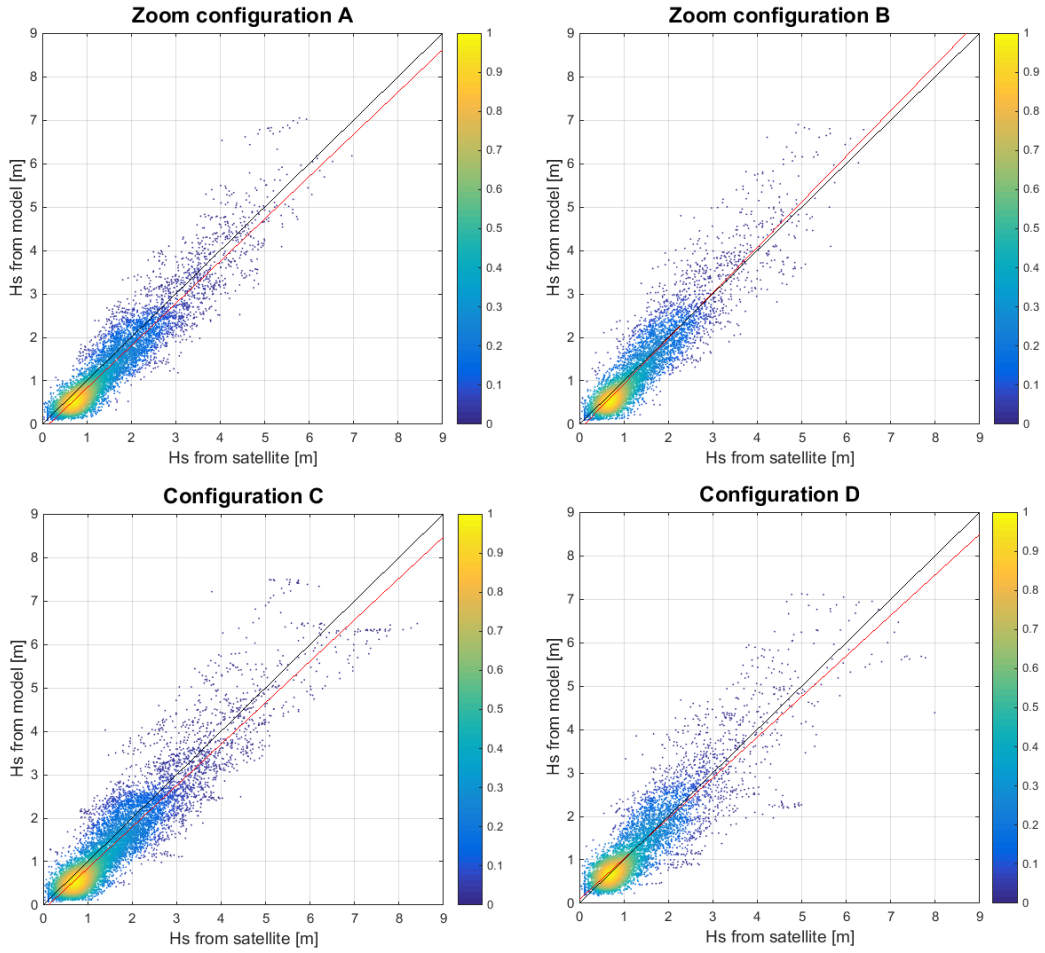

Figure 6.6: Comparison of observed (altimeter) and predicted significant wave height for the 2013, for the Balear Sea region. The colours represent the density of points.

In figure 6.5 the scatter diagrams of the collocated pairs of point for the Western Mediterranean sea region are presented, and in figure 6.6 the collocated pairs of point for the four configurations studied in the Balear Sea domain are presented. The colour scheme represents the number of values for box of 0.10 m normalized with the maximum number of values in a box. Each figure has two lines, the black line is the line of perfect agreement and the red line is the linear regression line, with formulation $a \cdot x + b$ (coefficients presented in table 6.5).

The statistics obtained from the validation process are presented in table 6.5. From these results a comparison between the regular nested grids and the unstructured grids can be easily performed, on the basis that the four configurations present acceptable values for the scatter index and the correlation coefficient. In fact, the dispersion of highest significant wave heights is considerable, probably due to the lower number of points compared to other measuring ranges.

Table 6.5: Statistics for the comparison of the collocated pair of points between the satellite measurements and four configurations model outputs, for the significant wave height; coefficients of the linear regression and number of collocated pairs of points.

Configuration	RMSE [m]	Bias [m]	SI	R	a	b	Number of values
A	0.42	-0.24	0.29	0.94	0.892	-0.081	72,520
B	0.40	-0.18	0.29	0.94	0.926	-0.078	31,991
A zoom	0.40	-0.18	0.30	0.93	0.974	-0.143	9,610
B zoom	0.41	-0.06	0.36	0.92	1.048	-0.120	6,596
C	0.46	-0.17	0.31	0.92	0.956	-0.103	12,583
D	0.50	-0.01	0.36	0.88	0.934	0.090	6,549

For the Western Mediterranean Sea domain the results obtained from configurations A and B are very similar, consistent with the situation previously observed in the buoy locations. Similar results are observed for the same configurations in a smaller region. However, the unstructured grid for the Balear Sea domain (configuration D) does not seem to work as good as the equivalent regular nested grids (configuration C). Hence, the small problems observed in configuration D for coastal areas are also appreciable when evaluating the entire domain with satellite measurements, with bigger RMSE, and worst scatter index and correlation coefficients. Further possible explanations for this discordances will be presented in the discussion section.

6.4.3 Storm analysis

The previous results show the average behaviour of the four configurations over a one-year period. However, one of the main purposes of an operational forecast system is to be able to predict a storm event a few days in advance. For this reason, the annual results have been analysed in order to identify all the storm events reaching the coast. The criteria used to define a storm were a significant wave height threshold of 2 m and a minimum duration of 8 h (Lin-Ye et al., 2016). At the Tarragona deep-water location seven storms were detected, with significant wave heights at the peak of the storm between 3 and 4.5 m. However, only three of them reached the coast and were detected from the Barcelona coast buoy or Tarragona coast buoy. The three storms had a similar pattern, occurring during autumn and winter and generated by important east winds. Since one of them was particularly intense and caused severe damages on the Catalan coast, it has been selected for the present study. The chosen storm occurred between the 26$^{\text{th}}$ of February 2013 and the 6$^{\text{th}}$ of March 2013, and it presents a two-peak profile. The first peak reaches a significant wave height of 4.5 m, and the second one between 3 and 4 m depending on the locations.

In figure 6.7 the time series for the significant wave height, the mean wave period and the direction, both observed and modelled, are presented for the Barcelona coast and Tarragona locations. The storm also reached the Tarragona coast buoy, but the results are not shown due to their similarity to the Barcelona buoy. From a qualitative analysis it seems that the four configurations tested work properly for the first storm peak but present some errors for the second one.

The statistics obtained for the Barcelona coast buoy, presented in table 6.6, show that for significant wave height there is almost no differences between configurations A, B and C, while configuration D presents the worst results, with a RMSE that doubles the others. It is interesting to remark that during the storm event configuration D presents an important negative bias in contrast with what is happening in the annual mean, where configuration D presents an overestimation. For the mean wave period, configurations A and B have similar behaviour, while C and D present some problems in the RMSE for the first one and the correlation coefficient in the second one. The bias for all the configurations is higher than that observed for the annual average. The direction is quite constant during the entire event and is well represented by the four configurations, although A and B present better results than C and D.

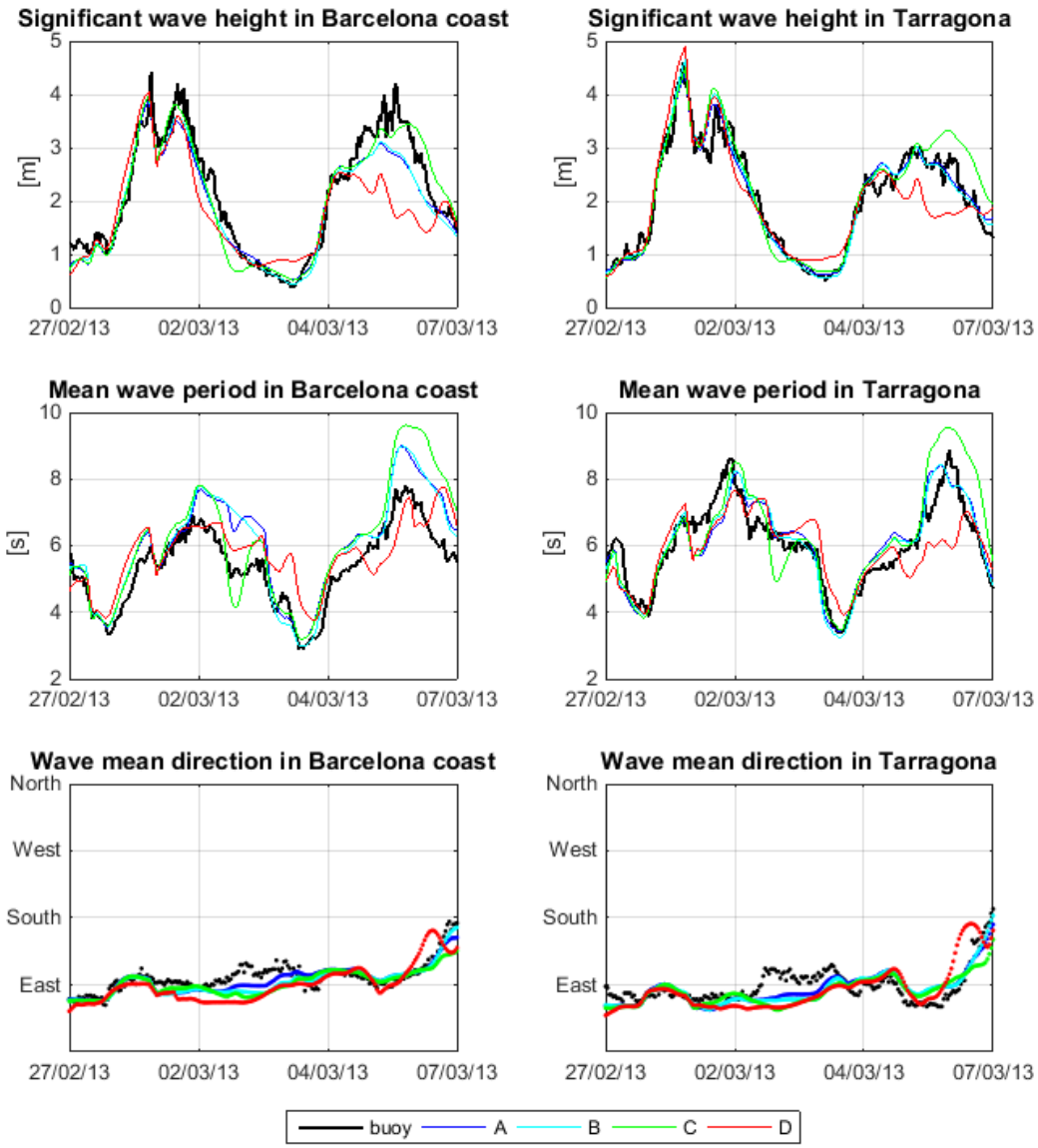

Figure 6.7: Time series for the significant wave height (first row), the mean wave period (second row) and the mean wave direction (third row) for the Barcelona coast location (first column) and the Tarragona location (right column) during the storm event. In black the buoy measurements are represented, while the colours correspond to the four configurations tested.

Table 6.6: Results of the validation of the four configurations including the significant wave height (m), the mean wave period (s) and the wave direction (degrees) for the storm event in Barcelona coast buoy location.

	Hs				Tm_{02}				Dir		
	RMSE [m]	Bias [m]	Si	R	RMSE [s]	Bias [s]	Si	R	RMSE [º]	Si	R
A	0.36	-0.19	0.17	0.97	0.87	0.66	0.16	0.94	11.31	0.03	0.94
B	0.35	-0.21	0.66	0.97	0.86	0.61	0.16	0.94	13.45	0.04	0.81
C	0.33	-0.07	0.15	0.96	1.05	0.69	0.20	0.93	16.29	0.05	0.69
D	0.69	-0.30	0.32	0.83	0.81	0.39	0.15	0.80	20.81	0.06	0.68

Table 6.7: Results of the validation of the four configurations including the significant wave height (m), the mean wave period (s) and the wave direction (degrees) for the storm event in Tarragona buoy location.

	Hs				Tm_{02}				Dir		
	RMSE [m]	Bias [m]	Si	R	RMSE [s]	Bias [s]	Si	R	RMSE [º]	Si	R
A	0.22	0.01	0.11	0.98	0.57	0.05	0.09	0.90	16.19	0.05	0.75
B	0.23	0.01	0.11	0.98	0.53	0.01	0.09	0.92	17.64	0.05	0.72
C	0.37	0.14	0.18	0.95	0.81	0.23	0.13	0.87	21.53	0.06	0.55
D	0.44	-0.06	0.21	0.90	0.82	-0.13	0.14	0.76	24.60	0.07	0.61

The results in deep waters, presented in table 6.7, show that, in contrast with the results for coastal areas, the significant wave height has better behaviour for configurations A and B than for configurations C and D, which depend on the boundary conditions obtained from the operational model. As previously seen, configuration D tends to underestimate the significant wave height during storm events as opposed to the annual behaviour. For the mean wave period and the mean wave direction similar observations can be made.

In conclusion, configurations A and B work best, and configuration D is the one presenting the worst results. The main difference can be found in configuration C, which works fine in coastal areas but not so well in deep waters.

6.4.4 Computational time requirements

Until now the comparison has been focused on the accuracy and quality of the results. However, there is another key point to account for in the comparison: the computational time required to obtain the results. This aspect can become vital in an early-warning system when the information is required as soon as possible in order to be able to take decisions.

Following this idea, a comparison of the four configurations described in section 6.3.1 has been carried out. The selected period for the comparison was June 2013, and the computer used is the one described in section 6.3.3.

Table 6.8: Computational time requirements for each of the grids used in the study (third column) and for each configuration tested (fourth column).

Configuration	Grids used	Grid time	Total time
A	Mediterranean regular	7 h 46 min	24 h 17 min
	Balear regular	8 h 10 min	
	Local regular	8 h 21 min	
B	Mediterranean unstrcutured	8 h 11 min	8 h 11 min
C	Balear regular	9 h 1 min	17 h 22 min
	Local regular	8 h 21 min	
D	Balear unstructured	14 h 33 min	14 h 33 min

The results for each of the grids are presented in the third column of table 6.8. The total time for each configuration can be obtained as the sum of the time required for each of the domains included in it. The results show a reduction of time of about 66% from the traditional way of providing a high-resolution wave forecast (the nested grids, configuration A) to the regional unstructured grid proposed in the present study (configuration B). Configuration C, using boundary conditions from an operational system, presents a reduction of time of about 23% with respect to configuration A. Finally, the Balear unstructured grid (configuration D) is faster than configuration C but slower than configuration B due to the time required to read the boundary conditions, despite configuration D having fewer nodes than B.

6.5 Discussion

In the present study the use of unstructured grids is presented as an alternative to the traditional downscaling methods consisting of a series of nested grids. The unstructured grids (figure 6.1) allow the boundary conditions to be removed, obtaining high-resolution forecasts in less computational time. However, it should be taken into account that designing an efficient unstructured grid is a long process, and still some small problems can appear, as happens with configuration D.

From the analysis of annual results, both in coastal areas and in deep waters, it can be concluded that using a system of nested grids (configuration A) or a regional unstructured grid (configuration B) provides almost the same results, so there is no effect of the meshes used on the accuracy of the forecast. Some differences may appear when nesting the local grids (regular as in configuration C or unstructured as in configuration D) due to the boundary conditions. These differences mainly depend on the quality of the boundary conditions for regular grids. From the present study it can be stated that using good boundary conditions generates forecasts very similar to the ones generated by a regional model, like happens with configuration C.

The mentioned differences are more relevant when nesting an unstructured grid into a regular regional system (configuration D), obtaining lower correlation coefficients and presenting a slight overestimation of the results not seen in the other configurations. It should be pointed out that in the SWAN model it is possible to introduce boundary conditions in two different ways: providing the full spectrum in all the boundary points, or providing some bulk parameters (significant wave height, wave period, wave direction and wave spread) and letting the model calculate a theoretical spectrum with this information. In both configurations C and D, the second option has been used, but only some problems have been detected with the unstructured grid (configuration D). In order to assure that the small problems in configuration D are due to the reading of the boundary conditions and not related to the grid design, some additional tests have been carried out.

The sensitivity test has been performed in order to evaluate the ability of the SWAN model to read different types of boundary conditions when using unstructured grids. Two situations are compared, consisting in (1) introducing boundary conditions in a parameter form (including the significant wave height, the mean wave period, the mean wave direction and the wave spread coefficient obtained from the operational service), and (2) introducing boundary conditions in a spectral form (directly obtained from the SWAN wave model using a regular coarser domain). The different options are used for both configurations C and D (corresponding to

the regular nested system and the unstructured Balear grid respectively).

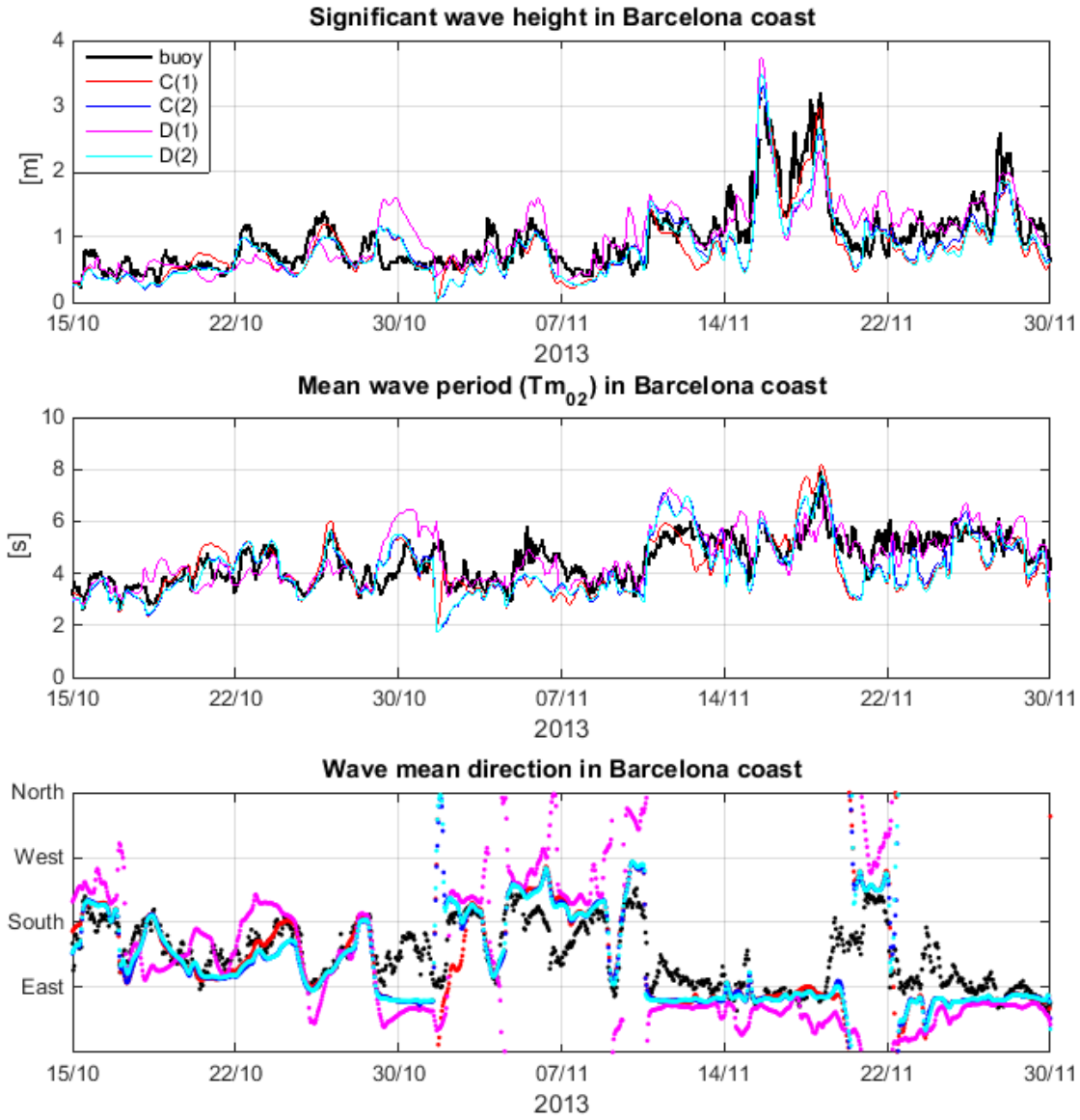

Figure 6.8: Time series for the significant wave height (top), the mean wave period (medium) and the mean wave direction (bottom) comparing the buoy measurements in black and the SWAN results for configurations C and D using boundary conditions in parameter form (1) and in spectral form (2).

The test is carried out for the two measurement locations, in the Barcelona coast buoy location and in the Tarragona buoy location, for a one year period. In figure 6.8 a time series for the significant wave height, the mean wave period (Tm_{02}) and the mean wave direction is presented during a one month and a half period, when a storm event reached the area. From the presented results it is clearly stated that the SWAN model has some problems when reading and/or processing the boundary conditions

in parametric form on unstructured grids (D(1)). This problems disappear using exactly the same boundary conditions in regular grids (C(1)) or when using spectral boundary conditions in the unstructured grid (D(2)).

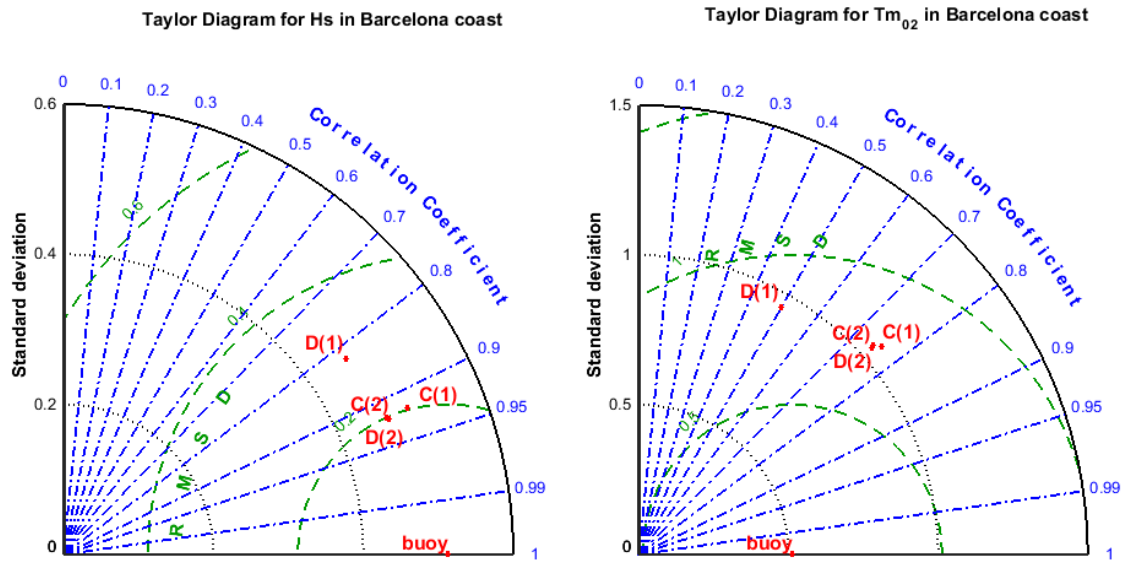

Figure 6.9: Taylor diagram of the significant wave height (left) and the mean wave period (right) for the annual analyse in the Barcelona coast location for configurations C and D using boundary conditions in parameter form (1) and in spectral form (2).

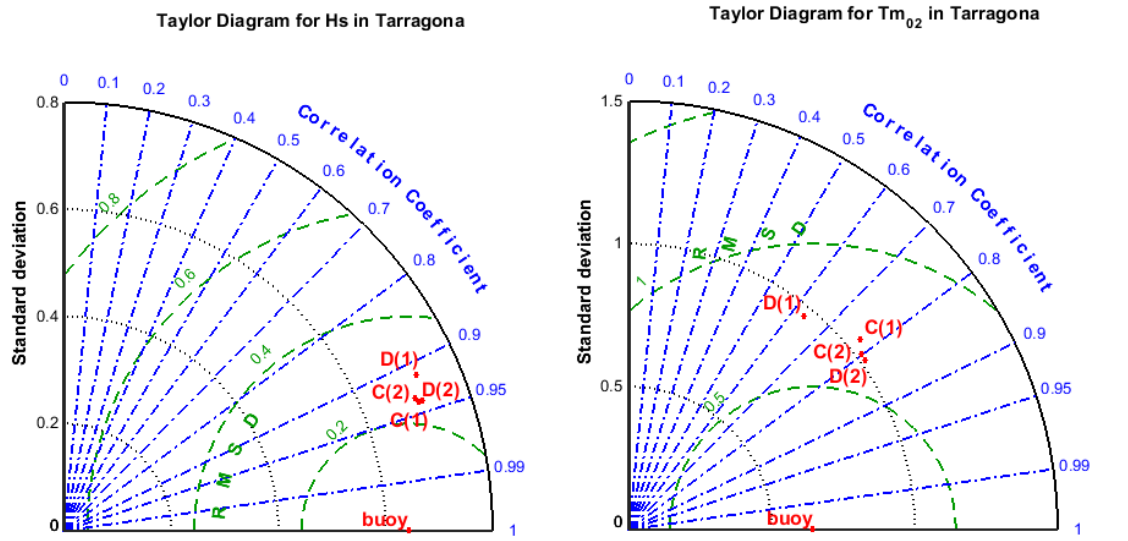

Figure 6.10: Taylor diagram of the significant wave height (left) and the mean wave period (right) for the annual analyse in the Tarragona location for configurations C and D using boundary conditions in parameter form (1) and in spectral form (2).

In order to quantify this errors, in figures 6.9 and 6.10 the Taylor diagrams for the significant wave height and the mean wave period are represented for both validation locations for the entire year, thereby confirming that is not a local problem.

The Taylor diagrams show that both configurations, C and D, present almost equivalent results when using the boundary conditions obtained from a coarser SWAN domain in spectral form (2). However, when using the boundary conditions obtained from the Puertos del Estado operational service in parameters form (1), the regular grids present similar results to the previous ones, while the unstructured grid is not able to properly use this boundary conditions providing worst results for the significant wave height and the mean wave period for both locations.

When running configuration D using the full spectra as boundary conditions, obtained directly from SWAN simulations in the biggest grid of configuration A, the obtained results are almost equivalent to the ones from configuration C (figures 6.9 and 6.10). From the analysis of the test it seems that the local unstructured grid only works properly when the boundary conditions are provided as a spectra (not always available from an operational forecast service), and some errors appear when the boundary conditions are provided in parameter form.

A storm event has also been analysed, with very similar conclusions. Although during energetic events the different configurations tend to work better than for the annual average, the behaviours of the different configurations are very similar. The regional configurations (A and B) present very similar results, confirming that there is almost no contrast between unstructured grids and regular nested grids. The differences, more important during energetic events, appear when introducing boundary conditions from an operational forecasting system.

The computational time required is the key point of the configuration comparison. All the considered configurations present a reduction of time with respect to the traditional methodology, with the unstructured regional grid being the most important, with a decrease of around 66% without losing quality in the wave forecast. The local regular domains nested in a forecast system also present very good results and a reduction of time of 23% with respect to the traditional methodology.

The unstructured grids have considerably fewer points than the regular grids (table 6.1). However, the numerical scheme for these grids is slower, obtaining a total computational time per grid of the same order of magnitude as a regular grid. The advantage derives from the fact that only one unstructured grid is necessary as compared to a system of several nested grids.

One last critical point is that the Mediterranean unstructured grid is faster than the Balear unstructured grid despite having a greater number of nodes. This increase

of time is due to the process of reading and interpolating the boundary conditions from several locations at the boundaries into the grid nodes located at the boundaries (not regularly distributed). When working with boundary conditions in spectral form, the time required to run the Balear unstructured grid is reduced to 5 h and 12 min.

6.6 Conclusions

In recent years the application of unstructured grids in wave modelling has been gaining relevance. In the present study an unstructured grid applied to a regional environment like a semi-enclosed sea is compared to the traditional downscaling method in terms of both the accuracy of the results and the computational time required. Two local grids (one regular and the other unstructured) nested in an operational system are also included in the comparison. The main conclusions obtained can be summarized in three points.

Designing a good unstructured grid is a hard process that only needs to be done once. After obtaining an efficient and accurate unstructured grid, it is possible to achieve the same forecast accuracy and costal resolution as the traditional downscaling method, with an important reduction of the computational time.

For semi-enclosed domains it is more interesting to generate a regional unstructured grid than a local grid nested into an operational forecasting system. However, if the operational system provides good boundary conditions, as happens in the present study, the local nested grid may provide accurate results with a reduction of time with respect to the traditional method.

Finally, the SWAN model presents some problems when using boundary conditions in parameter format in unstructured grids with respect to regular grids. These differences disappear when the boundary conditions come in a spectral format.

Chapter 7

Final discussion and conclusions

7.1 Summary

The main objective of this thesis is to improve the actual wave forecasting abilities for the Catalan Coast. Although several previous studies have identified some of the main characteristics of the wave climate and have improved considerably the wave prediction in the area, some progress can still be achieved which have not been acquired in previous contributions. In consequence, the chapters included in the thesis pointed out the different aspects which remain to be solved.

The work presented in chapter 3 has been motivated by the limited accuracy of wave models under short-duration and fetch-limited conditions. This applies particularly to the wave period, in semi-enclosed domains with highly variable wind patterns along the Catalan coast, where the wave growth rates included in the models are lower than the measured rates (Alomar et al., 2014). The spectral wave model SWAN was implemented in three nested grids covering all the North-western Mediterranean Sea with a grid resolution from 9 to 1 km, forced with high resolution wind patterns from BSC (Barcelona Supercomputing Center) for two study periods, the winter 2010 and the spring 2011. The results were validated in eight locations with different types of in-situ instruments.

In order to correct this systematic errors, a modification of the delta value in the Hasselmann (1974) whitecapping term formulation was performed, based on the Rogers et al. (2003) previous work, thus improving the prediction of the energy spectra at lower frequencies. This correction is appropriate only for young and moderate sea wave conditions. In fact, the SWAN team has recently modified this delta coefficient according to the findings presented in this thesis.

The appropriate frequency integral range used to calculate the integral wave parameters from the model results was also tested. This was done to compare the

simulation results and the instrument data for the same frequency interval.

The results obtained show a clear improvement of the mean wave period and the peak period for the study area, decreasing considerably the negative bias observed previously, while almost no change was observed in wave height due to the proposed modifications. These results can be generalized for the Spanish Mediterranean coast and may be applicable to study areas with similar characteristics as the ones presented here: semi-enclosed domains with fetch-limited conditions, variable wind conditions and young sea waves.

When working in coastal areas the interaction between wind, waves and currents fields is not negligible, and therefore it is recommendable to couple the different numerical models. The effect of the coupling in the wave modelling was analysed for the Catalan coast in chapter 4. Two different types of coupling were considered, the first one consists of a one-way coupling in which the current field is directly introduced in the SWAN wave model, and the second consists of a two-way coupling in which the wave model, the current model and the atmospheric model are run in parallel and information is transferred between them. Both coupling methodologies have been tested for a calm period but also during a local energetic event (when the effect of the coupling is expected to be more important): a current intensification in front of the Barcelona harbour and a wind jet event in the Ebro river shelf.

The results for the Catalan coast show that during clam events the one-way interaction between the waves and the ambient currents are negligible, even during storm events. However, during intense episodes of currents (one order of magnitude higher than usual) or when the wind is extremely intense and it interacts with opposite wave conditions, the effect of one-way or two-way coupling should be considered.

The main processes affecting the waves during the interaction are the wind-stress modification in the presence of currents, the wave refraction due to currents and the sea surface roughness modification.

It should be noted that the coupled models have higher computational requirements, mostly when a two-way coupling is performed and several models need to run at the same time in the same computer. For this reason, it is not always feasible to implement this kind of models in an operational forecasting system, especially when the benefits are only appreciable under very specific conditions.

In this sense, in chapter 5 the use of an unstructured grid with a varying resolution instead of a system of nested regular grids was considered, improving the resolution in coastal areas while reducing the computation time. The main advantage of using an unstructured grid for wave modelling is that it allows working with a single mesh with different resolutions in each of the sub-domains, and therefore

the nesting is not needed, avoiding the associated problems due to the internal boundary conditions. Another advantage is that the grid can reproduce the sharp coastline with more accuracy than regular meshes. Finally, unstructured grids allow in a natural manner to build in a two-way nesting, a process especially interesting in situations of land winds such as the Mistral case in the Mediterranean coast.

On the other hand, the use of unstructured grids in SWAN also has some drawbacks: the same parametrizations need to be used in all the domain, usually involving different scales. Additionally, in some local areas with step gradients and too coarse spatial resolution some unwanted accumulation of wave energy may occur due to the numerical scheme used in SWAN, which can be solved by activating a refraction limiter.

The design of the unstructured grid plays an important role in the quality of the results. In this sense, adding some size criteria to the basic distribution of grid sizes is decisive to obtain efficient grids with a cell refinement only where necessary. The first criteria presented depend on the distance to the coast, because it is in this areas where high resolution wave conditions are usually required, but also where more information is available (e.g. better wind forcing). The second criteria proposed increases the grid resolution as a function of the water depth and the bathymetric gradients where the influence of the bottom modifies the wave fields.

In chapter 5 two unstructured grids were designed according to the mentioned criteria, covering the Western Mediterranean Sea and the Balear Sea with coastal resolutions up to 800 m. The grids were tested for a one year period using two high resolution wind field domains from AEMET, and were validated with in-situ and remote-sensing measurements.

The results obtained for the coastal areas presented good agreement with buoy measurements, mainly for deep water buoys. The simulations in this areas showed that increasing the spatial resolution of the wind forcing slightly improved the significant wave height statistics in averaged yearly results. The validation with satellite data supports the previous results also in open waters, confirming the unstructured grids as a valid alternative to the nested regular systems.

Finally, in chapter 6, a direct comparison between the unstructured grids and the traditional downscaling method was presented. Traditionally, wave modellers used a downscaling process by means of successive nested grids to obtain high-resolution wave fields near the coast. This supposes an uncertain error due to internal boundary conditions and a long computational time. Unstructured grids avoid multiple meshes and thus also eliminating the problem of internal boundary conditions.

In the present study, high-resolution wave simulations were analysed for a full year where high-resolution meteorological models were available in the Catalan

coast, comparing the traditional nested sequence and a regional unstructured grid. Also a local unstructured grid nested in an operational forecast system was included in the analysis.

The obtained results were compared to wave observations from buoys near the coast and to satellite data along the simulation domain. In both cases, almost no differences were observed between the unstructured grids and the regular grids.

Simultaneously, tests have been carried out in order to analyse the computational time required for each of the alternatives, showing a decrease to less than half the time when working with regional unstructured grids and maintaining the forecast accuracy and coastal resolution with respect to the downscaling system. Despite the numerical scheme for unstructured grids is slower, the total time requirements were reduced since only one grid was necessary to cover different domains and resolutions.

An additional sensitivity test was performed in order to evaluate the performance of SWAN model using unstructured grids when boundary conditions were introduced in two different formats. For the first test, using boundary conditions in a spectral format (directly generated from a coarser domain SWAN simulation), the model performed properly, showing no differences between regular and unstructured grids. However, for the second test, when boundary conditions were obtained from an operational system in a parametric form (including the significant wave height, the mean wave period and the wave direction), SWAN unstructured grid simulations presented some discrepancies. This issue is still being investigated together with the SWAN team.

Despite these last small drawbacks, the unstructured grids are proved to be a better alternative to the traditional nested systems. The results obtained were as good as the ones obtained from regular grids or even better, providing high resolution only where the wave field is expected to present variations and reducing considerably the computation time. In conclusion, in few years the unstructured grids would be the preference for most of the wave modelling community.

7.2 Conclusions

According to the main objective of this thesis, consisting on improving the actual wave forecasting abilities for the Catalan Coast, the conclusions associated to each specific objective are:

1. *Improve the wave forecasting in the Catalan coast by tuning the wave model parametrizations related to the wave growth.*

    - The overall model performance is a combination of various terms contributing to the action balance. The whitecapping term is the easier parameter to tune, since it is the least well-known term in wave models. However, the problem also affects the growing terms.
    - The whitecapping term correction proposed by Rogers et al. (2003) is a good solution for young sea conditions, in which the growth rates are under predicted by the models. With this correction, an increase of the energy spectra at lower frequencies is presented, reducing the under-prediction of the wave period.
    - However, the proposed formulation is only suitable for the early stages of generation and should be discontinued after the waves reach a certain maturity.
    - Since this correction is based on the physics of the young sea evolution it should be applicable to other similar environments.
    - Finally, the integral wave parameters obtained from the wave simulations and the instrument measurements should be referred to the same frequency integration range in order to compare the two magnitudes under the same conditions, since the spectral high frequency tail is present in the wave model results but it is not included in the measurements.

2. *Evaluate the effect of the coupling between the wave model and the current and atmospheric models for different situations.*

    - Two different types of coupling were proposed, a one-way coupling consisting of introducing the current field as an input for the wave model to analyse the effect of ambient currents on the wave field, and a two-way coupling consisting of running at the same time an atmospheric, current and wave model. The interaction between fields is better represented in the second type, but this method also requires higher computational requirements which are not always available.

- During most of the time for the Catalan coast, under calm conditions, the coupling between models does hardly improve the results. Even when a storm event is reaching the coast, with significant wave height up to 2.5 m, if the current magnitude are not extremely intense the coupling can be neglected.
- However, during local energetic events the coupled predictions provide a more accurate reproduction of the situation. For the Catalan coast these energetic events correspond to superficial current intensifications and wind jet events.
- An equilibrium should be searched between the computational requirements associated to the coupled systems and the improvements obtained from the coupling.
- The main physical processes affecting the wave field due to the coupling are the sea surface roughness modification in presence of intense winds, and the wave refraction together with the wind-stress modifications in presence of intense currents.

3. *Consider the use of unstructured grids as an alternative of the regular nested grids.*

   - After a one-year period simulations analysis the unstructured grids are proved to be a good alternative to the traditional nested systems for the study area.
   - The results of the validation with in-situ measurements presented high correlation coefficients and RMSE and biases the same order of magnitude than the ones obtained in previous works using regular grids.
   - As expected, the wave simulations presented a better agreement in deep water areas than in coastal locations.
   - Improving the wind field resolution generated few variations on the wave predictions, only appreciable for the significant wave height.
   - The design of the unstructured grid is probably the most delicate part, and usually requires a lot of work and time. However, it should be considered a worthy investment due to the good results obtained.

4. *Define the criteria necessary to generate an efficient unstructured grids, considering the grid resolution and the distribution of cells in the domains.*

   - The basic unstructured grids obtained without any size criteria were not good enough, presenting an excess of cells in some areas and a lack of resolution in some subdomains.

- Two different criteria were proposed to increase the grid size: in the areas near the coast, as a function of the distance to the shore line, and also in intermediate and shallow waters, as a function of the depth and he bathymetric gradients.
- The resulting grids present less elements and nodes than the basic ones and, what it is more important, the triangles are better distributed along the domain.
- The criteria can be applied to other locations, but need to be calibrated depending on the geometric characteristics and the wave conditions of the domain to be simulated.

5. *Assess the viability of these improvements into an operational forecasting system.*

   - The important improvements obtained from tuning the wave model parameterizations are easy to implement in an operational system, and do not require any additional computational cost.
   - In contrast, the two-way coupling between models is not an easy process to incorporate in an operational forecasting system due to the high computational requirements associated to this methodology and the small benefits obtained, only appreciable in few situations and in punctual locations.
   - The one-way coupling can be considered in an operational forecasting system, since the computational cost associated is small (mainly related to computer memory necessary to save all the current fields files). However, in order to implement a one-way coupling the accuracy of the current fields should be guaranteed if one wants to avoid worsening the wave predictions.
   - Finally, unstructured grids can be considered a great alternative to regular nested grids systems, especially for an operational forecasting system, since the experience shows that the accuracy of the results is maintained and the computational time is highly reduced.
   - Some differences appear when working with regional unstructured grids (e.g. the Western Mediterranean grid presented in this thesis) and local nested grids (e.g. the Balear sea domain grid). The first involve several scales and so it will be difficult to determine which parametrizations to use. In contrast, this kind of grids is faster. The second grids cover smaller areas and thus the scales affected are also smaller. This grids

characteristic makes it easy to choose the coefficients and parametrizations. However, these grids are usually nested to other models and need boundary conditions that can incorporate important errors. Finally, the SWAN model presents some problems when reading boundary conditions in some specific formats, so special attention is required.

7.3 Future work

The work presented in this document sheds some light to some questions related to the wave forecasting in semi-enclosed domains and coastal areas with high variable wind conditions, including the adaptation of the spectral wave models to the wave growth characteristics of the area, the effect of coupling the wave model with a circulation and meteorological models, or the use of unstructured grids as an alternative to the traditional nested systems to obtain high resolution in coastal areas. However, new questions have also arisen from the work performed that are suggested in the following lines.

The actions proposed in this chapter 3 related to the wave growth implemented in the model and the rates measured in the area corrected part of the problem of the wave under prediction, but are far from a final solution since better formulations for the energy balance terms are necessary to reproduce the actually occurring growth and dissipation rates in coastal areas within semi-enclosed domains.

In this sense it is important to remark that the results presented in this document correspond to relatively small periods, so an analysis of extended periods (including several years) together with a discretization of the results depending on the season or the wave characteristics should be advisable.

Another aspect not treated in the thesis is the use of other models for wave prediction, and specifically the use of other numerical schemes when working with unstructured grids. The SWAN wave model uses an implicit numerical scheme that has been proven to properly solve the unstructured grids with a reduction of the computational time in comparison to the traditional nested grids system. However, a comparison between an implicit and an explicit numerical scheme would be very interesting in terms of computational requirements and results accuracy. In this sense, the Wave Watch III model offers the possibility to choose between the two numerical schemes mentioned. Additionally, the WWIII spectral wave model is continuously introducing new parametrizations that may be interesting to try for the study area, like the recent formulations to predict extreme waves not only considering the temporal variability but also the spatial variability (Barbariol et al., 2016).

Finally, despite every day the wave information provided by the models is improving in quality (including the resolution and the accuracy of the results), the wave forecast is based on a deterministic solution of the problem. In the recent years some efforts have been carried out in order to generate a methodology to determine the uncertainty associated with the wave forecast. Based on the meteorology progresses, the ensemble methodology has recently been applied to the wave

prediction (e.g. Bunney and Saulter, 2015). This methodology consists in using an ensemble of winds to force the wave model, obtaining a range of possible predictions for the following days. Once all the possibilities are simulated several statistics can be computed in order to define the most probable, and then add a probability accompanying the wave prediction. The first exercises performed in the Catalan coast in this direction were carried out using global ensemble wind fields, no accurate enough to capture the variability of the Western Mediterranean Sea. So that, high resolution ensemble winds should be generated before implementing an ensemble wave forecast, thing that will surely happen during the next few years.

Bibliography

Abdalla, S, J Bidlot, and P Janssen (2006), "Global validation and assimilation of envisat asar wave mode spectra." In *Proceedings of the Advances in SAR Oceanography from ENVISAT and ERS Missions, ESA-ESRIN*, Paper No. 176, Frascati, Rome, Italy.

Akpinar, A, G van Vledder, M Komurcu, and M Ozger (2012), "Evaluation of the numerical wave model (swan) for wave simulation in the black sea." *Continental Shelf Research*, 50, 80–99.

ALADINteam (1997), "The aladin project: Mesoescale modelling seen as a basic tool for weather forecasting and atmospheric research." *WMO bulletin*, 46, 317–324.

Alari, V, U Raudsepp, and T Koutsr (2008), "Wind wave measurements and modelling in küdema bay, estonian archipelago sea." *Journal of Marine Systems*, 74, 530–540.

Alomar, M (2012), *Improving wave forecasting in variable wind conditions. The effect of resolution and growth rate for the Catalan coast.* Ph.D. thesis, Universitat Politecnica de Catalunya.

Alomar, M, A Sanchez-Arcilla, R Bolaños, and A Sairouni (2014), "Wave growth and forecasting in variable, semi enclosed domains." *Continental Shelf Research*, 87, 28–40.

Alves, J, S Stripling, A Chawla, H tolman, and A van der Westhuysen (2015), "Operational wave guidance at the u.s. national weather service during tropical7post-tropical storm sandy, october 2012." *Monthly Weather Review*, 143, 1687–1702.

Ardhuin, F, L Bertotti, J Bidlot, L Cavaleri, V Filipetto, J Lefevre, and P Wittmann (2007), "Comparison of wind and wave measurements and models in the western mediterranean sea." *Ocean Engineering*, 34, 526–541.

Ardhuin, F and A Roland (2013), "The development of spectral wave modes: coastal and coupled aspects." *Coastal Dynamics*, 4, 833–846.

Ardhuin, F, J Torunadre, P Queffeulou, F Girard-Ardhuin, and F Collard (2011), "Observation and parameterization of small icebergs: Drifting breakwaters in the southern ocean." *Ocean Modelling*, 39, 405–410.

Arnau, P (2000), *Aspectos de la variabilidad de mesoescala de la circulación marina en la plataforma continental catalana*. Ph.D. thesis, Universitat Politecnica de Catalunya.

Barbariol, F, J Alves, A Benetazzo, F Bergamasco, S Carniel, Y Chao, A Chawla, A Ricchi, and M Sclavo (2016), "Extreme wave analysis in the space-time domain: from observations to applications." In *EGU 2016 – European Geoscience Union General Assembly 2016*, Vienna, Austria.

Battjes, J and J Janssen (1978), "Energy loss and set-up due to breaking of random waves." *Proceedings of th 16th International Conference on Coastal Engineering, ASCE*, 569–587.

Benetazzo, A, S Carniel, M Sclavo, and A Bergamasco (2013), "Wave-current interactions: effect on the wave field in a semi-enclosed basin." *Ocean modelling*, 70, 152–165.

Benoit, M, F Marcos, and F Becq (1996), "Development of a third generation shallow-water wave model with unstructured spatial meshing." In *Proceedings of the 25th International Conference in Coastal Engineering*, 465–478, Orlando, Florida.

Bertotti, L, L Cavaleri, A Soret, and R Tolosana-Delgado (2014), "Performance of global and regional nested meteorological models." *Continental Shelf research*, 87, 17–27.

Bidlot, J, D Holmes, P Wittmann, R Libeharry, and H Chen (2002), "Intercomparison of the performance of operational ocean wave forecasting systems with buoy data." *Weather and Forecasting*, 287–310.

Bidlot, J and M Holt (1999), "Statistical properties of global significant wave height and their use for validation." *Journal of Geophysical Research*, 103, 1153–1166.

Bilgili, A, K Smith, and D Lynch (2006), "Battri: a two-dimensional bathymetry-based unstructured triangular grid generator for finite element circulation modelling." *Computers and Geosciences*, 32, 632–642.

Bolaños, R (2004), *Tormentas de oleaje en el Mediterráneo: Física y Predicción*. Ph.D. thesis, Universitat Politecnica de Catalunya.

Bolaños, R, G Jorda, J Cateura, J Lopez, J Puigdefabregas, J Gomez, and M Espino (2009), "The xiom: 20 years of a regional coastal observatory in the spanish catalan coast." *Journal of Marine Systems*, 77, 237–230.

Bolaños, R, P Osuna, J Wolf, and A Sanchez-Arcilla (2011), "Development of the polcoms-wam current-wave model." *Ocean Modelling*, 36, 102–115.

Bolaños, R and A Sanchez-Arcilla (2006), "A note on nearshore wave features: Implications for wave generation." *Progress in Oceanography*, 70, 168–180.

Bolaños, R, A Sanchez-Arcilla, and J Cateura (2007), "Evaluation of two atmospheric models for wind–wave modelling in the nw mediterranean." *Journal of Marine Systems*, 65, 336–353.

Booij, N, R Ris, and L Holthuijsen (1999), "A third-generation wave model for coastal regions. 1. model description and validation." *Journal of Geophysical Research*, 104, 7649–7666.

Brown, G (1997), "The average impulse response of a rough surface and its applications." *IEEE Transactions on Antennas and Propagation*, 25.

Bunney, C and A Saulter (2015), "An ensemble forecast system for prediction of atlantic-uk waves." *Ocean Modelling*, 96, 103–116.

Cavaleri, L and L Bertotti (2004), "Accuracy of the modeled wind and wave fields in enclosed seas." *Tellus*, 56A, 167–178.

Cavaleri, L and P Malanotte-Rizzoli (1981), "Wind wave prediction in shallow water: Theory and applications." *Journal of Geophysical Research*, 86, 961–973.

Cerralbo, P, M Grifoll, J More, M Bravo, A Sairouni, and M Espino (2015), "Wind variability in a coastal area (alfacs bay, ebro river delta)." *Advances in Science and Research*, 12, 11–21.

Charnock, H (1995), "Wind stress over a water surface." *Quarterly Journal of the Royal Meteorological Society*, 81, 639–640.

Chawla, A, H Tolman, V Gerald, D Spindler, J Alves, D Cao, J Hanson, and E Devaliere (2013), "A multigrid wave forecasting model: a new paradigm in operational wave forecasting." *Weather and forecasting*, 28, 1057–1078.

Chen, H (1995), *Ocean surface waves*, volume 18 pp. TPB 426,NOAA/NWS/OM.

Clancy, R, J Kaitala, and L Zambreski (1986), "The fleet numerical oceanography center global spectral ocean wave model." *Bulletin of the American Meteorology Society*, 67, 498–512.

Datawell (2006), *Datawell waverider reference manual*. Datawell, BV.

Dietrich, J, S Tanaka, J Westerink, C Dawson, R Luettich, M Zijlema, L Holthuijsen, J Smith, L Westerink, and H Westerink (2012), "Performance of the unstructured-mesh, swan+adcirc model in computing hurricane waves ans surge." *Journal of Scientific Computing*, 52, 68–97.

Dietrich, J, J Westerink, A Keneddy, J Smith, R Jensen, M Zijlema, L Holthuijsen, C Dawson, R Luettich, M Powell, V Cardone, A Cox, G Stone, H Pourtaheri, M Hope, S Tanaka, L Westerink, H Westerink, and Z Cobell (2011a), "Hurricane gustav (2008) waves and storm surge: hindcast, validation and synoptic analysis in southern louisiana." *Monthly Weather Review*, 139, 2488–2522.

Dietrich, J, M Zijlema, P Aier, L Holthuijsen, N Booij, J Meixner, J Profit, C Dawson, C Bender, A Naimaster, J Smith, and J Westerink (2013), "Limiter for spectral propagation velocities in swan." *Ocean Modelling*, 70, 85–102.

Dietrich, J, M Zijlema, J Westerink, L Holthuijsen, C Dawson, R Luettich, R Jensen, J Smith, G Stelling, and G Stone (2011b), "Modeling hurricante waves and storm surge using integrally-coupled, scalable computations." *Coastal Engineering*, 58, 45–65.

Dinardo, S, J Benveniste, L Fegnolio-Marc, and R Scharroo (2014), "Validation of open-sea cryosat-2 data in sar mode in the german bight." In *40th COSPAR Scientific Assembly*, volume Abstract A2, 1-32-14, 710 p, Moscow, Russia.

Drenann, W, H Graber, D Hauser, and C Quentin (2003), "On the wave age dependence of wind stress over pure wind seas." *Journal of Geophysical research*, 108, 8062.

ESA and CNES (2016), "Radar altimetry tutorial and toolbox." *Retrieved from http://www.altimetry.info*.

et al., P Unden (2002), "Hirlam -5 scientific documentation." *Available online in:*, www.hirlam.org.

Ewing, J (1971), "A numerical wave prediction method for the north atlantic ocean." *Erganzungsheft zur Deutschen Hydrographischen Zeitschrift*, 24, 21–261.

Ferrarin, C, G Imguesser, A Cucco, A Roland, and C Amos (2008), "Development and validation of a finite element morphological model for shallow water basins." *Coastal Engineering*, 55, 716–731.

Font, J (1990), "A comparison of seasonal winds with currents on the continental slope of the catalan sea (northwestern mediterranean)." *Journal of Geophysical Research*, 95, 1537–1545.

Font, J, E Garcia-Ladona, and E Gorriz (1995), "The seasonality of mesoescale motion in the northern current of the western mediterranean: several years of evidence." *Oceanologia Acta*, 18, 207–219.

Francis, P and R Stratton (1990), "Some experiments to investigate the assimilation of seasat altimeter wave height data into a global wave model." *Quartery Journal of the Royal Meteorological Society*, 116, 1225–1251.

Garcia, M, A Sanchez-Arcilla, j Sierr, J Sospedra, and J Gomez (1993), "Wind waves off the ebro delta, nw mediterranean." *Journal of Marine System*, 4, 235–262.

Goldin, B (1983), "A wave prediction system for real time sea state forecasting." *Quarterly Journal of the Royal Meteoroogical Society*, 109, 393–416.

Gomez, M and J Carretero (2005), "Wave forecasting in the spanish coasts." *Journal of Atmospheric and Ocean Science*, 10, 389–405.

Gracia, V, M Garcia-Leon, A Sanchez-Arcilla, J Gault, P Oller, J Fernandez, A Sairouni, E Cristofoli, and R Toldra (2014), "A new generation of early warning system for coastal risk. the icoast project." In *International Conference in Coastal Engineering, ICCE 2014*, Seoul, Korea.

Grifoll, M, A Aretxabaleta, and M Espino (2015), "Shelf response to intense offshore wind." *Journal of Geophysical Research - Oceans*, 120, 664–658.

Grifoll, M, A Aretxabaleta, J Pelegri, M Espino, J Warner, and A Sanchez-Arcilla (2013), "Seasonal circulation over the catalan inner-shelf (northwest mediterranean sea)." *Journal of Geophysical research*, 118, 1–14.

Haidovel, D, H Arango, W Budgell, B Cornuelle, E Curchister, E di Lorenzo, K Fennel, W Geyer, A Hermann, L Lanerolle, J Levin, J McWilliams, A Miller, A Moore, T Powell, A Shcheoetkin, C Sherwood, R Signell, J Warner, and J Wilkin (2008), "Regional ocean forecasting in terrain-following coordinates: model formulation and skill assessment." *Journal of Computational Physics*, 227, 3595–3624.

Hasselmann, K (1960), "Grundgleichungen der seegangsvoraussage." *Schiffstechnik*, 7, 191–195.

Hasselmann, K (1974), "On the spectral dissipation of ocean waves due to white-capping." *Boundary-layer Meteorology*, 6, 107–127.

Hasselmann, K, T Barnet, E Bows, H Carlson, D Cartwrght, K Enke, J Ewing, H Gienapp, D Hasselmann, Kruseman, A Meerburg, P Muller, D Olbers, K Richter, W Sell, and H Walden (1973), "Measurements of wind-wave growth and swell decay during the joint north sea wave projec (jonswap)." *Erganzungsheft zur Deutschen Hydrographischen Zeitschrift, Reihe*, A(8),12, 95pp.

Hasselmann, K, K Hasselmann, J Allender, and T Barnett (1985), "Computations and parameterizations of the nonlinear energy transfer in a gravity wave spectrum. part ii: Parameterizations of the nonlinear transfer for application in wave models." *Journal of Physical Oceanography*, 15, 1378–1391.

Holt, J and I James (2001), "An s coordinate density evolving model for the northwest european continental shelf. model description and density structure." *Journal of Geophysical Research*, 9, 1087–1112.

Holt, M (1994), "Improvement to the ukmo wave model swell dissipation and performance in light winds." *Met Office Forecasting Research Division Tech. Rep.*, 119, 12pp.

Holthuijsen, L (2007), *Waves in Oceanic and coastal waters*, y schreer and o c zienkiewicz edition. Computer Modelling in Ocean Engineering.

Holthuijsen, L and S DeBoer (1988), *Wave forecasting for moving and stationary targets*, volume 387 pp. Cambridge University Press.

Hsu, T, S Ou, and J Liau (2005), "Hindcasting nearshore wind waves using a fem code for swan." *Coastal Engineering*, 52, 17–195.

Jacob, R, J Larson, and E Ong (2005), *M x N communication and parallel interpolation in CCSM using the Model Coupling Toolkit*. Preprints, Mathematics and Computer Science Division.

Jansa, A (1985), "The 'mistral-tramuntana' shear line. a satellite observation, scientific results of the alpine experiment (alpex)." *Grap publication series*, 27,Volume II, 577–591.

Janssen, P (1989), "Wave-induced stress and the drag of air flow over sea waves." *Journal of Physical Oceanography*, 19, 745–754.

Janssen, P (1991a), "Quasi-linear theory of wind-wave generation applied to wave forecasting." *Journal of Physical Oceanography*, 21, 1631–1642.

Janssen, P (1991b), "Quasi-linear theory of wind-wave generation applied to wave forecasting." In *International Union of Theory and Applied Mechanics (IUTAM)*, 193–198, Sydney, Australia.

Janssen, P (2008), "Progress in ocean wave forecasting." *Journal of Computational Physics*, 227, 3572–3594.

Janssen, P, S Abdalla, H Hersbach, and J Bidlot (2007), "Error estimation of buoys, satellite, and model wave height data." *Journal of Atmospheric and Oceanic technology*, 24, 1665–1677.

Janssen, P, B Hansen, and J Bidlot (1997), "Verification of the ecmwf wave forecasting system against buoy and altimeter data." *Weather and Forecasting*, 12, 763–784.

Janssen, P and P Viterbo (1996), "Ocean waves and the atmospheric climate." *Journal of Climate*, 9, 1269–1287.

Johnson, H, J Hojstruo, H Vested, and S Larsen (1998), "On the dependence of sea surface roughness on wind waves." *Journal of Physical Oceanography*, 28, 1702–1716.

Jones, P (1999), "First-and second-order conservative remapping schemes for grids in spherical coordinates." *Monthly Weather Review*, 3, 2204–2210.

Jorda, G (2005), *Towards data assimilation in the Catalan continental shelf. From data analysis to optimization methods*. Ph.D. thesis, Universitat Politecnica de Catalunya.

Jorda, G, R Bolaños, M Espino, and A Sanchez-Arcilla (2007), "Assessment of the importance of the current-wave coupling in the shelf ocean forecasts." *Ocean Science*, 3, 345–362.

Kandekar, M and R Lalbeharry (1996), "An evaluation of environment canada's operational ocean wave model based on moored buoy data." *Weather Forecasting*, 11, 137–152.

Klaic, Z, Z Pasaric, G Paklar, and P Oddo (2011), "Coastal sea responses to atmospheric forcings at two different resolutions." *Ocean Science*, 7, 521–532.

Komen, G, L Cavaleri, M Donean, K Hasselmann, S Hasselmann, and P Janssen (1994), *Dynamics and Modelling of Ocean Waves*. Cambridge University Press.

Komen, G, S Hasselmann, and K Hasselmann (1984), "On the existence of a fully developed wind-sea spectrum." *Journal of Physical Oceanography*, 14, 1271–1285.

Larson, J, R Jacob, and E Ong (2004), "The model coupling toolkit: A new fortran90 toolkit for building multiphysics parallel coupled models." *International Journal of High Performance Computing Applications*, 19, 277–292.

Legrand, S, E Deleersnijder, E Delhez, and E Legati (2007), "Unstructured, anisotropic mesh generation for the northwestern european continental shelf, the continental slope and the neighbouring ocean." *Continental Shelf Research*, 27, 1344–1356.

Legrand, S, E Deleersnijder, E Hanert, E Legat, and E Wolanski (2006), "High-resolution, unstructured meshes for hydrodynamic models of the great barrier reef, australia." *Estuarine, Coastal and Shelf Science*, 68, 36–46.

Legrand, S, V Legat, and E Deleersnijder (2000), "Delaunay mesh generation for an unstructured-grid ocean general circulation model." *Ocean Modelling*, 2, 17–28.

Lin, W, L Sanford, and S Suttles (2002), "Wave measurement and modelling in chesapeake bay." *Continental Shelf Research*, 22, 2673–2686.

Lin-Ye, J, M Garcia-Leon, V Gracia, and A Sanchez-Arcilla (2016), "A multivariate model of nw mediterranean extreme events: hydrodynamics, energy and duration." *Coastal Engineering*, In press.

Luettich, R and J Westerink (1994a), *The model coupling toolkit: A new Fortran90 toolkit for building multiphysics parallel coupled models*. User's Manual V50. www.adcirc.com.

Luettich, R and J Westerink (1994b), *A (parallel) Advanced Circulation Model for oceanic, coastal and estuarine waters*. User's Manual V50. www.adcirc.com.

Malhadas, M, R Neves, P Leitao, and A Silva (2010), "Influence of tide and waves on water renewal in obidos lagoon, portugal." *Ocean Dynamics*, 60, 40–55.

Mendoza, T, J Jimenez, and J Mateo (2011), "A coastal storms intensity scale for the catalan sea (nw mediterranean)." *Natural Hazards and Earth System Sciences*, 11, 2453–2462.

Mestres, M, M Grifoll, and A Sanchez-Arcilla (2016), "Analysis of current intensification in the northwest mediterranean shelf." *Continental Shelf Research*, 114, 29–40.

Miles, J (1957), "On the generation of waves by shear flows." *Journal of Fluid Mechanics*, 3, 185–204.

Millot, C (1999), "Circulation in the western mediterranean sea." *Journal of Marine Systems*, 20, 423–442.

Monaldo, F (1988), "Expected differences between buoy and radar altimeter estimates of wind speed and significant wave height and their implications on buoy-altimeter comparisons." *Journal of Geophysical Research*, 93, 2285–2302.

Olabarrieta, M, J Warner, B Amstrong, J Zambon, and R He (2012), "Ocean–atmosphere dynamics during hurricane ida and nor'ida: An application of the coupled ocean–atmosphere–wave–sediment transport (coawst) modeling system." *Ocean Modelling*, 43, 112–137.

Oost, W, G Komen, C Jacobs, and C van Oort (2002), "New evidence for a relation between wind stress and wave age from measurements during asgamage." *Boundary Layer Meteorologhy*, 103, 409–438.

Osuna, P and J Wolf (2005), "A numerical study of the effect of wave-current interaction processes in the hydrodinamics of the irish sea." In *International Conference on processes in ocean Waves and Analysis. WAVES*, Madrid, Spain.

Palanques, A, P Puig, J Guillen, J Jimenez, V Gracia, A Sanchez-Arcilla, and O Madsen (2002), "Near bottom suspended sediment fluxes on the microtidal low energy ebro continental shelf (nw mediterranean sea)." *Continental Shelf Research*, 22, 285–303.

Philips, O (1957), "On the generation of waves by turbulent wind." *Journal of Fluid Mechanics*, 2, 417–445.

Pierson, W and L Moskowitz (1964), "A proposed spectral form for fully developed wind seas based on the similarity theory of s.a. kitaigorodskii." *Journal of Geophysical Research*, 69, 5181–5190.

Qi, J, C Chen, R Beardsley, W Perrie, G Celes, and Z Lai (2009), "An unstructured grid finite-volume surface wave mode (fvcom-swave): implementation, validations and applications." *Ocean Modelling*, 28, 153–166.

Queffeulou, P (2004), "Long term validation of wave height measurements from altimeters." *Marine Geodesy*, 27, 495–510.

Queffeulou, P, F Ardhuin, and J efevrer (2011), "Wave height measurements from altimeters: validation status and applications." In *OSTST meeting*, San Diego,USA.

Queffeulou, P, A Bentamy, and J Guyader (2004), "Satellite height validation over the mediterranean sea." In *Proceedings of the 2004 Envisat and ERS Symposium (ESA SP-752)*, Salzburg, Austria.

Queffeulou, P and D Croize-Fillon (2016), "Gobal altimeter swan data set – february 2016." *Report available at:*, ftp://ftp.ifremer.fr/ifremer/cersat/products/swath/altimeters/waves/documentation/.

Radnoti, G, R Ajjajii, R Bubnova, M Caian, E Corconeanu, K von der Emde, J Gril, J Hoffman, A Horanyi, S Issara, V Ivanovici, M Janousek, A Joly, P le Moigne, and S Malardel (1995), "The spectral limited area model arpege/aladin." *PWPR report series 7*, WMO-TD 699, 111–117.

Rebay, S (1993), "Efficient unstructured mesh generation by means of delaunay triangulation and bowyer-watson algorithm." *Journal of Computational Physics*, 105, 125–138.

Ris, R, L Holthuijsen, and N Booij (1999), "A third-generation wave model for coastal regions. 2. verification." *Journal of Geophysical Research*, 104, 7667–7681.

Rogers, W, P Hwang, and D Wang (2003), "Investigation of wave growth and decay in the swan model: Three regional-scale applications." *Journal of Physical Oceanography*, 33, 366–389.

Roland, A, A Cucco, C Ferrarin, T Hsu, J Liau, S Ou, G Umgiesser, and U Zanke (2009), "On the development and verification of a 2-d coupled wave-current mode on unstructured meshes." *Journal of Marine Systems*, 78, 244–254.

Roland, A, U Zanke, T Hsu, S Ou, and J Liau (2006), "Spectral wave modelling on unstructured grids with the wwm (wind wave model) i: The deep water case." In *Third Chinese-German Joint Symposium on Coastal and Ocean Engineering*, Tainan, Taiwan.

Rusu, L and C Guedes Soares (2011), "Modelling the wave-current interactions in the offshore basin using the swan model." *Ocean Engineering*, 38, 63–76.

Sanchez-Arcilla, A, D Gonzalez-Marco, and R Bolaños (2008), "A review of wave climate and prediction along the spanish mediterranean coast." *Natural Hazards and Earth System Sciences*, 8, 1217–1228.

Sanchez-Arcilla, A, J Wolf, and J Monbaliu (2014), "Oceanography at coastal scales: Introduction to the special issue and results from the eu fp7 field ac project." *Continental Shelf Research*, 87, 1–6.

Sandhya, K, T Balakrishnan Nair, L Sabique, N Arun, and K Jeykumar (2014), "Wave forecasting system for operational use and its validation at coastal puducherry, east coast of india." *Ocean Engineering*, 80, 64–72.

Santos, J (1995), *Modelo Hidrodinamico Tridimensional de Circulaçao Oceanica e Estuarina*. Ph.D. thesis, Universidade Técnica de Liscoa, Instituto Superior Técnico.

Schaeffer, A, P Garreau, P Molcard, P Fraunie, and Y Seity (2011), "Influence of high-resolution wind forcing on hydrodynamic modeling of the gulf of lions." *Ocean Dynamics*, 61, 1823–1844.

Sembiring, L, M van Omondt, A van Dongeren, and D Roelvink (2015), "A validation of an operational wave and surge prediction system for the dutch coast." *Natural Hazards and Earth System Sciences*, 15, 1231–1242.

Sepulveda, H, P Queffeulou, and F Ardhuin (2014), "Evaluation of saral/altika observations of small (¡1.5m) significant wave height: comparison with buoy and jason-2 data." In *The WISE 2014 meeting - Waves in Shallow Water Environment*, Reading, United Kingdom.

Sepulveda, H, P Queffeulou, and F Ardhuin (2015), "Assessment of saral altika wave height measurements relative to buoy, jason-2 and cryosat-2 data." *Marine Geodesy*, 3, 449–465.

Shchepetkin, A and J Williams (2005), "The regional ocean modeling system (roms): a split-explicit, free-surface, topography-following-coordinates ocean model." *Ocean Modelling*, 9, 347–404.

Shchepetkin, A and J Williams (2009), "Corrections and commentary for 'ocean forecasting in terrain-following coordinates: Formulation and skill assessment of the regional ocean modeling system' by haidvogel et al., j. comp. phys. 227, pp. 3595-3624." *Jorunal of Computational Physics*, 228, 8985–9000.

Shewchuk, J (2002), "Delaunay refinement algorithms for triangular mesh generation." *Computational Geometry: Theory and Applications*, 22, 21–74.

Shimada, T and H Kawamura (2006), "Wind-wave development under alternating wind jets and wakes induced by orographic effects." *Gephysical REsearch Letters*, 33, L02602.

Siadatmousavi, S, F Jose, and G Miot da Silva (2015), "Sensitivity of a third generation wave model to wind and boundary condition sources and model physics: A casa study from the south atlantic ocean off brazil coast." *Computers and Geosciencesg*, 90, 57–65.

Siadatmousavi, S, F Jose, and G Stone (2012), "In the importance of high frequency tail in third generation wave models." *Coastal Engineering*, 60, 248–260.

Skamarock, W, J Klemp, J Dudhia, J Gill, D Baker, W Wang, and J Powers (2005), "A description of the advanced research wrf version 2." *NCAR Technical Note*, NCAR/TN-468+STR.

Smith, J, A Sherlock, and D Resio (2001), *STAWE: Steady-State Spectral Wave Model User's Manual for STWAVE, Version 3.0*. US Army Corps of Engineering.

Snyder, R, F Dobson, J Elliott, and R Long (1981), "Array measurement of atmospheric pressure fluctuations above surface gravity waves." *Journal of Fluid Mechanics*, 102, 1–59.

Soares, C Guedes, L Rusu, M Bernardino, and P Pilar (2011), "An operational wave forecasting system for the portuguese continental coast area." *Journal of Operational Oceanography*, 4, 17–27.

Sorensen, O, H Kofoed-Hansen, M Rugbjerg, and L Sorensen (2004), "A third-generation spectral wave model using an unstructured finite volume technique." In *Proceedings of the 29th International Conference in Coastal Engineering, ASCE*, 894–906.

Souza, A, A Brown, J Williams, and G Lymbery (2013), "Application of an operational storm coastal impact forecasting system." *Journal of Operational Oceanography*, 6, 23–26.

SWAMPgroup (1985), "Sea wave modelling project (swamp). an intercomparison study of wind wave predictions models, part i: principal results and conclusions." *Ocean Wave Modelling*, 8, 1217–1228.

SWANteam (2015a), "Swan scientific and technical documentation. swan cycle iii version 41.01ab." *Delft University of Technology*, Technical documentation.

SWANteam (2015b), "Swan user's manual. swan cycle iii version 41.01ab." *Delft University of Technology*, Technical documentation.

Taylor, K (2001), "Summarizing multiple aspects of model performance in a single diagram." *Journal of Geophysical Research*, 106, 7183–7192.

Taylor, P and M Yelland (2001), "The dependence of sea surface roughness on the height and steepness of the waves." *Journal of Physical Oceanorgraphy*, 572–590.

Tolman, H (1992a), "Effects of numeric on the physics in a third-generation wind-wave model." *Journal of Physical Oceanography*, 22, 1095–1111.

Tolman, H (1992b), "An evaluation of expressions for the wave energy dissipation due to bottom friction in the presence of currentsl." *Coastal Engineering*, 16, 165–179.

Tolman, H (2008), "A mosaic approach to wind wave modelling." *Ocean Modelling*, 25, 35–47.

Tolman, H, B Balasubramaniyan, L Burroughts, D Chalikov, Y Chao, H Chen, and V Gerald (2002), "A mosaic approach to wind wave modelling." *Weather Forecast*, 17, 311–333.

Tolman, H, M Banner, and J Kaihatu (2013), "The nopp operational wave model improvement project." *Ocean Modelling*, 70, 2–10.

Tonani, M, A Teruzzi, G Korres, N Pinardi, A Crise, M Adani, P Oddo, S Dobricic, C Fratianni, M Drudi, S Salon, A Grandi, G Girardi, V yubartsev, and S Marino (2014), "Proceedings of the sixth international conference on eurogoos 2011." In *Eurogoos Publication no. 30* (N.C. Fleming H. Dahlin and S. E. Petersson, eds.), , Sopot, Poland.

van der Westhuysen, A, M Zijlema, and J Battjes (2007), "Nonlinear saturation-based whitecapping dissipation in swan for deep and shallow water." *Coastal Engineering*, 54, 151–170.

van Vledder, G and A Akpinar (2015), "Wave model predictions in the black sea: sensitivity to wind fields." *Applied Ocean Research*, 53, 161–178.

WAMDIgroup (1988), "The wam model – a third generation ocean wave prediction model." *Journal of Physical Oceanography*, 18, 1775–1810.

Warner, J, B Armstrong, R He, and J Zambon (2010), "Development of a coupled ocean–atmosphere–wave–sediment transport (coawst) modeling system." *Ocean Modelling*, 35, 230–244.

Warner, J, N Perlin, and E Skyllingstad (2008a), "Using the model coupling toolkit to couple earth system models." *Environmental Modelling and Software*, 23, 1240–1249.

Warner, J, C Sherwood, R Signell, C Harris, and H Arango (2008b), "Development of a three-dimensional, regional, coupled wave current, and sediment-transport model." *Computers and Geosciences*, 34, 1284–1306.

Whitham, G (1974), *Linear and nonlinear waves*, volume 636p. Wiley.

WISEgroup (2007), "Wave modeling – the state of the artl." *Progress in Oceanography*, 75, 603–674.

Yan, L (2007), "An improved wind input source term for third generation ocean wave modeling." *Scientific report WR-No 87-8*, De Bilt, The Netherlands.

Young, I (1988), "A shallow water spectral wave model." *Journal of Geophysical Research*, 95, 5116–5126.

Zambon, J, R He, and J Warner (2014), "Investigation of hurricane ivan using the coupled ocean–atmosphere–wave–sediment transport (coawst) model." *Ocean Dynamics*, 64, 1535–1554.

Zanke, U, A Roland, T Hsu, S Ou, and J Liau (2006), "Spectral wave modelling on unstructured grids with the wwm (wind wave model) ii: The shallow water case." In *Third Chinese-German Joint Symposium on Coastal and Ocean Engineering*, Tainan, Taiwan.

Zhai, P and A Bower (2013), "The response of the red sea to a strong wind jet near the tokar gap in summer." *Journal of Geophysical Research - Ocean*, 118, 421–434.

Zijlema, M (2010), "Computation of wind-wave spectra in coastal waters with swan on unstructured grids." *Coastal Engineering*, 57, 267–277.